Investigating actomyosin mediated nuclear force coupling in Hutchinson Gilford Progeria Syndrome

Thesis submitted in accordance with the requirements of the University of Liverpool for the degree of Doctor in Philosophy by Thomas Waring.

November 2021

Abstract

Investigating acto-myosin mediated nuclear force coupling in Hutchinson Gilford Progeria Syndrome

Thomas Waring

Mechanotransduction is the process whereby a cell converts mechanical stimuli into a biological response. This process allows cells that are subject to mechanical stresses to adapt and thereby avoid damage, as well as initiate force-sensitive responses such as differentiation, cell polarisation, and cell cycle activation. Mechanotransduction can be facilitated by the channelling of external forces from the extracellular environment to the nuclear interior, which can activate biochemical signalling pathways, trigger the import of transcription factors, and alter gene expression by modifying chromatin structure. The structures through which these forces are transmitted include focal adhesions, actin stress fibres, the LINC complex, and the nuclear lamina. HGPS is a premature ageing disease, caused by a point mutation in *LMNA*, where the primary cause of death is cardiovascular disease, and there is mounting evidence to suggest that this vascular deterioration is due to cells affected by HGPS being unable to adequately adapt to force stresses. This study therefore aimed to assess the structures involved in mechanotransduction in the context of HGPS to identify any changes in these structures that would explain the inability to adapt to force stresses.

To investigate force transmission at key junctions of the pathway, FRET-based tension biosensors were employed to observe the tensile force applied to talin (located in focal adhesions) and nesprin-2 (located in the LINC complex). Whilst tensile forces across talin were elevated in HGPS cell lines, tension across nesprin-2 was reduced. A morphological assessment of the focal adhesions revealed that they were enlarged in HGPS cells. Atomic force microscopy was used to investigate cytoskeletal stiffness, as an indirect measure of stress fibre tension, and it was found that the fibres running over the nucleus had higher stiffness values in HGPS cell lines, suggesting increased fibre tension. Immunofluorescence of YAP, a transcription factor that typically localises to the nucleus in response to force stimuli, revealed that on 15kPa and 1.5kPa 2-D substrates, the nuclear localisation of YAP was reduced in the majority of HGPS cell lines. An assessment of RhoA activity, a small GTPase that can regulate adhesion maturation and acto-myosin contractility, using a FRET-based activity sensor showed elevated RhoA activity in the HGPS cell line assessed.

From these observations, a model for force sensitivity in HGPS cell lines is proposed. In this model, elevated RhoA activity leads to the reinforcement of focal adhesions and increased acto-myosin contractility, which in turn leads to increased force transmission into the cell. These increased forces are not however felt at the nuclear envelope, and thus cannot influence nuclear import/export. This prevents the dynamic regulation of RhoA, which maintains an elevated activity level, as well as preventing the proper regulation of mechanically sensitive genes. This results in cell damage, death and ultimately the breakdown of the arterial walls.

Acknowledgements

I would first like to thank my supervisors Tobias Zech, Iakowos Karakesisoglou and Luning Liu for their help and support over the course of my studies; their sage advice and keen insight were of immeasurable aid, and their support has allowed me to develop both my academic and personal skills to new heights.

I would also like to thank the members of Zech lab, both past and present, for their companionship. Special thanks go to Louise Brown, Ewan MacDonald, Daniel Newman, and Jessica Bithell, who warmly welcomed me into the lab. They helped me find my feet and set off on this long journey. Thanks go to Milan Collins, who assisted with the traction force microscopy contained within this project. Thanks also go to Lorna Young, who assisted with the RhoA activity experiments and imaging of the lonafarnib treated cells.

My thanks also go to the staff at the Centre for Cell Imaging (University of Liverpool) for allowing access to their facility and providing initial training for the atomic force microscopy work. I would also like to thank them for allowing me to be their colleague for the past year; it was truly a pleasure to work with each and every one of them.

I would finally like to thank the BBSRC, who gave me the opportunity to conduct this work and provided the necessary funding.

COVID-19 Statement

The final two years of this project, 2020-2021, were conducted during the COVID-19 pandemic. The University of Liverpool was locked down entirely for three months between March and June 2020, with heavy restrictions on in-lab working time in place well into 2021. These lockdowns and restrictions were highly disruptive to efficient laboratory work, and thereby resulted in reduced productivity in this time. This was compounded by my own personal difficulties, for I must confess that I struggled with my mental health for many months after the lockdown was lifted; fuelled in part by the high degree of uncertainty that was abound during that time. As a result of these factors, I was unable to conduct all the work that I would have desired by the end of this project. I hope that this can be taken into consideration when assessing the content of this work, and some clemency given to account for these factors that ultimately lay outside of my control.

Table of Contents

List of Figures

List of Tables

Abbreviations

2-D – Two dimensional

3-D – Three dimensional

ABD – Actin binding domain

ABP – Actin binding protein

ABS – Actin binding site

ADP – Adenosine diphosphate

AFM – Atomic force microscopy

ATP – Adenosine triphosphate

DLC1 – Deleted in liver cancer 1

DSB – Double stranded break

ECM – Extracellular Matrix

ELC – Essential Light Chain

FAK – Focal adhesion kinase

FAT – Focal adhesion targeting

FERM – Four-point-one, ezrin, radixin, moesin

FRET - Förster resonance energy transfer

GAP - GTPase activating protein

GDI – Guanine nucleotide dissociation inhibitor

GDP – Guanosine diphosphate

GEF - Guanine nucleotide exchange factor

GTP – Guanosine triphosphate

HR – Homologous recombination

HGPS – Hutchinson Gilford progeria syndrome

HRP – Horse radish peroxidase

INM – Inner nuclear membrane

LAD – Lamina associated domain

LINC – Linker of nucleoskeleton and cytoskeleton

MEF – Mouse embryonic fibroblast

PAA – Polyacrylamide

PDMS – Polydimethylsiloxane

PEG – Polyethylene glycol

PFA – Paraformaldehyde

PCR – Polymerase chain reaction

MLC – Myosin light chain

NE – Nuclear envelope

NHEJ – Non-homologous end joining

NMII – Non-muscle myosin II

NPC – Nuclear pore complex

ONM – Outer nuclear membrane

RLC – Regulatory Light Chain

ROCK - Rho-associated, coiled-coil containing kinase

ROI – Region of interest

SH-2/3 – Src homology 2/3

TAZ – Transcriptional co-activator with PDZ-binding motif

TFM – Traction force microscopy

TFP – Teal fluorescent protein

YAP – Yes-associated protein

1. Introduction

1.1. Mechanotransduction

Cells embedded within the body's tissues are subjected to a variety of external forces. Smooth and skeletal muscle cells will be stretched, osteoblasts will be compressed, and endothelial cells will be sheared by the flowing of blood. These cells will also be surrounded by environments with different mechanical properties; bone will be stiffer than muscle, which in turn will be stiffer than brain (Guimarães *et al.*, 2020). The cell must be able to sense these environmental cues and respond accordingly. This process of converting a mechanical stimulus into a biological response is referred to as mechanotransduction. Mechanotransduction lies at the heart of many cellular processes, including control of the cell cycle (Huang and Ingber, 1999), cell differentiation (Engler *et al.*, 2006; Le *et al.*, 2016,), tissue development (Wozniak and Chen, 2009), and migration (Lo *et al.*, 2000). The ability of mesenchymal stem cells to sense the stiffness of their surrounding matrix, for example, informs them whether to undergo osteogenesis, myogenesis or neurogenesis; with stiff matrix inducing osteogenesis, intermediate stiffness inducing myogenesis and low stiffness inducing neurogenesis (Engler *et al.*, 2006). Bovine aortic endothelial cell (BAEC) monolayers subject to shear stresses will align their long axis and actin stress fibres in the direction of the flow (Galbraith *et al.*, 1998). Quiescent kidney epithelial (MDCK) cells can be stimulated to enter the cell cycle by the application of a persistent stretching force (Benham-Pyle *et al.*, 2015). In each of these cases, mechanotransduction allows the cells to sense mechanical cues and coordinate an appropriate response. Given the variety of processes that mechanotransduction plays a part in, it is no surprise that the loss or subversion of this ability leads to a wide range of diseases including muscular dystrophies, premature ageing diseases, and cancer (Jaalouk and Lammerding, 2009).

There are several different mechanisms via which mechanotransduction can occur. Ion channels within the plasma membrane can act as force sensors by undergoing conformational changes in response to tensile forces along the plasma membrane, opening their channels and allowing the entry of ions into the cytoplasm (Jin *et al.*, 2020; Martinac, 2004); though the exact mechanism via which these conformational changes are facilitated remains unknown (Jin *et al.*, 2020). These mechanosensitive

ion channels play a role in a diverse range of processes including hearing, touch, and flow sensing (Jin *et al.*, 2020).

There are another group of structures within the cell that can facilitate mechanotransduction. These structures, through a continuous connection to each other, allow external forces to be transmitted from the extracellular matrix (ECM) to the nuclear interior. The structures involved in this connection are the focal adhesions, actin stress fibres, the linker of nucleoskeleton and cytoskeleton (LINC) complex and the nuclear lamina (Fig 1.1). The focal adhesions bridge the plasma membrane via proteins called integrins, which connect the ECM to actin stress fibres through actin-binding adapter proteins. These actin stress fibres, via the perinuclear actin cap (or an unknown actin structure in 3-D), then link to the nucleus by interacting with another trans-membrane protein complex known as the LINC complex (Fig 1.1). This complex spans the nuclear envelope (NE) and links the actin cytoskeleton to the nuclear lamina via the outer nuclear membrane (ONM) spanning nesprins and the inner nuclear membrane (INM) spanning SUN proteins. Within the nuclear interior, proteins within the INM that bind to both lamins and chromatin then act to link the LINC complex directly to the chromatin, in regions known as lamina associated domains (LADs). This pathway of structures can channel forces directly into the nuclear interior, where it can influence global gene expression via effects upon chromatin organisation (Gauthier *et al*., 2012; Heo *et al.*, 2015; 2016; Iyer *et al*., 2012; Poh *et al*., 2012). It can also facilitate the localisation of transcription factors into the nucleus in response to force application (Elosegui-Artola *et al.*, 2017).

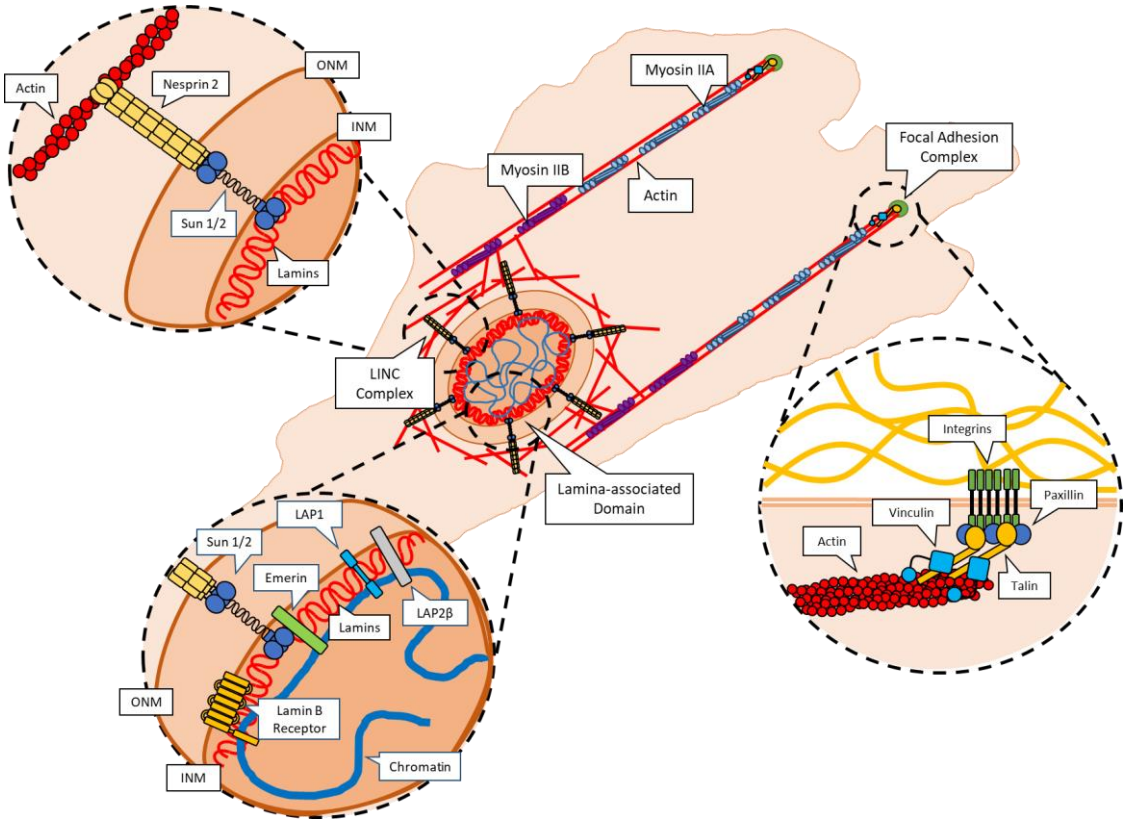

Fig 1.1. Summary of connection between the extracellular environment and the nuclear interior that facilitates mechanotransduction. Forces from the extracellular environment can be channelled to the nuclear interior through a series of physical connections involving focal adhesion complexes, acto-myosin stress fibres, LINC complexes and LADs.

1.1.1. The Extracellular Matrix

The ECM is a fundamental part of the form and function of soft connective tissues. There are approximately 300 proteins, 200 glycoproteins and 20 proteoglycans that constitute the ECM (Hynes and Naba, 2012). Despite this large number of different constituents, one of the features that they share is that they typically contain repeats of a select number of domains (Hynes and Naba, 2012), and these domains can be used to characterise the different components of the ECM into broad groups. One such group is the collagens. Collagens are typified by the presence of a repeating Gly-X-Y domain, where X is frequently proline and Y is frequently 4-hydroxyproline (Hynes and Naba, 2012). There are a total of 28 members of the collagen superfamily in vertebrates, which are denoted by Roman numerals (Ricard-Blum, 2011). The collagens commonly form homotrimer α chains, or less commonly heterotrimers, which comprise of the Gly-X-Y repeat domains (Ricard-Blum, 2011). These trimeric

collagens can then form supramolecular structures, which can be divided into different groups: fibrils, beaded filaments, anchoring fibrils, and networks (Ricard-Blum, 2011). Collagen fibrils, which are then further assembled into collagen fibres, provide the ECM with its mechanical stiffness and strength (Humphrey *et al.*, 2014).

Fibronectin is a glycoprotein found within the ECM that forms a meshwork between neighbouring cells (Singh *et al.*, 2010). It consists of numerous repeating modules, which can be divided into three types (I, II, and III) (Singh *et al.*, 2010). Two intramolecular disulphide bonds form within each type I and II module, stabilising fibronectin's folded structure (Singh *et al.*, 2010). Type III modules are seven-stranded β-barrel structures which lack disulphides. Further disulphide bonds between the C-termini of two fibronectin molecules brings them together into a dimer (Singh *et al.*, 2010). Numerous cell surface integrins can bind to the modules within fibronectin (including module III_{10}, which contains the well-studied RGD sequence), which mediates cellular control of fibronectin filament assembly (Pankov and Yamada, 2002; Singh *et al.*, 2010). As part of this process, the binding of fibronectin to integrins promotes integrin clustering, which brings numerous fibronectin molecules together to form intermolecular connections (Singh *et al.*, 2010). Fibronectin is also able to bind a variety of other ECM components, including collagen, heparin, and fibrillin (Pankov and Yamada, 2002; Singh *et al.*, 2010), and the fibronectin matrix is known to play a role in the matrix assembly of a range of these ECM components (Singh *et al.*, 2010).

The ECM can take on a variety of different structures, which are influenced by the proteins that compose it (Theocharis *et al.*, 2016). One of these structures, known as a basement membrane, takes the form of a 40–120nm sheet that acts to separate cells from the surrounding connective tissue, as well as acting as a scaffold on which epithelial and endothelial can grow (Paulsson *et al.*, 1992). Collagen IV is a major component of the basement membrane and provides a scaffold for the assembly of the other structural components (Paulsson *et al.*, 1992). Among these other components are the laminins. These laminins exist as heterotrimers, consisting of one α chain, one β chain and one γ chain (Shaw *et al.*, 2021). There are five α chains, four β chains and three γ chains, which can combine into 16 known heterotrimers (Aumailley *et al.*, 2005; Shaw *et al.*, 2021). The α chains have a large C-terminal globular G domain, a coiled-coil domain, and an N-terminal short arm (whose length varies between α

chains) with a number of laminin-type epidermal growth factor-like repeats located between globular L domains (Domogatskaya *et al.*, 2012). The β and γ chains share the coiled-coil domain, as well as the N-terminal short arm domain, with the α chains (Domogatskaya *et al.*, 2012). It is the coiled-coil domains that interact to facilitate trimerization of the chains, whilst the N-terminal domains allow the polymerisation of heterotrimers into higher order networks (Shaw *et al.*, 2021). Laminins can interact with a range of different cell surface receptors, including integrins (Domogatskaya *et al.*, 2012) and mutations in the laminins has been linked to a range of diseases with distinct pathologies (Shaw *et al.*, 2021).

Another ECM constituent that can define the mechanical properties of the ECM is the glycoprotein elastin. It is first produced as a precursor protein called tropoelastin, which is then assembled and crosslinked to form an insoluble polymer (Arribas *et al.*, 2006). This assembly is guided by microfibrils produced at the cell surface, which themselves are composed of numerous glycoproteins, such as fibrillin-1 and fibrillin-2, microfibril-associated glycoproteins (MAGP1 and MAGP2) and the latent transforming growth factor β (TGF-β)-binding proteins (Arribas *et al.*, 2006). These elastic fibres bestow the ECM with its extensibility (elastic fibres can extend up to 150% without failure) and resilience (the ability to recoil upon unloading) (Humphrey *et al.*, 2014).

The regulation of the ECM constituents, and the mechanical properties that they impart to the ECM, is important for the maintenance of tissue homeostasis. As such, cells possess an array of negative feedback loops that allow them to sense changes in the mechanical properties of the ECM and return them to desired levels (Humphrey *et al.*, 2014). The loss of these feedback loops, or their reversal into a positive feedback loop, can cause tissue homeostasis to be lost and thereby result in pathology. Fibrosis, for example, is caused by the excessive production and deposition of collagen into the ECM by fibroblasts. This then leads to a stiffening of the ECM, which in turn promotes the production of more collagen in a positive feedback loop that ultimately leads to tissue pathology (Henderson *et al.*, 2020). The proteoglycan decorin, important for collagen fibrillogenesis (Reed and Iozzo, 2002), acts at various stages in the progression of atherosclerosis to attenuate its progression, and lower levels of this ECM component correspond to increased rates of atherosclerosis progression (Singla

et al., 2011), highlighting the importance of ECM composition in tissue homeostasis and disease progression. The loss of ECM mechanical homeostasis also plays an important role in ageing, with tissues such as the skin and arterial walls displaying increased stiffness with advanced age due to progressive degradation of the ECM (Birch, 2018). The cell's ability to sense and properly adjust the composition and mechanical properties of the ECM is therefore vitally important to maintaining a healthy tissue state.

1.1.2. The Focal Adhesion Complex

The focal adhesion complex acts as both a platform for mechanically activated biochemical signalling pathways and as a relay for force transmission between the ECM and the nuclear interior. The complex itself consists of a wide variety of proteins, which associate with the adhesion at varying stages of its life cycle. The use of proximity labelling probes, combined with mass spectroscopy, has allowed for the identification of proteins associated with focal adhesions. Horton *et al.* (2015) used data from seven such datasets, based upon fibronectin induced adhesions, to build a picture of which proteins are universally identified across differing cell lines and methodologies. This study identified 60 proteins that were termed the 'consensus integrin adhesome'; proteins that were enriched in at least five of the datasets. Amongst these were proteins that are known to play an important role in transmitting mechanical forces, as well as in mechanically induced biochemical signalling.

1.1.2.1. Integrins

Integrins form the bedrock of the focal adhesions and are the component of the complex that spans the plasma membrane and engages with components of the ECM. Integrins exist as non-covalent heterodimers, which consist of a single α subunit and a single β subunit. There are a total of 18 α and 8 β subunits, which can combine into 24 different integrins (Hynes, 2002). The component α and β subunit of the heterodimer determine the ligand specificity of the integrin, and each combination of subunits has its own specific, non-redundant function (Hynes, 2002). The α and β subunits have different molecular structures. The α subunit consists of a β-propeller head domain connected to a thigh, calf-1, and calf-2 domain, which collectively form the leg structure (Barczyk *et al.*, 2010). 9 of the α subunits also have an αI domain, inserted

into the β-propeller (Larson *et al.*, 1989). The β subunit consists of a plexin-sempahorin-integrin (PSI) domain, a hybrid domain, a βI domain and four cysteine-rich epidermal growth factor (EGF) repeats (Barczyk *et al.*, 2010). Both subunits also contain a single membrane-spanning helix and a short cytoplasmic tail (Campbell and Humphries, 2011).

Integrins can exist in three conformational states: "bent closed", "extended closed" and "extended open" (Luo *et al.*, 2007). The "bent closed" state has a low ligand affinity, and thus represents an inactive conformation; with integrin activation being the transition of integrin into its "extended open" conformation (Luo *et al.*, 2007; Sun *et al.*, 2019). Activated integrins that are bound to their ligands will cluster together, leading to the formation of focal adhesions. Mechanical force is an important factor in integrin activation, with low level tensile forces being needed to stabilise the "extended open" conformation (Sun *et al.*, 2019). Intermediate tensile forces promote the clustering of integrins and the strengthening of the attachment between the ECM and integrins into mature focal adhesions (Humphrey *et al.*, 2014; Sun *et al.*, 2019). The activation and clustering of integrins can also be promoted by the binding of proteins to their cytoplasmic tails, namely talin and kindlin (Sun *et al*, 2019). Ligand binding that promotes integrin clustering is often referred to as "outside-in" signalling, as it is the ECM outside the cell that triggers the clustering of integrins and the subsequent recruitment of focal adhesion proteins inside the cell. In the reverse, the binding of proteins such as talin to integrin is referred to as "inside-out" signalling, as it is the binding of these proteins inside the cell that promotes integrin clustering and the subsequent recruitment of ECM components outside the cell.

1.1.2.2. Talin

Talin is a large (270kDa) multidomain protein that acts as a bridge between integrins and the actin cytoskeleton. It binds to the cytoplasmic tail of integrins via an N-terminal FERM domain, and to actin filaments via two actin binding sites (ABS) within its C-terminal rod domain (Goult *et al.*, 2018). The FERM domain consists of four globular segments (F0-F3), whilst the rod domain consists of 13 helical bundles (R1-13) terminated by a single α-helix that mediates homodimerization; the two domains are connected by a disordered linker segment (Goult *et al.*, 2018). Talin natively exists in an autoinhibitory state, with the rod domain binding to the FERM

domain at a position overlapping the site of integrin binding, thus preventing talin's binding to the cytoplasmic tail of integrin (Goksoy *et al.*, 2008). Talin binding to phosphatidylinositol 4,5-bisphosphate (PIP_2) disrupts the interaction between the FERM and rod domains, unveiling the integrin binding site (Goksoy *et al.*, 2008). Talin is recruited to the plasma membrane via its interaction with Rap1/RIAM, which is required for its activation and binding to integrin (Lee *et al.*, 2009).

Talin has been shown to be subject to tensile forces whilst within the adhesion (Kumar *et al.*, 2016), and plays a role in propagating forces from the adhesions to the actin cytoskeleton (Elosegui-Artola *et al.*, 2016). Talin has also been shown to play a role in orchestrating adhesion formation and maturation via its interaction with vinculin (Humphries *et al.*, 2007), and in defining the structure of the adhesion (Liu *et al.*, 2015). These roles of talin have been directly linked to its ability to transmit forces; indeed, force application across talin is required for its functions in regulating focal adhesions (Rahikainen *et al.*, 2019). Some of these functions, including the recruitment of vinculin to the adhesion, are accomplished by force-induced unfolding of the helical bundles within talin's rod domain, which reveals previously inaccessible binding sites and allows vinculin to bind (del Rio *et al.*, 2009; Rahikainen *et al.*, 2019). This mechanical unfolding of domains can itself act as a signalling method, with each of the helical bundles within the rod domain having unique force-extension profiles that can facilitate differing combinations of ligand binding at different tensile force thresholds (Goult *et al.*, 2018). Vinculin has also been shown to be subject to tensile forces within the adhesion, and this tension promotes focal adhesion assembly and maturation (Grashoff *et al.*, 2010). Together, talin and vinculin thereby act as the principal mechanism via which forces from the extracellular environment are transmitted to the actin cytoskeleton, and in so doing also act to activate mechanically induced signalling pathways.

1.1.2.3. Focal Adhesion Kinase

One of the main signalling proteins within the adhesion is focal adhesion kinase (FAK). FAK consists of an N-terminal FERM domain, followed by a ~40 residue linker region, a central kinase domain, a ~220 residue proline rich low complexity region and a C-terminal focal adhesion targeting (FAT) domain (Lietha *et al.*, 2007). The FERM domain shares a similar structure to that of talin, kindlin, and a range of

other proteins (Frame *et al.*, 2010). In a similar manner to talin, FAK natively exists in an autoinhibitory conformation with the FERM domain binding to the kinase domain, which blocks the autophosphorylation of Tyr397 in FAK (Cooper *et al.*, 2003; Lietha *et al.*, 2007); the first step in FAK activation. Integrin binding activates FAK by releasing FERM domain binding, revealing autophosphorylation sites (including Tyr397) and binding sites for SH-2 domain containing proteins, allowing for activation of FAK via tyrosine phosphorylation (Chen *et al*., 1996; Han and Guan, 1999; Schaller *et al.*, 1994; Xing *et al.*, 1994). The FAT domain of FAK localises it to the focal adhesions via interaction with various adhesion proteins, including talin and paxillin (Chen *et al.*, 1995; Hildebrand *et al.*, 1993, 1995).

FAK is activated in response to a variety of force stresses and plays a role in mediating an array of force-sensitive cellular behaviours, including cell spreading and cell migration (Zebda *et al.*, 2012). Src, specifically, forms a complex with FAK, activating both proteins via phosphorylation of FAK and a conformational change that relieves its own auto-inhibition (Calalb *et al.*, 1995; Matsui *et al.*, 2012). Src activity can be activated in response to direct mechanical stimulation, even at sites distal to the application point (Wang *et al.*, 2005). FAK/Src activate a wide range of biochemical signalling pathways in response to integrin engagement with the extracellular environment, which coordinate to regulate processes such as cellular migration, cell spreading, focal adhesion turnover and formation (Boutahar *et al.*, 2004; Mitra *et al.*, 2005; Stutchbury *et al.*, 2017; Webb *et al.*, 2004; Zhao *et al.*, 2011). FAK activity can also control the expression level of lamin A/C, a function that controls the progression of cellular senescence and is co-opted in cancer to promote tumour growth (Chuang *et al.*, 2019).

1.1.2.4. Paxillin

A key protein within the adhesion that is phosphorylated by FAK is paxillin (Bellis *et al.*, 1995). Paxillin's structure consists of five repetitive leucine-rich LD (Leu-Asp) motifs located at the N-terminus (LD1 to LD5) and four cysteine-histidine-enriched LIM domains at the C-terminus. Additionally, it contains a proline-rich sequence that anchors SH-3 domain-containing proteins, located within the N-terminus, as well as numerous serine and tyrosine residues throughout the protein which bind to SH-2

domains (López-Colomé *et al.*, 2017). The LIM2 and 3 domains are required to localise paxillin to the focal adhesions (Brown *et al.*, 1996). The LD domains of paxillin facilitate binding with a wide variety of proteins associated with focal adhesions, including FAK and vinculin (Brown *et al.*, 1996; Hildebrand *et al.*, 1995; López-Colomé *et al.*, 2017; Wood *et al.*, 1994). The proline rich region also facilitates binding to the tyrosine kinase Src (Weng *et al.*, 1993). Through these numerous interactions, paxillin plays a pivotal role within the adhesion as a central hub for the coordination of focal adhesion-based signalling.

Multiple tyrosine, serine and threonine phosphorylation sites exist throughout paxillin (Webb *et al.*, 2005), which are targeted for phosphorylation by a wide variety of kinases, including FAK/Src (Deakin *et al.*, 2008; López-Colomé *et al.*, 2017). Stimulation with growth factors, neuropeptides, ligands for G-protein coupled receptors and physical stress all trigger the phosphorylation of paxillin (Schaller, 2001), giving it an important role in coordinating the signalling pathways necessary for controlling cell migration and adhesion dynamics (Brown and Turner, 2004; Deakin *et al.*, 2008; Schaller, 2001). Indeed, paxillin is among the first proteins to be recruited to forming adhesions (termed nascent adhesions) (Zaidel-Bar *et al.*, 2003) and remains present throughout the life cycle of the adhesion, controlling their growth and ultimate disassembly (Webb *et al.*, 2004).

1.1.3. The Actin Cytoskeleton

1.1.3.1. Actin Filament Assembly

Actin is a monomeric globular protein (G-actin) that can be polymerised into a filamentous polymer (F-actin). Monomeric actin has two major α/β-domains, which are divided into four subdomains (Dominguez and Holmes, 2011). There are two clefts between these two domains; the smaller of these binds ATP, while the larger cleft is the primary binding site for most actin binding proteins (Dominguez and Holmes, 2011), as well as coordinating the binding between actin monomers within the filamentous polymer (Oda *et al.*, 2009). Actin polymerisation itself is not an energetically favoured process, with the limiting step in fibre assembly being the formation of an initial actin dimer (Sept and McCammon, 2001). As such, actin nucleating factors, such as the Arp2/3 complex, are used to facilitate the formation of

an actin trimer, which can then act as a base for further polymerisation (Dominguez, 2009). Due to the nature of the interaction between the actin monomers, each of the monomers adopts the same orientation within the filamentous polymer and as a result actin filaments are polarised. The ends of the polarised filament are referred to as the barbed (+) end and the pointed (-) end. Actin monomers in an ATP-bound state associate more readily with the barbed end of the filament than the pointed end (Wegner and Isenberg, 1983), resulting in assembly generally occurring at the barbed end and disassembly occurring at the pointed end. The hydrolysis of ATP within the actin filament also results in the loss of actin monomers from the filament at the pointed end, as ADP-bound actin has a much higher dissociation rate than ATP-bound actin (Pollard, 1986). The rates of assembly/disassembly of the filaments can also be controlled by the binding of various actin binding proteins (ABPs), which can either promote or prevent actin filament polymerisation (Pollard, 2016).

1.1.3.2. Actin Binding Proteins and Actin Nucleation/Bundling

These ABPs are vitally important for the regulation of actin assembly/disassembly in cells. Actin concentration in cells ranges from ~25–100μM, which lies well beyond the critical concentration for actin polymerisation; and yet half of the total actin in cells is unpolymerized (Pollard, 2016). This is due to the regulation of actin dynamics by ABPs, which can control nearly every aspect of actin assembly; they can sequester and store actin monomers, nucleate actin filament polymerisation, promote filament elongation, cap actin filaments to prevent assembly/disassembly, sever actin filaments and bundle filaments (Pollard, 2016).

Profilin is an actin monomer binding protein that inhibits the nucleation and polymerisation of actin at the pointed ends of actin filaments, though not the barbed end (Pollard, 2016). Actin-profilin complexes can assemble at the barbed end of the filament, where profilin is then released due to its low affinity for ATP-bound actin filaments (Courtemanche and Pollard, 2013). Profilin also acts as a nucleotide exchange factor, promoting the exchange of ADP for ATP in the nucleotide binding site (Mockrin and Korn, 1980). Profilin can be recruited to the barbed ends of actin filaments by its interaction with polyproline sequences in various elongation mediating proteins (Ferron *et al.*, 2007). Through these various functions, profilin acts to store

and recycle actin monomers and facilitate their incorporation into growing actin filaments.

Formins are one group of proteins that can bind to the barbed end of actin filaments and control filament elongation. Formins typically have two formin homology domains, FH1 and FH2, which bind to profilin (via a varying number of polyproline sequences) and the barbed end of actin filaments respectively (Paul and Pollard, 2009). Formin FH2 domains will dimerise and bind to the actin filament barbed end, and then control the addition of actin monomers by switching between an "open" and "closed" conformation (Paul and Pollard, 2009 Vavylonis *et al.*, 2006). mDia1 is one example of a FH2 domain containing formin, which can promote rapid actin polymerisation at the barbed end of filaments (Kovar *et al.*, 2006). The activity of mDia1 can be controlled by the binding of the small GTPase RhoA, which binds at a site at the N-terminal end of mDia1 and thereby relieves mDia1 autoinhibition (Li and Higgs, 2005; Otomo *et al.*, 2005).

The Arp2/3 complex can act as a nucleator of actin filaments that branch from an existing actin filament. The binding of the Arp2/3 complex to an existing actin filament causes a conformational change in the complex, which allows the Arp2 and Arp3 subunits of the complex to act as the initial dimer for actin polymerisation (Rouiller *et al.*, 2008). The nucleating activity of the Arp2/3 complex requires the binding of a nucleation promoting factor (NPF), a group of proteins that includes WASP family verprolin-homologous protein (WAVE), Wiskott–Aldrich syndrome protein (WASP), neural WASP (NWASP), WASP and SCAR homologue (WASH), and junction-mediating and regulatory protein (JMY) (Rotty *et al.*, 2013). The activity of these NPFs, and by extension the Arp2/3 complex, can be controlled by small GTPases; WASP can be activated by Cdc42 binding (Kim *et al.*, 2000) and WAVE can be activated by Rac1 (Eden *et al.*, 2002).

α-actinin is an ABP that acts to bundle actin filaments by cross-linking the individual actin filaments and thereby keep them in proximity with one another (Sjöblom *et al.*, 2008). There are six isoforms of α-actinin in mammalian cells, which can be split into two groups; those expressed in muscle tissue and those expressed in non-muscle cells (Sjöblom *et al.*, 2008). Isoform 1 is the isoform that distributes along actin stress fibres in motile non-muscle cells (Sjöblom *et al.*, 2008). α-actinin consists of an N-terminal

actin binding domain (ABD), a central rod region of four spectrin repeats, and a C-terminal calmodulin (CaM) like domain (Sjöblom *et al.*, 2008). Two α-actinin molecules form a functional dimer via interaction between their spectrin repeats, and the two molecules are oriented in the opposite direction so that each end of the homodimer has one ABD and one CaM-like domain (Sjöblom *et al.*, 2008). This allows each end of the dimer to bind to an actin filament, and thus facilitates its ability to cross-link actin filaments.

1.1.3.3. Actin Stress Fibres

Stress fibres are bundles of filamentous actin, with alternating polarity, which are associated with bi-polar arrays of non-muscle myosin II (NMII) and bound by α-actinin (Langanger *et al.*, 1986). The stress fibres are not universal in their morphology, however, and can be divided into three groups (found in 2-D): dorsal and ventral stress fibres, and transverse arcs. Transverse arcs are curved filaments which are not associated with focal adhesions and span the apical surface of the cell. In migrating cells, these arcs flow backward from the lamellipodia towards the cell centre (Heath, 1983), a process that is dependent upon contraction within the arcs (Zhang *et al.*, 2003). This contractility can be transmitted to the focal adhesions, and thus the extracellular environment, via the dorsal stress fibres. These fibres are associated with focal adhesions at one end, whilst the other end is attached to transverse arcs. Unlike other stress fibres, dorsal fibres do not contain NMII and thus are not contractile (Tojkander *et al.*, 2011). Ventral stress fibres are attached to focal adhesions at both ends and constitute the main contractile force generating component within the cell. The mechanism via which stress fibres are formed differs between the different types of fibre (Pellegrin and Mellor, 2007). Dorsal stress fibres elongate from focal adhesions to form short filaments containing α-actinin. Clusters of myosin are then woven into these structures, displacing α-actinin. Transverse arcs form by end-to-end joining of short bundles of actin to bundles of myosin. Ventral stress fibres form by the end-to-end joining of two dorsal stress fibres to form a structure that is anchored at both ends by a focal adhesion (Pellegrin and Mellor, 2007).

1.1.3.4. Non-Muscle Myosin II

The ability of actin stress fibres to contract, and thus exert force, is imparted by the incorporation of NMII isoforms. The myosins are a superfamily of proteins, which typically contain three domains: a motor domain, a neck domain, and a tail domain (Sellers, 2000). The motor domains are relatively well conserved and are the domain that interacts with the actin filament and possess an ATP binding site. The neck incorporates a conserved IQ motif that binds to light chains, whilst the tail domain can vary widely between the different myosins; a range of different binding domains, including SH-3 domains, GAP domains, FERM domains, and pleckstrin homology (PH) domains can be found within the tail domain of myosins (Sellers, 2000). There are 25-30 different myosins in mammals, split between 9 of the 15 different classes of myosin; the classes generally being unified by phylogenetic analysis of the motor domains (Sellers, 2000). The myosins of class II constitute the major contractile myosin found in skeletal and smooth muscle, as well as being present in all non-muscle eukaryotic cells (Vicente-Manzanares *et al.*, 2009). NMII is constructed from three peptides: a non-muscle myosin II heavy chain (NMIIHC), a regulatory light chain (RLC), and an essential light chain (ELC). The RLC and ELC bind to the heavy chain via the IQ motifs in the neck domain of the heavy chain. The tail domain of NMIIHC forms an α-helical coiled-coil with another heavy chain, creating a homodimer. The fully formed NMII therefore consists of 2 heavy chains, 2 RLC and 2 ELC, with the two head domains of NMIIHC at one end of the molecule (Vicente-Manzanares *et al.*, 2009). These NMII molecules can then associate with one another via their coiled-coils, forming bipolar filaments, though this assembly is reliant on RLC phosphorylation (Vicente-Manzanares *et al.*, 2009). These bipolar filaments, associated with anti-parallel actin filaments, form the basis of contractile actin stress fibres. There are three isoforms of NMIIHC in mammals, encoded by three genes; myosin heavy chain 9 (MYH9), MYH10 and MYH14 encode the heavy chains NMHC IIA, NMHC IIB and NMHC IIC, respectively (Vicente-Manzanares *et al.*, 2009).

The activity of NMII isoforms is controlled by the phosphorylation of the RLC. Phosphorylation at ser19 greatly increases the ATPase activity of the myosin head domain in the presence of actin, which stimulates head domain movement and thus pulling on the actin filament (Vicente-Manzanares *et al.*, 2009). This activity can be

further stimulated by the additional phosphorylation of Thr18 (Vicente-Manzanares *et al.*, 2009). The phosphorylation of these two sites is controlled by a variety of different kinases, namely myosin light chain kinase (MLCK), Rho-associated, coiled-coil containing kinase (ROCK), citron kinase, leucine zipper interacting kinase (ZIPK) and myotonic dystrophy kinase-related CDC42-binding kinase (MRCK) (Vicente-Manzanares *et al.*, 2009). The activity and assembly of NMII isoforms can also be controlled by phosphorylation at several sites within both the light chains and the heavy chains. (Pecci *et al.*, 2018; Vicente-Manzanares *et al.*, 2009).

1.1.3.5. Acto-Myosin Contractility

The contractility of the stress fibres plays a pivotal role in the regulation of the focal adhesions, with inhibition of NMII activity leading to focal adhesion disassembly and a blocking of focal adhesion maturation (Chrzanowska-Wodnicka and Burridge, 1996; Helfman *et al.*, 1999). NMII activity has also been shown to play a role in recruiting FAK and vinculin to adhesions, as well as promote FAK mediated phosphorylation of paxillin, facilitating adhesion maturation (Pasapera *et al.*, 2010). Contractility is also important for the maintenance of the stress fibres themselves, as NMII inhibition leads to their disassembly (Chrzanowska-Wodnicka and Burridge, 1996; Helfman *et al.*, 1999). Focal adhesion maturation can however be triggered in the absence of NMII contractility if external forces are present (Bershadsky *et al.*, 2005; Riveline *et al.*, 2001). Actin stress fibre contractility is also important for the stress fibre's role in propagating forces from the extracellular environment. The actin cytoskeleton is maintained under a constant state of contraction and stretching, which is generated by NMII activity within the stress fibres (Guolla *et al.*, 2012). This places the cytoskeleton under tension, or pre-stress, which facilitates force propagation by making the cell more sensitive to applied forces (Hu *et al.*, 2005), as well as allowing the propagation of locally applied forces over greater distances within the cell (Hu *et al.*, 2003). This long-distance force propagation allows for forces exerted locally at the focal adhesions to be transmitted all the way to the nuclear interior, where it can directly regulate protein interactions within nuclear structures (Poh *et al.*, 2012) as well as alter chromatin structure and regulate gene transcription (Tajik *et al.*, 2016). This cytoskeletal tension can be related to cellular stiffness, with increased contractility correlating with increased cellular stiffness (Wang *et al.*, 2002). As such, one can gain insight into the underlying tension state of a cell by assessing its overall cytoskeletal

stiffness and draw conclusions about the ability of that cell to propagate external forces exerted at the focal adhesions.

While stress fibre organisation and formation been studied extensively in cells grown upon a 2-D substrate, the question has been raised as to whether actin structures such as stress fibres even exist within cells grown in 3-D matrices (Burridge and Wittchen, 2013). Whilst cells within most tissues may never develop actin stress fibres, it has been demonstrated that those cells that experience high mechanical forces do undertake stress fibre formation (Burridge and Wittchen, 2013), making observations of stress fibre mediated force propagation in 2-D physiologically relevant. Indeed, stress fibre contractility, and resulting transmission of forces across focal adhesions to the ECM, has been demonstrated in fibroblasts migrating through a 3-D fibrin matrix, with the mechanism for this force transmission having many characteristics in common with that observed for 2-D migration (Owen *et al.*, 2017).

1.1.3.6. Perinuclear Actin Cap

The perinuclear actin cap is a name given to a subset of actin stress fibres that run along the top of the nucleus and are directly linked to the NE via their interaction with nesprin-2 (Khatau *et al.*, 2009). Like ventral stress fibres, they are anchored at both ends by focal adhesions, though these adhesions differ from typical focal adhesions in their morphology and function (Kim *et al.*, 2012). The perinuclear actin cap helps define the shape of the nucleus, a process that is important for persistent migration (Razafsky *et al.*, 2014), as well as control the movement of the nucleus during cell polarisation (Maninová and Vomastek, 2016). How the perinuclear actin cap is formed is currently not fully understood, however the work of Maninová and Vomastek (2016) suggests that the stress fibres of the cap are formed from the fusion of dorsal and peripheral stress fibres, whose movement over the nucleus is facilitated by transverse arcs. The stress fibres of the perinuclear actin cap display a greater level of acto-myosin contractility than other types of stress fibre (Maninova *et al.*, 2017).

1.1.4. Small GTPases

The small guanosine triphosphatases (GTPases), or the Ras superfamily, are a large group of proteins that control many aspects of cell behaviour (Reiner and Lundquist,

2018). They act as molecular switches for cell signalling, existing in either an active or inactive state. The active state is GTP bound, whilst the inactive state is GDP bound. Control of the switching between these states is facilitated by three groups of regulators, guanine nucleotide exchange factors (GEFs), GTPase activating proteins (GAPs), and guanine nucleotide dissociation inhibitor (GDI) (Fig 1.2). The Ras superfamily can be divided into five families: Ras, Rho, Arf, Rab and Ran. Each of these families generally controls different aspects of cellular behaviour (Reiner and Lundquist, 2018). There are 20 members of the Rho family of small GTPases in eukaryotes, which generally act to control the organisation and dynamics of cytoskeletal components (Heasman and Ridley, 2008). Among these are Cdc42, Rac1 and RhoA. The activity of each of these proteins promotes the formation of different actin structures and has been linked to a variety of cellular behaviours including cell division, polarisation, migration, and morphology (Etienne-Manneville and Hall, 2002; Heng and Koh, 2010; Sit and Manser, 2011).

1.1.4.1. RhoA

RhoA activity promotes the formation of actin stress fibres, with microinjection of activated recombinant RhoA into fibroblasts resulting in extensive stress fibre formation (Paterson *et al.*, 1990). This stress fibre formation is facilitated by the activation of two downstream effectors, mDia1 and ROCK, which work cooperatively to bring about the reorganisation of actin into stress fibres (Leung *et al.*, 1996; Pellegrin and Mellor, 2007; Watanabe *et al.*, 1999). ROCK acts to increase acto-myosin contractility via two main mechanisms. It firstly increases the activity of NMII isoforms via phosphorylation of the RLC, which enhances NMII ATPase activity (Amano *et al.*, 1996). It also phosphorylates myosin light chain (MLC) phosphatase, inhibiting its activity and thereby preventing inactivation of the RLC (Kimura *et al.*, 1996). ROCK also acts to stabilise the actin cytoskeleton via phosphorylation and activation of LIM kinase, which in turn phosphorylates and deactivates cofilin, an actin filament severing protein (Maekawa *et al.*, 1999). mDia1, meanwhile, promotes the formation of new actin filaments via its ability to act as an actin nucleation factor (Watanabe *et al.*, 1999).

RhoA has been demonstrated to play a role in the formation of stress fibres in response to mechanical stretching, where its activity ensures the proper organisation of the

fibres relative to the stretch axis (Kaunas *et al.*, 2005). The modulation of RhoA activity in response to shear forces is also important for mediating endothelial cell alignment in the direction of flow (Tzima *et al.*, 2001). p190GAP, a RhoGAP, plays a role in the initial phase of the shear stress response by supressing RhoA activity and thereby facilitating the re-organisation of the stress fibres (Yang *et al.*, 2011). Two GEFs that are known to activate RhoA, LARG and GEF-H1, are activated by tensile forces applied across the focal adhesions (Guilluy *et al.*, 2011). By facilitating the formation of stress fibres and promoting acto-myosin contractility RhoA can trigger the nuclear localisation of YAP/TAZ, a pair of transcriptional regulators important for the coordination of gene expression in response to mechanical stimulation (Dupont *et al.*, 2011). Signalling at focal adhesions via FAK can also supress the activity of RhoA, promoting adhesion turnover and facilitate migration (Ren *et al.*, 2000). Deleted in liver cancer 1 (DLC1), for example, is a RhoGAP that is recruited to focal adhesions via it's binding to the R8 domain of talin (Haining et al., 2018), where it is activated and inhibits RhoA activity (Li et al., 2011). Unfolding of this domain by tensile forces prevents the binding of DLC1 and thereby inhibits its activity (Haining et al., 2018).

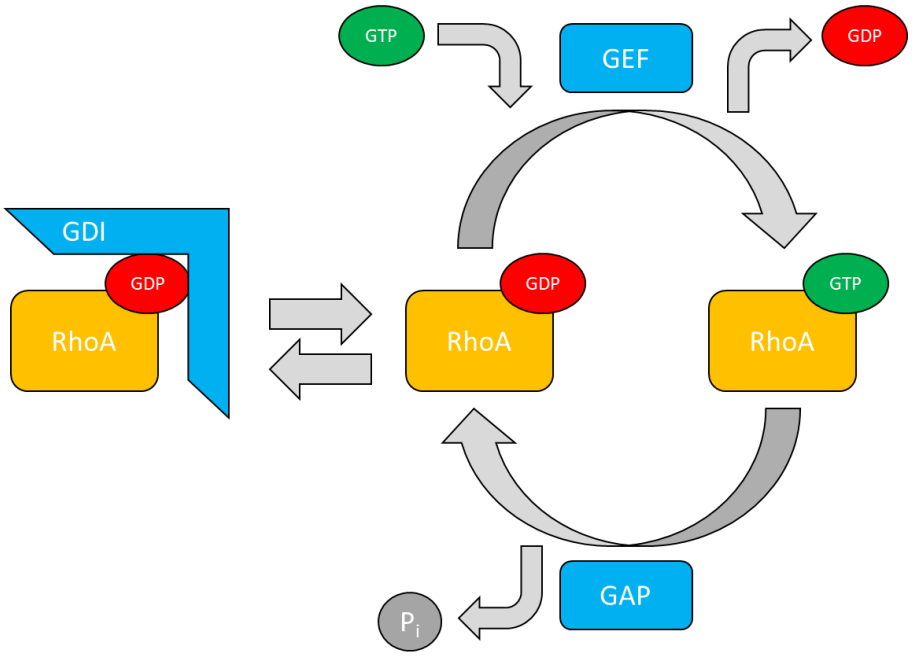

Figure 1.2: Regulation of small GTPase activity via GAPs, GEFs and GDIs. The switch between the inactive (GDP bound) and active (GTP bound) forms of small GTPases can be triggered by GEFs, which promotes the release of GDP and allows GTP to bind (GTP binding preferred due to higher cytosolic concentration). GAPs catalyse GTP hydrolysis, switching the small GTPase from the active to inactive state. GDIs can sequester inactive small GTPase, preventing the release of GDP and activation by GEFs.

1.1.5. The LINC Complex

For forces to be propagated to the nuclear interior, they must first cross the nuclear envelope (NE), a double layered lipid bilayer consisting of an outer nuclear membrane (ONM) and an inner nuclear membrane (INM) separated by a ~40nm gap known as the perinuclear space. The ONM is continuous with the endoplasmic reticulum (ER), with the perinuclear space being an extension of the ER lumen. The INM and ONM are also continuous with one another, with the membrane folding at the nuclear pores to form the two membranes. The role of propagating forces across this membrane is fulfilled by the LInker of Nucleoskeleton and Cytoskeleton (LINC) complex (Cartwright and Karakesisoglou, 2014) (Fig 1.3). This complex consists of two protein families, nesprins and SUNs. Nesprins (nuclear envelope spectrin-repeat proteins), unified by their conserved C-terminal KASH (Klarsicht/ANC-1/Syne Homology) domain, span the ONM and act as the link to the cellular cytoskeleton, with either direct or indirect binding to all three components of the cytoskeleton (Cartwright and Karakesisoglou, 2014; Crisp *et al.*, 2006; Zhang *et al.*, 2001). The SUN proteins, so named because of their conserved C-terminal SUN (Sad1p, UNC-84) domain, span the INM and act to link the nesprins to the nucleoskeleton via interactions with lamin A/C (Cartwright and Karakesisoglou, 2014; Sosa *et al.*, 2012).

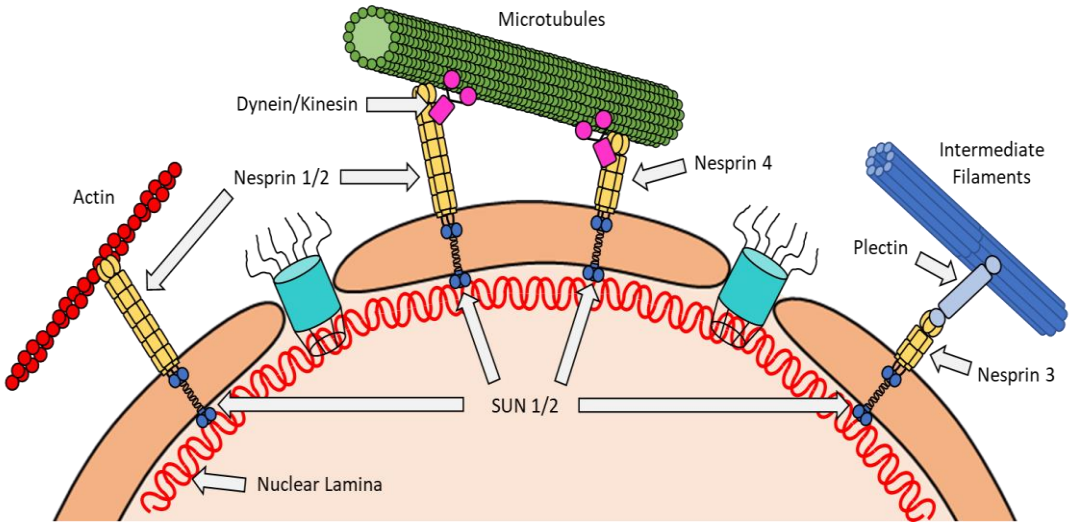

Fig 1.3. Illustration of the LINC complex connections to the cytoskeleton. The nesprins each bind to elements of the cytoskeleton, either directly or indirectly via adaptor proteins, as well as being linked to the nuclear lamina via their interaction with SUN proteins in the perinuclear space.

1.1.5.1 Nesprins

In mammals there are five known nesprins, named nesprin-1, -2, -3, -4 and KASH5, each of which has a variety of alternative-splice variants (Cartwright and Karakesisoglou, 2014). Those variants that form a part of the LINC complex all contain a KASH domain, which consists of a single transmembrane segment followed by a short (~40 residue) sequence that lies within the perinuclear space (Cartwright and Karakesisoglou, 2014). Indeed, it is the presence of the KASH domain that facilitates the localisation of these nesprins to the ONM, where they then form the LINC complex via binding to SUN proteins (Crisp *et al.*, 2005; Padmakumar *et al.*, 2005). The five nesprins each associate with different cytoskeletal components (Fig 1.3). Nesprin-1 and nesprin-2, the largest of the nesprins at ~ 976 kDa and ~ 764 kDa respectively, have N-terminal calponin-homology (CH) domains that facilitate binding to filamentous actin (Warren *et al.*, 2005). Nesprin-3 binds to the actin binding domain of plectin, a linker protein that binds to intermediate filaments (Wilhelmsen *et al.*, 2005). Nesprin-4, meanwhile, binds to kinesin-1 and thereby links to the microtubule cytoskeleton (Roux *et al.*, 2009). Each of these linkages to the cytoskeletal networks plays a role in nuclear function. Nesprin-4's link to microtubules is important for establishing cell polarisation, with the loss of nesprin-4 function leading to a loss of polarised centrosomal positioning and changes in the polarisation of organelles such as the Golgi (Roux *et al.*, 2009). Nesprin-2 can also associate with microtubules via binding sites for dynein and kinesin-1 within its spectrin-repeat domains that form the rod, and this binding plays a similar role in controlling centrosomal/nuclear positioning (Schneider *et al.*, 2011; Zhang *et al.*, 2009; Zhu *et al.*, 2017). Nesprin-3 plays as role in organising the perinuclear cytoskeleton, as well as aiding in nuclear positioning, though its influence in these functions appears dispensable for development in zebra fish and mouse models (Ketema *et al.*, 2013; Morgan *et al.*, 2011; Postel *et al.*, 2011). KASH5 is specific to meiotic cells, where it's interaction with microtubules facilitates the movement of chromosomes during meiosis via interactions with dynein/dynactin and SUN1 (Morimoto *et al.*, 2012). Nesprin-2 anchoring to the actin cytoskeleton mediates the movement of the nucleus via retrograde actin flow during polarisation (Luxton *et al.*, 2010), as well as mediating rearward movement of nuclei in fibroblasts (Zhu *et al.*, 2017). In the context of mechanotransduction, it is nesprin-1/2's binding to the actin cytoskeleton that is

important for receiving and transmitting forces across the NE, due to actin filaments being the prominent vehicle via which internal forces are generated and external forces are propagated. Indeed, it has been shown that nesprin-2 is subject to tensile forces generated within the acto-myosin cytoskeleton whilst at the NE (Arsenovic *et al.*, 2016; Woroniuk *et al.*, 2018).

1.1.5.2. SUN 1/2

At the INM there are two SUN proteins in humans, SUN1 and SUN2 (Cartwright and Karakesisoglou, 2014). These proteins bind to the KASH domain of nesprins within the perinuclear space via their C-terminal SUN domain (Padmakumar *et al.*, 2005), whilst their N-terminus resides within the nucleoplasm and binds to variable components of the nucleoskeleton, including lamin A/C and emerin (Crisp *et al.*, 2006; Haque *et al.*, 2006; Haque *et al.*, 2010). Interestingly, however, lamin A/C is not required for the localisation of SUN1/2 to the INM (Crisp *et al.*, 2006; Haque *et al.*, 2006; Haque *et al.*, 2010). SUN1/2 have two coiled-coil domains, which sit within the perinuclear space and facilitate the formation of a trimer complex (Sosa *et al.*, 2012; Wang *et al.*, 2012). This trimeric SUN complex can then bind to three KASH domains, with the binding pocket being formed at the interface between two SUN domains (Sosa *et al.*, 2012; Wang *et al.*, 2012). The SUN domains of SUN1/2 display no inherent preference in which KASH domains they bind, with both SUN proteins being able to bind the KASH domains of multiple nesprins (Stewart-Hutchinson *et al.*, 2008; Sosa *et al.*, 2012). As a result, it is possible to disrupt the LINC complex via overexpression of a KASH domain, which competitively excludes endogenous nesprins from the complex (Stewart-Hutchinson *et al.*, 2008). However, the incorporation of SUN1/2 into the LINC complex is not equivalent. In HeLa cells it was demonstrated that, under endogenous conditions, the proportion of SUN1 incorporated into LINC complexes was far greater than that of SUN2 (May and Carroll, 2018). These proportions could be reversed via SRF/Mkl1 signalling, and it has also been demonstrated that this change in LINC composition may play a role in regulating RhoA activity (May and Carroll, 2018; Thakar *et al.*, 2017). A link between RhoA regulation and the LINC complex has also been demonstrated in vascular smooth muscle cells (Porter *et al.*, 2020). These results suggest that altering LINC complex compositions may be used as a mechanism for regulating cellular responses.

Disrupting the LINC complex leads to the loss of proper nuclear positioning and cell polarisation/migration, which is linked to the roles that the nesprins play in anchoring the nucleus to the cellular cytoskeleton (Schneider *et al.*, 2011; Zhang *et al.*, 2009; Zhu *et al.*, 2017). LINC complex disruption also results in a decrease in cellular stiffness (Schneider *et al.*, 2011), suggesting that engagement of the cytoskeleton with the NE is critical for maintaining cytoskeletal tension.

1.1.6. The Nuclear Lamina

The LINC complex acts to propagate forces to the chromatin through their mutual connection to the nuclear lamina. The main structural component of the nuclear lamina is a network of type V intermediate filament proteins, termed lamins, that line the inside of the INM. The lamins have a short N-terminal head, a central alpha-helical coiled-coil rod domain and a globular tail-domain (Stuurman *et al.*, 1998). The nuclear lamina in mammalian cells will consist of four lamins; lamin A, C, B1 and B2 (Bridger *et al.*, 2007). These lamins derive from three genes; *LMNA*, which encodes lamin A and lamin C (termed A-type lamins), and *LMNB1* and *LMNB2*, which encode lamin B1 and B2 (termed B-type lamins), respectively (Almendáriz-Palacios *et al.*, 2020). Electron microscopy imaging of *Xenopus* oocytes has suggested that the structure of the nuclear lamina is that of a meshwork, with interconnected lamin fibres running parallel along the inside of the INM (Aebi *et al.*, 1986; Goldberg *et al.*, 2008). Cryo-EM has observed a similar structure in somatic cells, with the lamina being formed of ~3.5nm thick filaments that form a complex meshwork along the INM (Turgay *et al.*, 2017). It has been observed that lamins form separate, but interacting, networks that together form the lamina; with A-type lamins forming one network, and B-type lamins forming another (Shimi *et al.*, 2008; 2015). Lamin filaments are formed from a series of coiled-coil lamin dimers, which then associate head-to-tail with one another to form polar polymers (Stuurman *et al.*, 1998). These dimer polymers then associate with each other to form bundled fibres (Stuurman *et al.*, 1998).

Other components of the nuclear lamina include a group of proteins known as nuclear envelope transmembrane proteins (NETs). This group includes lamina associated peptide (LAP) 1, LAP2a, lamin B receptor (LBR) and emerin (Almendáriz-Palacios *et al.*, 2020). These proteins span the INM and can bind to both the nuclear lamina and

chromatin, thereby anchoring chromatin to the nuclear lamina (Almendáriz-Palacios *et al.*, 2020; Briand and Collas, 2020). These anchorage points are known as lamina associated domains (LADs), and ~ 40% of the genome is organized into ~ 1300 LADs (Almendáriz-Palacios *et al.*, 2020). These LADs act to compartmentalise the chromatin, allowing for the spatial organisation of genes and the regulation of their expression by conversion into heterochromatin (Briand and Collas, 2020). This conversion into heterochromatin is facilitated by the interaction of LAP2β and emerin with HDAC3, which deacetylases histone within the chromatin. By interacting with both HDAC3 and chromatin, LAP2β and emerin act to bring the two into proximity and thus facilitate histone modification of the chromatin (Briand and Collas, 2020).

The lamina is not only a platform for protein/chromatin binding but also plays an active role in determining the mechanical properties of the nucleus. This is partly accomplished through tuning of the levels of lamin A within the nuclear lamina. Indeed, the loss of lamin A from the nuclear lamina greatly diminishes the stiffness of the nucleus, as well as leading to a variety of nuclear deformities (Lammerding *et al.*, 2006). These nuclear mechanical properties are important for maintaining the integrity of the nucleus under force stresses. Cells use differing expression levels of lamin A to adapt their nuclei to the stiffness of the surrounding matrix, increasing its levels in stiffer surroundings to maintain nuclear integrity (Swift *et al.*, 2013). The nuclear lamina also imparts an element of protection against compressive forces onto the nucleus (Dahl *et al.*, 2004). It has also been demonstrated that cells with low levels of lamin A are susceptible to nuclear damage during migration in constrictive environments, though those that survived showed increased migratory potential due to increased malleability of the nucleus (Harada *et al.*, 2014).

1.1.7. The Nuclear Interior

Lamin proteins are not only found within the nuclear lamina at the NE but can also be found within the nuclear interior, forming stable higher order structures (Moir *et al.*, 2000) that facilitate a variety of processes, including DNA replication, repair, transcription, and telomere homeostasis (Dorner *et al.*, 2007; Lambert, 2019; Gonzalo, 2014; Shumaker *et al.*, 2003). Both A and B type lamin act to regulate various proteins involved in double-stranded break (DSB) repair and control the choice between non-

homologous end joining (NHEJ) and homologous recombination (HR) (Lambert, 2019). Just as the nuclear lamina can control the positioning of chromatin through LADs, lamin within the nucleoplasm can bind to chromatin within the nuclear interior (Lund *et al.*, 2015) and act to control the structure and positioning of chromatin within the nucleoplasm (Bera and Sengupta, 2020, Dechat *et al.*, 2008). As such, lamins play a crucial role in the regulation of numerous nuclear activities, which extend beyond its place in the nuclear lamina.

Actin is also found within the nuclear interior and can be found in both monomeric (Gonsior *et al.,* 1999) and filamentous form (Belin *et al.*, 2013); both of which play a role in regulating nuclear activities. The control of actin dynamics and polymerisation within the nuclear interior is orchestrated by ABPs also found within the cytoplasm, including mDia (Baarlink *et al.*, 2013), cofilin (Chhabra and dos Remedios, 2005) and Arp2/3 (Schrank *et al.*, 2018). In its monomeric form, actin can bind to RNA polymerases I (Philimonenko *et al.*, 2004), II (Hofmann *et al.*, 2004) and III (Hu *et al.*, 2004), facilitating gene transcription. It can also control the expression of a variety of genes important for the control of cytoskeletal and focal adhesion organisation (Sharili *et al.*, 2016). Monomeric actin also forms a part of the INO80 complex, providing evidence to suggest that it can influence chromatin remodelling (Kapoor *et al.*, 2013). In its filamentous form, actin plays a role in the repair of both NHEJ and HR DSBs (Lambert, 2019), a role that is partly reliant on the action of nuclear myosins (Caridi *et al.*, 2018). Actin filaments may also have a role in chromatin repositioning, which in turn can control the expression of genes (Chuang *et al.*, 2006; Dundr *et al.*, 2007).

1.2. Force Dependent Responses

Through these cellular components, the cell is capable of transmitting forces from the extracellular environment directly to the nuclear interior. This pathway also allows the cell to generate its own forces, via acto-myosin stress fibre contraction. These forces provide an alternate regulatory stimulus to traditional biochemical signalling, allowing the cell to react to changes in its mechanical environment, such as matrix stiffness.

1.2.1. Gene Expression and Regulation

One way in which forces can regulate cell behaviour is through alteration of gene expression. This is accomplished through two main mechanisms: the targeting of transcription factors to the nucleus, and the manipulation of chromatin structure. One of the best characterised pair of mechanically targeted transcription regulators is YAP/TAZ. These transcriptional coregulators are shuttled between the cytoplasm and the nucleus, a process that can be controlled by a variety of signalling pathways including the Hippo and Wnt pathways (Dupont, 2016). When within the nucleus, YAP/TAZ interact with DNA binding transcription factors, such as TEAD, and thereby activate wide ranging gene expression (Zanconato *et al.*, 2015; Zhao *et al.*, 2008). Nuclear YAP/TAZ localisation can also be controlled by mechanical stimuli, such as increased ECM stiffness and changes in cell shape (Dupont *et al.*, 2011; Elosegui-Artola *et al.*, 2017). The response of YAP/TAZ to such mechanical cues is independent of its regulation by the Hippo pathway and dependant on RhoA activity, acto-myosin contractility, and an intact LINC complex, suggesting that YAP/TAZ localisation can be directly regulated by force propagation to the nucleus (Dupont *et al.*, 2011; Elosegui-Artola *et al.*, 2017). This regulation in response to mechanical cues is not just important for somatic cells but also plays a role in stem cell differentiation. Mesenchymal stem cells can be stimulated to develop into osteogenic, myogenic, or neurogenic cell lineages by growing them on stiff, intermediate, or soft matrices respectively; a process that is dependent on acto-myosin contractility (Engler *et al.*, 2006) and controlled by YAP/TAZ localisation (Dupont *et al.*, 2011). On top of this, YAP/TAZ has been shown to play an important role in cardiovascular development/homeostasis. Nuclear localisation of YAP can be triggered by exposure to laminar shear stresses, a process that is important for the maintenance of the vasculature in developing zebrafish via a mechanism that is again independent of Hippo pathway signalling (Nakajima *et al.*, 2017). These, along with other findings, identify YAP/TAZ as a central hub for transducing a range of mechanical stimuli into a cellular gene expression response, and a source of pathology in a variety of cancers and diseases (Dupont, 2015; Halder *et al.*, 2012; Panciera *et al.*, 2017).

Whilst transcriptional regulators play an important role in mediating gene expression, another mechanism of controlling expression is via changes in chromosome structure.

By altering the 3-D positioning of their chromatin, and bringing certain elements closer together or further away, cells can regulate their gene expression on a global level (Dekker and Mirny, 2016; Lanctôt *et al.*, 2007). The anchoring of chromatin to the nuclear lamina in LADs can also act to control gene expression by altering the structure and spatial organisation of chromatin (Shevelyov and Ulianov, 2019). Given that the LINC complex acts to link the cytoskeleton directly to the nuclear lamina, it stands to reason that forces propagated across the actin cytoskeleton may be directly felt by chromatin and result in altered chromatin structure/positioning. Indeed, the ability of extracellular forces to cause movement within nuclear structures has long been known (Maniotis *et al.*, 1997). Since then, the role that force-mediated chromatin re-arrangement plays in cellular development has been further explored. Traction force microscopy has been used to demonstrate that there is a correlation between the forces a cell exerts upon the substratum via the focal adhesions and the movement of heterochromatin within the nucleus, and that the time scale for these events were similar (~40 sec) (Li *et al.*, 2015). The perinuclear actin cap can mediate the polarisation of transcriptionally active heterochromatin via a re-distribution of lamin A/C towards the apical surface; a process that is dependent upon the contractility of the cap (Kim and Wirtz, 2015). Force application onto HeLa cells results in rapid decompaction of heterochromatin (< 5 sec), which was reversed when force application was ceased (Iyer *et al.*, 2012). Force induced changes in chromatin organisation have also been linked to the regulation of mesenchymal stem cell differentiation, with force application resulting in a rapid increase in chromatin condensation in a process dependent on acto-myosin (Heo *et al.*, 2015; 2016). Taken together, these observations highlight that forces from the extracellular environment can indeed alter chromosomal structure, and that this response allows cells to adapt to force-stimuli in the long term. Recent work has also demonstrated that chromatin stretching induced by extracellular forces can directly activate gene transcription, in a process dependent upon acto-myosin (Tajik *et al.*, 2016). Indeed, the degree of gene activation depended upon the angle of the applied force (relative to cell long axis) opening the possibility that cells may even be sensitive to the direction from which forces are applied (Tajik *et al.*, 2016).

1.2.2. Nuclear Import

Another aspect of nuclear behaviour that is be regulated by force stimuli is nuclear import. The transport of factors into the nucleus is a process mediated by a protein complex known as the nuclear pore complex (NPC). This complex acts as a selective barrier between the cytoplasm and the nucleoplasm, preventing the passive entry of factors larger than 40kDa (Keminer and Peters, 1999). These factors, if they are required to cross the NE, must be actively transported through the NPC; a process that is facilitated by a group of proteins termed importins. These importins act to shuttle proteins across the NPC via their interactions with the luminal FG-nup proteins, which fill the lumen of the NPC and constitute the barrier to passive entry (Lim *et al.*, 2006). However, the exact mechanism via which importin/FG-nup interactions facilitate nuclear import is up for debate (Donnaloja *et al.*, 2019; Kabachinski and Schwartz, 2015; Wente and Rout, 2010). The process of active transport across NPC's is regulated by a gradient of GTP-bound Ran. Ran-GTP accumulates within the nucleus and acts to dissociate incoming importins from their cargo, releasing the cargo within the nucleoplasm (Rexach and Blobel, 1995; Wente and Rout, 2010) (Fig 1.4).

As previously mentioned, certain transcription factors (such as YAP/TAZ) are imported into the nucleus in response to forces applied at the NE. However, there is evidence to suggest that forces at the NE may facilitate the import of a much wider variety of factors via a more general mechanism. Work from Elosegui-Artola *et al.* (2017) demonstrates that direct force application onto the nucleus can trigger an increased nuclear import of YAP even when cells are cultured on soft substrates, a condition in which YAP would usually localise to the cytosol. YAP nuclear localisation could even be triggered in the absence of talin and filamentous actin, suggesting that nuclear localisation of YAP can be triggered solely by force application onto the nucleus. However, the blockage of active nuclear import prevented YAP localisation into the nucleus even under direct force. Elosegui-Artola *et al.* (2017) conclude that force applied to the nucleus, or growth upon stiff substrates, acts to stretch the NE and thereby open the NPC, reducing the strength of the FG-nup barrier within the lumen and making it easier for YAP to pass through the NPC. Whilst this mechanism of force-induced import was only demonstrated for YAP, there is little reason why this model could not be applied to other imported factors of similar size,

providing a general mechanism via which cells can regulate their nuclear import in response to mechanical cues.

It is also possible that forces transmitted to the NE may be able to exert a more direct influence upon the NPC. Donnaloja *et al.* (2019) posit that forces may be felt at the NPC itself through a connection between Nup153, a component of the NPC nuclear basket, and SUN1. This connection would allow a force stimulus to upregulate nuclear import by causing the opening of the nuclear basket, thereby increasing the permeability of the NPC.

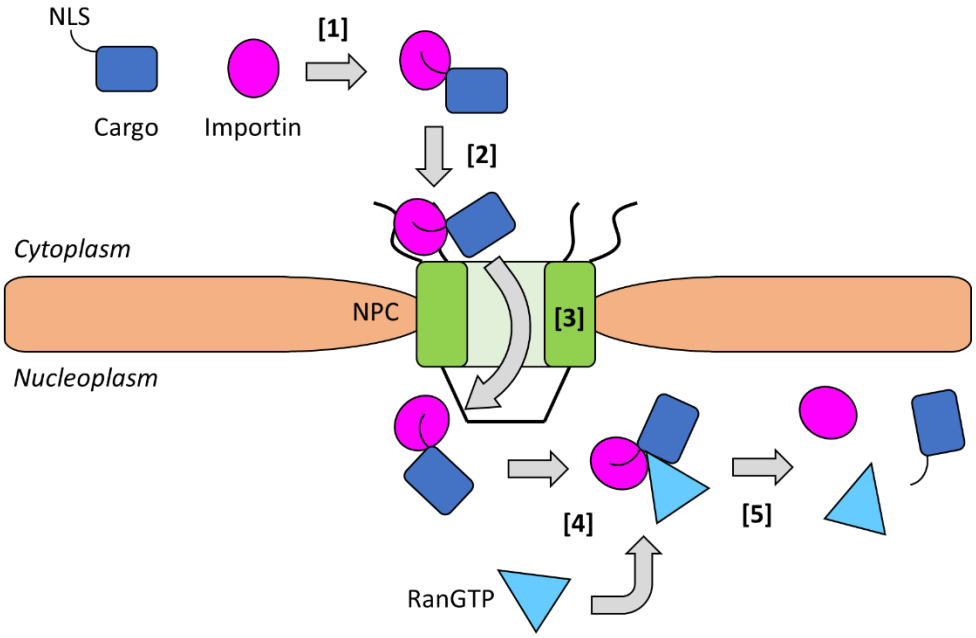

Fig 1.4. Illustration of Ran mediated nuclear import. Import of cargo labelled with a nuclear localisation signal (NLS) is facilitated by binding to an importin (1). Importins will then localise cargo to the nuclear pore complex (NPC) via interactions with the cytoplasmic filaments (2), before translocating cargo through the pore lumen via interactions with luminal FG-Nups (3). Once within the nucleoplasm, RanGTP binds to the complex (4) and disassembles it, releasing the cargo (5).

1.3. Laminopathies

Given the role of the nuclear lamina in mechanotransduction and chromatin organisation, it is understandable that mutations that affect the functioning of lamins can lead to disease. Indeed, there are a range of diverse diseases that result from mutations in lamin genes, which are broadly termed laminopathies. Mutations in *LMNA* are the most numerous cause of these laminopathies, likely due to the essential role of B-type lamins in development and organogenesis making mutations in *LMNB1* and *LMNB2* embryo lethal (Donnaloja *et al.*, 2020). Mutations in *LMNA* can lead to a range of different diseases, including Emery–Dreifuss muscular dystrophy (EDMD), dilated cardiomyopathy (DCM), Dunnigan-type familial partial lipodystrophy (FPLD), Charcot–Marie–Tooth disease type 2B1 and Werner syndrome (Davidson and Lammerding, 2014; Kang *et al.*, 2018; Worman and Bonne, 2007). The mutations in *LMNA* can have numerous different effects on the nuclear lamina, depending on how the mutation affects lamin A function. The mutations that cause EDMD and DCM, for example, impair the ability of lamin A to form head-to-tail polymers, thereby disrupting the higher order assembly of lamins into fibres (Davidson and Lammerding, 2014). This not only reduces nuclear mechanical stability, but also impairs the activity of various signalling pathways and gene regulation that rely on nuclear lamina binding (Davidson and Lammerding, 2014).

1.3.1. Hutchinson Gilford Progeria Syndrome

Hutchinson-Gilford Progeria Syndrome (HGPS) is another example of a laminopathy, termed a pre-mature ageing disease. Those affected by this genetic disease experience symptoms such as a loss of subcutaneous fat, severe growth retardation, hair loss, bone deformations, osteoporosis, delayed dentition, joint stiffness, hip dislocations, sclerodermatous areas, and progressive arteriosclerosis. The average age of death of HGPS patients is 14.6 years, with the primary cause of death being cardiovascular disease (Gordon *et al.*, 2014). On a cellular level, the nucleus displays a highly deformed appearance and shows an increased nuclear stiffness (Dahl *et al.*, 2006). Defective DNA repair and telomere dysfunction also contribute to a decrease in genetic stability (Gonzalo and Kreienkamp, 2015; Liu *et al.*, 2005).

HGPS results from a mutation within the *LMNA* gene; the most reported HGPS causing mutation being a *de novo* single nucleotide substitution at codon 608 (GGC > GGT; G608G) (Eriksson et al., 2003). This promotes activity at a cryptic splicing site in the primary transcript, which results in the loss of 150 nucleotides from exon 11 (Eriksson et al., 2003). These lost nucleotides translate to the loss of 50 amino acids from the immature pre-lamin A protein. Pre-lamin A, in a healthy context, undergoes a series of maturation steps to generate the final lamin-A protein (Fig 1.5) (Sinensky et al., 1994). The final step of this maturation involves the endoproteolytic cleavage of the C-terminal 18 amino acids by the endoprotease Zmpste24, which includes a farnsylated C-terminal cysteine. In the pre-lamin A mutant, the cleavage site for Zmpste24 is lost, resulting in incomplete maturation of pre-lamin A (Eriksson et al., 2003). This is supported by studies of Zmpste24 deficient mice, with *Zmpste24*$^{-/-}$ mice showing symptoms and nuclear phenotypes similar to those seen in HGPS patients (Bergo *et al.*, 2002; Pendás *et al.*, 2002). This uncleavable pre-lamin A, also known as progerin, then accumulates within the nuclear lamina in an age-dependant manner, and results in a progeria phenotype in affected cells (Bridger and Kill, 2004; Goldman et al., 2004).

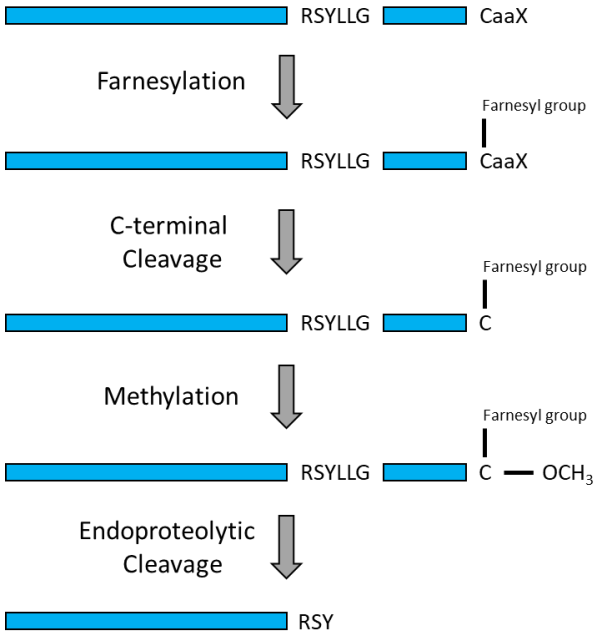

Fig 1.5: Processing steps of pre-lamin A. Pre-lamin A undergoes a series of processing steps, including farnesylation, methylation and cleavage, before yielding the final mature form of lamin A.

1.3.1.1. Mechanotransduction in HGPS

This accumulation of progerin has been shown to alter the response of cells to mechanical cues in several ways. Dahl *et al.* (2006) demonstrated that the nuclear lamina of progerin-expressing cells had drastically altered organisation and mechanical properties and showed a reduced ability to re-organise its structure under mechanical strain. Verstraeten *et al.* (2008) demonstrated that cells from HGPS patients have impaired cell cycle activation stimulated by biomechanical strain, as well as an increased sensitivity to mechanical strain. This increased sensitivity to strain can be linked to the progressive atherosclerosis seen in HGPS patients, since vascular smooth muscle and endothelial cells have been observed to be a primary target of progerin accumulation (McClintock *et al.*, 2006). Booth *et al.* (2015) observed that cells expressing progerin showed a loss of force propagation from the cytoskeleton to the nucleus, and that this results in a loss of chromatin movement in response to stress. HUVEC cells, an endothelial cell line, that expressed progerin were also shown to have reduced chromatin movement in response to shear stress (Booth *et al.*, 2015). Together, these studies suggest that a perturbed response to mechanical strain in progeria expressing vascular cells could be a causative factor that leads to the development of cardiovascular disease in HGPS patients. Indeed, recent work from Kim *et al.* (2018) has shown that vascular damage in the aorta of mice expressing progerin was concentrated at branching points and the inner curvature of the aorta; areas where the vasculature would experience the greatest fluctuations in shear stress (Suo *et al.*, 2007). Smooth muscle cells expressing progerin that were cultured *in vitro* were then shown to have increased levels of cell death when subjected to mechanical stretching. This death was rescued by disruption of the LINC complex, and LINC complex disruption within the mouse model reduced the levels of vascular damage within the aorta (Kim *et al.*, 2018). Autopsies within HGPS patients has also shown a marked depletion of smooth muscle cells within the aorta and other major arteries, which were replaced by fibrous matrix consisting of multiple collagen types; a finding that was attributed to degeneration of the muscle tissue (Stehbens *et al.*, 2001). These findings provide strong evidence for the hypothesis that sensitivity to mechanical force is a major component of the pathology of HGPS.

Broers *et al.* (2004) observed that *LMNA*$^{-/-}$ MEFs had disorganised peri-nuclear cytoskeletal networks, including the loss of actin stress fibres from the nuclear periphery. Chang *et al.* (2019) reported that actin filament coupling to the NE was reduced in HGPS patient fibroblasts, and that there was a reduction in retrograde actin flow speed in NIH-3T3 cells expressing progerin. Lammerding *et al.* (2004) demonstrated that the cytoskeleton of *LMNA*$^{-/-}$ MEFs has altered mechanical properties, being much more malleable to mechanical forces. This could also negatively affect mechanotransduction, as the stiffness of the cytoskeleton would influence the forces that are transmitted to the nucleus. HGPS may also act to the detriment of mechanotransduction through the disruption of the LINC complex. Work on another progeria generating mutant, p.S143F (Kirschner *et al.*, 2005), showed that nesprin-2 localisation to the NE was severely reduced in deformed mutant nuclei (Kandert *et al.*, 2007). SUN1 localisation to the INM was also affected in G608G mutants, though high progerin levels acted to increase SUN1 levels at the INM rather than decrease them, despite a reduction in the binding of SUN1 and SUN2 to progerin relative to wild type lamin A (Haque *et al.*, 2010). Nesprin 2 and SUN2 have also been shown to have reduced mobility within the NE of HGPS fibroblasts (Chang *et al.*, 2019).

1.3.1.2. Nuclear Import Defects

Whilst the classical view of HGPS would suggest that the loss of telomeres and impaired DNA repair are the ultimate cause of the senescence phenotype, recent findings suggest that a loss of nuclear import plays a key role. Larrieu *et al.* (2018) reported nuclear import defects in fibroblasts from HGPS patients, with the levels of cytoplasmic Ran being far higher than in healthy cells. They attribute this defect in import to the mislocalisation of transportin-1, an importin that is responsible for the import of various cargo, including Nup153. Whilst the paper does not draw any links between defective import and mechanotransduction it is interesting to note that Nup153, as previously mentioned, may play a role in mediating force-induced regulation of nuclear import (Donnaloja *et al.*, 2019). It may therefore be possible that the mislocalisation of transportin-1 may also impact the ability of the cell to regulate nuclear import via force stimuli, due to the loss of Nup153 from the NPC. Given that

restoring transportin-1 localisation rescued the HGPS phenotype (Larrieu *et al.*, 2018), it may be that this loss of function plays a significant role in the disease pathology.

1.3.1.3 HGPS as a Model for Physiological Aging

Understanding the mechanistic causes of HGPS is important for the treatment of this disease, however it also has importance as a window into the natural physiological ageing process. Increased levels of wild type lamin A have been shown to re-capitulate some of the phenotypic features of HGPS cells, and imaging of young verses old human diploid fibroblasts have shown that lamin A may be accumulating in the nuclei of older cells (Candelario *et al*., 2008). The presence of progerin itself within the cells of older individuals has also been shown (Cao *et al.*, 2007; McClintock D *et al.*, 2007; Ragnauth *et al.*, 2010; Scaffidi and Misteli, 2006). This accumulation of progerin within ageing cells is due to sporadic use of the cryptic splicing site that is mutated within G608G mutants, resulting in low levels of progerin being expressed in non-HGPS cells (Scaffidi and Misteli, 2006). This low level progerin expression recapitulated the HGPS phenotype in aged cells and resulted in cells reaching senescence at an earlier timepoint (Scaffidi and Misteli, 2006). Low level progerin expression in aged cells also interferes with the mitotic process in a manner similar to that seen in HGPS (Cao *et al.*, 2007). McClintock *et al*. (2007) demonstrate that this accumulation of progerin with age occurs *in vivo*, with skin biopsies from non-HGPS affected individuals showing an increase in the levels of progerin with increasing age in a subset of cells. These studies suggest that the accumulation of progerin occurs not only within HGPS affected cells, but also within healthy cells as part of the physiological ageing process, and that the induction of senescence and aberrations in mitosis resulting from progerin accumulation could contribute to this process. Accumulation of progerin has also been shown to affect vascular smooth muscle cells in a similar manner (Ragnauth *et al.*, 2010), providing a link between progerin accumulation with age and the development of atherosclerosis in older individuals. And whilst progerin expression is only seen in a subset of cells, work by Philip and Dahl (2008) raises the possibility that only a subset of cells need to express progerin in order for the response of the entire cell population to be affected, as progerin expressing HeLa cells perturbed the response of their non-expressing neighbours to shear stresses. This raises the question of whether aberrant

mechanotransduction, as seen in HGPS patients, could also be playing a role in physiological ageing through the subset of cells that accumulate progerin.

1.4. Measuring Forces

Through the combination of focal adhesions, actin cytoskeleton and LINC complex, the cell can respond to mechanical cues both in the short term via biochemical signalling and in the long term through changes in chromatin organisation and gene expression. One of the best ways to study these responses is to observe cells whilst they are experiencing force stimuli. However, cells in their native environment will experience distinct types of force, which based on their directionality and type can be divided into shear, tensile, compressive, and rotatory. Given this range of different force types, the study of mechanotransduction requires different methodologies to probe cell responses to these ranging force types.

1.4.1. Traction Force Microscopy

Traction Force Microscopy (TFM) is a technique commonly used to study the forces applied onto a substrate by a spreading cell, which are termed traction forces (Hur *et al.*, 2020). This method relies upon observation of the movement of a substrate of known mechanical properties to indirectly measure the force that must have been applied to induce that movement (Hur *et al.*, 2020; Polacheck and Chen, 2016). The properties of the substrate can also be altered to observe how the cells responds to a stiffer or softer substrate, or the substrate coated with varying ECM components to assess the effect of cell receptor binding on cell behaviour. The material composition of the substrate, as well as its structure, can vary between different techniques. The first TFM technique to be developed used a deformable material, such as polyacrylamide (PAA), polyethylene glycol (PEG), and polydimethylsiloxane (PDMS), which are known to have linearly elastic and isotropic properties in response to external force (Hur *et al.*, 2020). These materials are embedded with fluorescent beads, whose movement can be tracked. Tracking the movement of these beads can then be used to calculate the traction forces that facilitated that movement (Hur *et al.*, 2020). An alternative approach to this is to use a micropost substrate. This method seeds cells onto an array of micrometer scale posts, whose deformation by the cell can be tracked (Tan *et al.*, 2003). Due to the material properties of these posts being known,

the force needed to bend the posts can be calculated, giving a measurement of the local traction forces (Tan *et al.*, 2003). These techniques are inherently 2-D in their measurements, however recent experimental setups using 3-D collagen and PEG hydrogels have allowed measurement of traction forces in three dimensions (Hur *et al.*, 2020).

1.4.2. Magnetic/Optical Tweezers

Magnetic Twisting/Pulling Cytometry (MTC/MPC) is a more direct method for measuring cellular responses to force. These techniques both rely upon the use of coated ferromagnetic microbeads, which are bound to the surface of the cell to be probed. The bead is then magnetised, and a magnetic field used either to twist the bead (MTC) (Deng *et al.*, 2004) or a magnetic needle used to pull the bead away from the cell surface (MPC) (Overby *et al.*, 2005). These techniques allow for controlled force application onto the cells, applying either a tensile force (in the case of MPC) or a shear force (in the case of MTC). Observations of cell mechanical properties, such as local cell stiffness, can also be gleaned from the delay between the changes in the magnetic field and the movement of the bead. Another method that operates on a similar premise is known as Optical Tweezers (OT). This technique uses focused lasers to trap small objects within their beam, and then manipulate the object by altering the intensity of the beams (Zhang and Liu, 2008). This technique has been used extensively for the manipulation of single molecules (Zhang and Liu, 2008). In the context of mammalian cells, this technique can be used to probe cells via the attachment of dielectric beads to their surface. Whilst the cells themselves are often too large to manipulate directly using OT, the beads are readily moveable; thus, the beads can be used as contact points for cell manipulation, allowing the application of tensile and shear forces.

1.4.3. Atomic Force Microscopy

Atomic Force Microscopy (AFM) is another methodology that allows for the direct manipulation of cells. An atomic force microscope uses a small cantilever as the cell probe. The bending of the cantilever can be measured via changes in the path of a laser that is reflected off the top surface of the cantilever onto a position sensitive detector. By calibrating the cantilever (using its known dimensions), the spring constant of the

cantilever can be calculated, and the deflection of the cantilever as detected by the laser equated to a force. This allows the cell surface to be probed, and the forces being applied to both the cantilever and the cell (being equal and opposite forces) measured. AFM can therefore be used to probe the mechanical properties of a cell; by indenting the surface of the cell with a tip of known shape and dimensions, the elasticity and Young's modulus of the cell can be estimated (Akhremitchev and Walker, 1999) (Fig 1.6). A variety of tip shapes can be used, such as pyramidal or spherical, using adjusted fitting models. This methodology can be extended to provide detailed information about the distribution of mechanical properties, such as stiffness, by taking an array of readings across the cell.

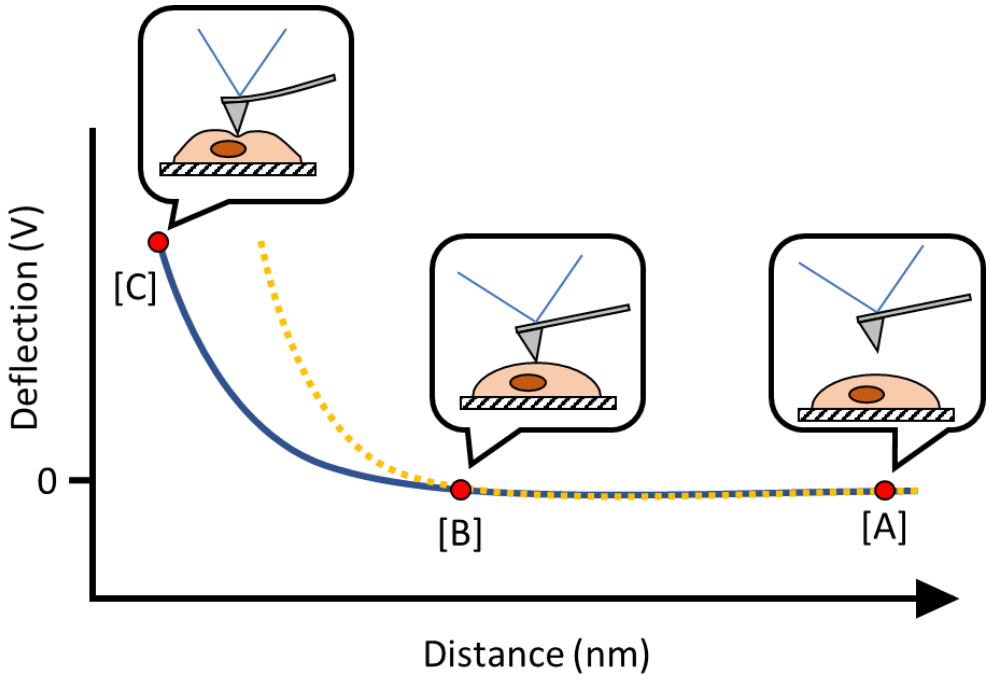

Fig 1.6. Young's modulus measurement using atomic force microscopy (AFM). A tipped cantilever can be used to observe the mechanical properties of a cell using a force(deflection)/distance curve, simplified above. (A) The cantilever approaches the surface of the cell, during which there is no deflection. (B) The cantilever contacts the surface of the cell. From this point, as the probe moves downward the cell will resist this movement, causing the cantilever to bend and increasing the deflection of the laser. (C) The cantilever is now indenting the surface of the cell and has reached a pre-defined deflection threshold. The slope of the curve between (B) and (C) can be determined and, alongside the known parameters of the cantilever, be used to calculate the Young's modulus (stiffness) of the cell. Simplified examples show measurements of a softer (solid blue) and stiffer (dotted yellow) cell.

AFM has also been used to study the adhesive properties of cell receptors involved in transmitting mechanical force, both on a single molecule and whole cell level

(Helenius *et al.*, 2008). On the whole cell level, this is accomplished in one of two ways; either a cell is attached to a functionalised cantilever and then probed against a coated surface, or a coated bead attached to the cantilever is used to probe cells cultured onto a coated surface (Helenius *et al.*, 2008). In either case, the force of adhesion is calculated using the force required to detach the cantilever from the surface, as well observations of the smaller force peaks known as 'steps' and 'jumps' (Helenius *et al.*, 2008).

1.4.4. Tension Biosensors

Whilst these methods provide a range of different ways to study mechanotransduction, they are not truly reflective of *in vivo* conditions. And methods such as AFM may be able to probe the strength and mechanical properties of single molecules, but they cannot determine the extent of forces applied to these molecules when they are fulfilling their function within the cell. To answer these questions, a different type of technique needs to be employed. One such technique, that has seen increasing use in recent years, is to use Förster Resonance Energy Transfer (FRET) based tension biosensors. FRET is a phenomenon that occurs when two fluorophores, one of whom (the donor) has an emission spectrum that overlaps with the excitation spectrum of the other (the acceptor), are in close proximity (<10nm). Excitation of the donor fluorophore causes it to enter an excited state and ordinarily this excitation energy would be released in the form of a longer wavelength photon. However when in proximity to the acceptor fluorophore that energy can instead be transferred from the donor to the acceptor, causing the acceptor to enter an excited state. The acceptor will then release this energy in the form of a photon. The probability of energy transfer is correlated with the distance between the two fluorophores, with the transfer efficiency relating to fluorophore separation being defined by the following equation:

$$\mathbf{E} = \frac{\mathbf{1}}{\mathbf{1} + \left({}^{\mathbf{r}}/_{\mathbf{R^0}}\right)^{\mathbf{6}}}$$

Where *E* is equal to the FRET efficiency, *r* is equal to the donor-to-acceptor separation and R^0 is equal to the distance at which transfer efficiency is 50%. This relation between FRET efficiency and the donor-to-acceptor separation is the core principle

behind the FRET based tension sensors. In these sensors, the fluorophores are joined by an elastic linking region. This elastic linker will unravel and elongate when placed under tensile force, increasing the distance between the two fluorophores. This will, as defined above, reduce the efficiency of FRET. Therefore, by observing changes in the FRET efficiency one can determine whether the sensor is being placed under tensile force. This has been used to study mechanotransduction across single molecules by embedding a tension sensing module within a protein of interest. The first study that developed FRET based tension biosensors was the work of Meng *et al.* (2008), who used a tension sensor (termed stFRET) incorporating the fluorescent proteins Cerulean (donor) and Venus (acceptor) linked by a stable α-helix. They incorporated this biosensor into α-actinin and filamin and showed that in 3T3 cells these proteins are under increased tension at the leading edges of the cell comparative to the lagging edge, which would be expected in migrating cells. This group would later go on to develop another FRET tension sensor (termed sstFRET), using the same fluorescent proteins as stFRET but replacing the stable α-helix with a spectrin repeat (Meng and Sachs, 2011). This sstFRET sensor was then incorporated into α-actinin and used to investigate tensile forces applied across actinin during cell migration and in hypertonic and hypotonic stress. Another FRET tension sensor (termed TSMod) was developed by Grashoff *et al.* (2010), which incorporated the fluorophores mTFP1 (donor) and Venus (acceptor) linked by a 40-amino acid long elastic region derived from the spider silk protein flagelliform. This biosensor was incorporated into the focal adhesion adaptor protein vinculin to discern the role of force upon vinculin function. The observations made indicated that vinculin was subject to tensile force when within the focal adhesions and that that force decreased as the focal adhesion matured and enlarged but did not change as the focal adhesion disassembled (instead remaining at a low level). What's more, by calibrating TSMod (using optical tweezers to apply known tensile force across the sensor) the force being applied across vinculin within the focal adhesions could be estimated. A related tension sensor, which used the same elastic linker but differing fluorescent proteins, has also been used to study tensile forces across talin (Kumar *et al.*, 2016). Using this sensor, they demonstrated that talin is under differential tension between peripheral and central focal adhesions, and that talin was subjected to greater tensile force when cells were cultured on stiffer substrates, suggesting that it could play a role in the mechanosensing pathway that adapts cells to matrix stiffness. The study also investigated the roles of two ABS within

talin, ABS2 and ABS3, as well as the role of vinculin, on these observed changes in forces applied to talin.

A FRET based tension biosensor has also been used to study forces at the LINC complex. Our lab has utilised the TSMod sensor to study tensile forces applied to the LINC complex by inserting the sensor into nesprin-2. This in-house sensor has been used to study the Rac1 GEF STEF and its role in regulating perinuclear actin (Woroniuk *et al.*, 2018). During this study, it was confirmed that nesprin-2 is subject to acto-myosin dependant tensile forces, as a combination of ROCK and myosin light chain kinase (MLCK) inhibitors increased FRET within the sensor.

1.5. Project Aims

Mechanotransduction, the conversion of a force stimulus into a biological response, is critical for a variety of cellular functions; both to fulfil their given roles and to adapt to external force stresses. Many structures and mechanisms exist, both inside and outside of the cell, that facilitate this process. Forces from the cell exterior are transmitted to the cell surface through the ECM, across the plasma membrane by the focal adhesions, and then converted into a biological response either via biochemical signalling or via direct transmission of the force into the nuclear interior. The loss or subversion of this ability has been shown to play a role in a variety of diseases. One disease in which the role of mechanotransduction is less clear is HGPS. There is mounting evidence to suggest that the loss of mechanotransduction in progeria-expressing cells contributes to the deterioration of the vascular tissue seen in HGPS patients, which is the cause of death in the majority of these patients. However, little is known about the changes in cellular phenotype that cause this loss of mechano-sensing. The goal of this project is therefore to investigate the cellular structures involved in the process of mechanotransduction and assess whether there are any changes within these structures that could contribute to the loss of mechano-sensing in progerin-expressing cells. Through this investigation, potential treatment avenues may be identified that could alleviate this phenotype in HGPS patients. This would hopefully mitigate the vascular deterioration of these individuals, and in so doing extend the lifespan of children who suffer from this premature ageing disease.

2. Materials and Methods

2.1. Materials

2.1.1. Antibodies

2.1.1.1 Primary Antibodies

Table 2.1: Primary antibodies for Immunofluorescence/Immunoblotting

Target	Clone	Host Species	Dilution	Application	Supplier (Cat #)
Paxillin	177	Mouse	1:100	IF	BD Biosciences (610569)
Lamin A/C	4C11	Mouse	1:200	IF	Cell Signalling Technology (4777S)
Nup153	Polyclonal	Rabbit	1:200	IF	Bethyl Laboratories (A301-788A)
Ran	20	Mouse	1:200	IF	BD Biosciences (610340)
Phospho-FAK (Tyr397)	Polyclonal	Rabbit	1:1000	WB	Cell Signalling Technology (3283S)
FAK	Polyclonal	Rabbit	1:1000	WB	Invitrogen (AHO0502)
GAPDH	Polyclonal	Rabbit	1:10,000	WB	Proteintech (10494-1-AP)

2.1.1.2. Secondary Antibodies for Immunofluorescence/Immunoblotting

Table 2.2: Secondary antibodies for Immunofluorescence/Immunoblotting

Target	**Conjugate**	**Host Species**	**Dilution**	**Application**	**Supplier (Cat #)**
Mouse IgG	Alexa-Fluor® 488	Goat	1:200	IF	Invitrogen (A11029)
Rabbit IgG	Alexa-Fluor® 488	Goat	1:200	IF	Invitrogen (A11008)
Rabbit IgG	Alexa-Fluor® 594	Donkey	1:200	IF	Invitrogen (A21207)
Mouse IgG	horseradish peroxidase (HRP)	Horse	1:2000	WB	Cell Signalling Technology (7076P2)
Rabbit IgG	horseradish peroxidase (HRP)	Goat	1:2000	WB	Cell Signalling Technology (7074P2)

2.1.1.3. Protein Stains for Immunofluorescence

Acti-Stain^{TM} 670 conjugated phalloidin (Cytoskeleton Inc., Cat #PHDN1) was reconstituted in 500µl of methanol following supplier's instructions and used at a dilution of 1:100.

Hoescht 33342 nucleic acid stain (Thermo Scientific, Cat# H3570) was reconstituted in deionized water following supplier instructions and stored at a concentration of 10mg/ml. The stock was then used at a dilution of 1:2000.

2.1.2. Buffers

PBS(-): Made 1x from Dulbecco's Phosphate Buffered Saline, 10× (Invitrogen, Cat # 70011036). Modified, without calcium chloride and magnesium chloride, liquid, sterile filtered, suitable for cell culture.

50x TAE Buffer: To Make 1L - 242g Tris-Base, 57.1mL Acetic Acid, 100mL 0.5M EDTA.

5x Reducing Sample Buffer: 15% Sodium dodecyl sulfate, 312.5 mM Tris pH 6.8, 50% Glycerol, 16% β-Mercaptoethanol.

RIPA Lysis Buffer: 150 mM NaCl, 1% (v/v) NP-40, 0.5% (w/v) Sodium deoxycholate, 0.1% Sodium dodecyl sulfate, 50 mM Tris pH 8.0.

20x Tris-Buffered Saline (TBS): To make 1L: 127 g Tris-HCl, 23.6 g Tris-Base, 175.2 g NaCl. pH was then adjusted to 7.5.

Tris-Glycine-SDS running buffer: Made 1x from 10x stock of Tris-Glycine buffer (BioRad, Cat # 1610771) diluted in double distilled water, to give final concentrations of 25mM Tris, 192mM glycine, pH 8.3. 0.1% v/v of SDS added.

2.1.3. Reagents

Table 2.3: List of reagents

Reagent	Supplier	Product #
(3-Aminopropyl)trimethoxysilane	Sigma-Aldrich	281778
Agarose	Invitrogen	16500-500
Ammonium persulfate	Sigma-Aldrich	215589
β-Mercaptoethanol	Sigma-Aldrich	M3148
Concanavalin A	Sigma-Aldrich	C2010
DMSO	Fisher Scientific	10080110
Ethanol	Physical Sciences Stores, University of Liverpool	
Fibronectin	Sigma-Aldrich	F1141
Glutaraldehyde	Sigma-Aldrich	G7651
Halt™ Phosphatase Inhibitor Cocktail (100x)	Thermo Scientific	78427
Halt™ Protease Inhibitor Cocktail (100x)	Thermo Scientific	1861279
HEPES Buffer (1M)	Sigma-Aldrich	H0887
Hygromycin B	Invitrogen	10687010
NaCl	Fisher Scientific	S.3160/60
Normal Donkey Serum	Sigma-Aldrich	D9663
NP-40 - Nonidet™ P 40 Substitute	Sigma-Aldrich	74385
Opti-MEM®	Thermo Scientific	11058-021
Paraformaldehyde	Sigma-Aldrich	158127
Ponceau S	Sigma-Aldrich	P7170
ProLong™ Gold Antifade Mountant	Thermo Scientific	P36930
Sodium bicarbonate	Sigma-Aldrich	S5761
Sodium deoxycholate	Sigma-Aldrich	30970
Sodium dodecyl sulfate	Fisher Scientific	S/5200/53

Continued on next page

sulfo-SANPAH	Fisher Scientific	10474005
SYBR® Safe DNA gel stain	Thermo Scientific	S33102
Tetramethylethylenediamine	Sigma-Aldrich	T9281
Tris-base	Fisher Scientific	BP152-1
Tris-HCL	Fisher Scientific	T/P631/53
Triton x-100	Sigma-Aldrich	X100

2.1.4. DNA Constructs

Table 2.4: List of DNA plasmids employed for cloning/transfection

Construct	**Source**	**Comment**
Talin-TS	Addgene (Plasmid # 83376)	
Talin-CS	Addgene (Plasmid # 83377)	
mN2-TS	Zech lab	
GFP-Lamin A	Gift from Iakowos Karakesisoglou	Vector used to clone mRuby2-Lamin A construct
GFP-Δ50 progerin	Gift from Iakowos Karakesisoglou	Vector used to clone mRuby2- Δ50 progerin construct
pOG44	ThermoFisher Scientific	Flp recombinase expression plasmid
pcDNA5/FRT	ThermoFisher Scientific	Expression vector for Flp-In™ System

2.1.5. Primers

Table 2.5: List of primers employed for vector cloning

Name	Description	Sequence
mRuby2-FWD	Forward primer for Cloning of mRuby2 into the pcDNA3.1 backbone. Incorporates KpnI restriction site	AGT ACT GGT ACC CAC CAT GGT GTC TAA GGG CGA A
mRuby2-REV	Reverse primer for Cloning of mRuby2 into the pcDNA3.1 backbone. Incorporates BamHI restriction site.	AGT ACT GGA TCC CTT GTA CAG CTC GTC CAT
LMNA-FWD	Forward primer for Cloning of LMNA/mutants into the pcDNA3.1 backbone. Incorporates EcoRI restriction site.	AGT ACT GAA TTC GAT GGA GAC CCC GTC CCA G
LMNA-REV	Reverse primer for Cloning of LMNA/mutants into the pcDNA3.1 backbone. Incorporates XBaI restriction site.	AGT ACT TCT AGA TTA CAT GAT GCT GCA GTT
LMNA-REV for pcDNA5-FRT	Reverse primer for cloning of LMNA/Δ50 progerin into pcDNA5-FRT vector. Incorporates EcoRV restriction site. Used in conjunction with mRuby2-FWD	ACT CAT GAT ATC TTA CAT GAT GCT GCA GTT

2.2. Methods

2.2.1. Collagen Extraction and Purification

Collagen to be used for the creation of gels was extracted from adolescent rat tails obtained from the Biomedical Service Unit (University of Liverpool) as follows. The tails were obtained and stored at -70ºC until ready for use. The tails were then thawed and washed in 70% ethanol for 1-2 hours before use. Once thawed, a scalpel was used to remove the skin from the tail by making an incision at the proximal end of the tail and cutting down to the distal end, taking care not to penetrate deeper than the skin, and then peeling the skin down the length of the tail. The tendons of the tail were then removed using teethed forceps. Removed tendons were kept in 70% ethanol to prevent drying, and the tail was kept from drying by routinely dipping it in 70% ethanol. The tendons were then dissolved in pre-cooled 0.5M acetic acid by stirring at 4ºC for 48 hours. Once dissolved, the extract was centrifuged at 7500 x g for 30 minutes, discarding the pellet and transferring the supernatant to a pre-cooled beaker. 10% (w/v) NaCl was then added to the supernatant and stirred for 30-60 minutes. The mixture was then centrifuged at 10,000 x g for 30 minutes, discarding the supernatant and re-dissolving the pellet in 0.25M acetic acid by stirring at 4ºC for 24 hours. The collagen was then dialysed using dialysis tubes immersed in 17.5mM acetic acid dissolved in Millipore water, with 6-8 changes (twice daily) in total being made. The dialysed collagen was then centrifuged at 30,000 x g for 1.5 hours, removing the supernatant and placing it in a sterile flask and discarding the pellet.

2.2.2. DNA Cloning

2.2.2.1. Polymerase Chain Reaction

Polymerase chain reaction mixtures were prepared with the following composition: 10µl PrimeStar Max premix (2x) (Takara), 1µl of template DNA (1ng), 1µl of each primer (5pmol), and made up to 20µl with ddH_2O. PCR was then run with the following conditions:

Segment	Cycles	Temperature	Time
1	1	98°C	1 min
2	35	98°C	10 secs
		55°C	5 secs
		72°C	5 sec/kb product length
3	1	72°C	10 min

2.2.2.2. Restriction Digestion

Restriction mixtures were prepared with the following composition: 5µl of 10x CutSmart buffer (New England BioLabs), 1µl (or 10 units) of each restriction enzyme to be used and DNA (volume dependent on experiment), made up to 50µl with ddH_2O. Restriction mixtures were then incubated at 37°C in a temperature-controlled water bath for either 2 hours or overnight. Restriction mixtures were then either heat inactivated by incubation at the appropriate temperature for 20 minutes or run on an agarose gel to separate DNA from the enzymes.

2.2.2.3. Agarose Gel Electrophoresis

Depending on the size of the expected DNA product(s), a 0.8-1.2% (w/v) agarose solution in TAE buffer was heated until agarose dissolved. The solution was then cooled prior to the addition of SYBR® Safe DNA gel stain. The agarose was then poured into a mould and allowed to set. Loading dye was then added to the DNA solution before it was loaded into the agarose gel. The gel was run at a constant voltage of 120V until desired separation had been achieved. DNA was visualised using an E-Gel Imager system (Life Technologies).

2.2.2.4. DNA band excision

The desired DNA band was cut from the agarose gel using a clean scalpel. The DNA was extracted from the excised gel using a Zymoclean™ Gel DNA Recovery Kit (Zymo Research, Cat # D4002) according to the manufacturer's protocol.

2.2.2.5. DNA Ligation

DNA ligation mixtures were prepared with the following composition: 1µl of T4-DNA ligase (New England BioLabs), 2µl of 10x DNA ligase buffer (New England BioLabs), and restricted vector and insert at a weight ratio of 1:3, which was then made up to 20µl with ddH_2O. Mixtures were then incubated at room temperature for 10 minutes. The DNA ligase was then deactivated by incubation at 65°C for 10 minutes.

2.2.2.6. Bacterial Transformation

25µl of α-Select Chemically Competent Cells (Bioline, Cat # BIO-85046) was mixed with either 1µl of mini-prep/maxi-prep DNA or 3µl of ligated DNA and incubated on ice for 20 minutes. The bacteria were then heat shocked by incubation at 42°C for 45 seconds, after which they were incubated on ice for 2 minutes. 500µl of SOC medium (Invitrogen) was added to the bacteria, which was followed by incubation of the bacteria at 37°C in a bacterial shaker incubator for 1 hour. Bacteria were then spread onto agar plates supplemented with the appropriate selection factor and incubated overnight at 37°C. Singular colonies were picked for further growth using a 20µl pipette tip.

2.2.2.7. Mini-prep

Approximately 6 mL of LB Broth containing the appropriate antibiotic was inoculated with bacteria. The bacteria were grown overnight at 37 °C in a bacterial shaker incubator. Bacteria from 3 mL of the culture were pelleted via centrifugation. Plamid DNA was extracted from the bacterial pellets using Zyppy™ Plasmid MiniPrep Kit (Zymo Research) following the manufacturer's protocol.

2.2.2.8. Maxi-prep

Approximately 150ml of LB Broth containing the appropriate antibiotic was inoculated with bacteria. The bacteria were grown overnight at 37°C in a bacterial shaker incubator. Bacteria were then pelleted via centrifugation for 10 minutes at 4000 x g. Plasmid DNA was extracted from the bacterial pellets using a PureLink® HiPure

Plasmid Maxiprep kit (Invitrogen, Cat # K210007) following the manufacturer's protocol.

2.2.3. Cell Culture

MDA-MB-231, NIH-3T3 Flp-In and primary fibroblast cell lines were cultured in a humidified incubator at 37ºC with 5% CO_2 in DMEM GlutaMax media (Thermo Fisher Scientific) supplemented with 10% (MDA/3T3) or 15% (primary fibroblasts) Foetal Bovine Serum (Thermo Fisher Scientific) and 1% Penicillin and Streptomycin (Sigma-Aldrich).

2.2.3.1. Subculture

Cell culture media was aspirated, and the cells washed with sterilised PBS. 3ml of 1x Trypsin solution (Sigma-Aldrich) per 75cm^2 area was then added. The cells were returned to a humidified 37ºC incubator with 5% CO_2 until the majority of cells were seen to detach via brightfield observation. Appropriate cell culture media was then added to the cell suspension at 5-fold volume. A suitable portion of this cell suspension would then be taken and seeded into a fresh culture vessel.

For HGPS cell lines, cells were passaged once confluency reached ~70% of the vessel surface, as judged by brightfield observation. 1/3 of the total cell suspension was used for new continual cultures. Cell populations were sub-cultured up to six times before being replaced. For NIH-3T3 cells lines, cells were passaged once confluency reached ~70% of the vessel surface, as judged by brightfield observation. 1/12 of the total cell suspension was used for new continual cultures. For MDA-MB-231 cells lines, cells were passaged once confluency reached ~80% of the vessel surface, as judged by brightfield observation. 1/6 of the total cell suspension was used for new continual cultures. Cells were observed by brightfield illumination prior to each passage to check for undesirable cell phenotypes, such as changes in cell shape and cell death.

2.2.3.2. Cryopreservation

Cells were detached from the culture surface and suspended following the same protocol as for subculture. The cell suspension was then transferred to an appropriate vessel and centrifuged at 280 x g for 4 minutes. The media was then aspirated, and the cell pellet resuspended in DMSO supplemented with 10% FBS. The suspension was then subdivided into cryo-vials, which were then placed into a freezing container (Mr. Frosty) and placed at -80°C. For long term preservation cryo-vials were transferred to liquid nitrogen storage.

To resurrect, frozen cells were thawed quickly in a temperature-controlled water bath at 37°C. The thawed cell suspension was added to 10-fold volume of culture media before being pelleted via centrifugation at 280 x g for 4 minutes. The cell pellet was re-suspended in culture medium and transferred to a culture vessel.

2.2.3.3. Coating 2-D Surfaces with Extracellular Matrix Proteins

All extracellular matrix proteins were diluted in 4°C sterile PBS. Fibronectin (from bovine plasma) or collagen type I (from rat tails, see previous) was diluted to a concentration of 10μg/ml. Surfaces to be coated were then incubated in the diluted protein and rocked for either 45 minutes at room temperature or overnight at 4°C. The surface was then washed twice with sterile PBS before being used for cell seeding.

2.2.3.4. Embedding Cells within a 3-D Collagen Matrix

Collagen gels were prepared on ice, and all gel constituents were kept on ice throughout gel preparation. Gels consisted of the following components: collagen type I (made to required concentration from stock), 10μg/ml fibronectin, 1x DMEM (from 10x stock), and 0.46M sodium bicarbonate (from 1M stock), made up to required volume with PBS. For fluorescent gels, the collagen mixture was spiked with 2% collagen-AlexaFluor® 647. Gels were pH balanced to ~7.4 using 1M NaOH. Cells were then suspended by trypsinisation and centrifuged at 280 x g for 4 minutes to obtain a cell pellet. The pellet was then resuspended in 500ml of collagen gel before being placed into a 35mm imaging dish. Gels were incubated under standard culture conditions for 1 hour, before appropriate culture media pre-warmed to 37°C was added

to the dish. Gels were then left to continue setting overnight under standard culture conditions.

2.2.3.5. DNA Transfection

For NIH-3T3 Flp-In cells, cells were grown to 80% confluence in a 6-well plate in standard culture conditions. 2µg of plasmid DNA was then mixed with 3µl of Lipofectamine® 2000 reagent (Thermo Fisher Scientific, Cat # 11668027) and made up to 100µl in Opti-MEM™ media. The mixture was then incubated at room temperature for 5 minutes, before being added directly to the wells containing 2ml of appropriate cell culture media. Cells were left under standard culture conditions overnight prior to seeding into 35mm imaging dishes for imaging. For primary fibroblasts, cells were grown to 80% confluence within 35mm imaging dishes and transfected using the same protocol, then left overnight under standard culture conditions. The culture media was then aspirated, the cells washed twice in PBS, and then fresh culture media added. All cells were imaged within 24 hours of transfection.

For MDA-MB-231 cells, cells were grown to 80% confluence in culture conditions as stated previously. The cells were then detached and suspended as for subculture, and the cell number per millilitre counted using a haemocytometer. A volume of cell suspension equivalent to ~2 x 10^6 cells was then centrifuged at 280 x g for 4 minutes to obtain a cell pellet. The pellet was then washed with PBS and centrifuged again, before being transfected with 2µg of plasmid DNA. Transfection was carried out using Nucleofector™ kit V (Lonza, Cat # VVCA-1003), following the manufacturer's protocol. Cells were seeded into a 10cm culture dish and left to recover under cell culture conditions for a minimum of four hours prior to use.

2.2.3.6. Clonal Selection

NIH-3T3 Flp-In cells were transfected following the previously stated protocol, except that the cells were grown to confluence in a 6cm culture dish. Transfection was carried out with the appropriate FRT construct and the pOG44 construct at a weight ratio of 1:10, to a total DNA weight of 1µg. One dish was transfected with an unmodified FRT construct as a negative control. Transfected cells were then left overnight under standard culture conditions. The culture media was substituted for fresh culture media

the next day, and then the cells were transferred into a 10cm culture dish the day after. 3 hours after passage, hygromycin was added to the culture media to a final concentration of 200μg/ml. The culture media was then exchanged for fresh media containing 200μg/ml hygromycin every two days. Once cell colonies had developed, and the negative control showed complete cell death, the clones were detached and seeded into a fresh culture vessel for further passage.

2.2.3.8. Drug Treatment

Lonafarnib

For lonafarnib treatment, cells were passaged into 6-well plates one day prior to the first treatment. The cells were then treated with standard culture medium supplemented with 2μM Lonafarnib (or equivalent volume of vehicle control) for three days, the medium being refreshed with 2μM lonafarnib media daily. Prior to the third treatment (start of day 3/3), cells were passaged onto coverslips coated with 10μg/ml fibronectin, left to settle for 1 hour, and then treated with lonafarnib. At the end of the third day, the cells were fixed and stained following the standard protocol. A lonafarnib stock was prepared fresh from desiccated powder (Tocris, Cat # 6265), at a concentration of 2mM, prior to the first treatment of each experiment. That stock was then used only for the three treatments of that experiment to avoid drug degradation and stored at -20ºC between uses.

Y-27632

For Y-27632 treatment, cells were seeded onto coverslips coated with 10μg/ml fibronectin one day prior to the first treatment. The cells were then treated with standard culture medium supplemented with 10μM Y-27632 (or equivalent volume of vehicle control) for two days, the medium being refreshed with 10μM Y-27632 media daily. At the end of the second day, the cells were fixed and stained following the standard protocol.

For Y-27632/ML-7 combination treatment, cells embedded in collagen gels were treated with standard culture medium supplemented with 20μM Y-27632 and 20μM ML-7 (or equivalent total volume of vehicle control) 2 hours prior to imaging.

2.2.4. Western Blotting

2.2.4.1. Cell Lysis

The cell culture vessel was placed on ice, and all reagents were pre-cooled on ice. The cells were washed with PBS twice, with care being taken to remove as much PBS as possible from the second wash. RIPA lysis buffer (supplemented with 1x HALT protease and phosphatase inhibitor) was then added to the cells, and the surface scraped with a cell scraper (Greiner Bio-One, Cat # 541070). The lysate was then transferred to a pre-cooled 1.5ml Eppendorf tube and incubated on ice for 10 minutes. The lysates were then centrifuged at 15,000 x g for 10 minutes at 4°C, before the supernatant was transferred to a fresh pre-cooled 1.5ml Eppendorf tube. Samples were then either processed or stored at -80°C for future use.

2.2.4.2. Protein Concentration Assessment

Protein concentration was calculated using a Precision Red Advanced Protein Assay. 990µl of Precision Red reagent (Cytoskeleton, Cat # ADV02-A) was mixed with 10µl of cell lysate in a plastic cuvette and incubated at room temperature for 1-2 minutes. The cuvette was then loaded into a spectrophotometer and the absorbance of the sample at 600nm measured. This absorbance value was then used to calculate the concentration of protein within the lysate in µg/ml.

2.2.4.3. Polyacrylamide gel electrophoresis

All samples within a singular experiment used the same protein concentration (25-50µg typically) and total volume. Appropriate volume of cell lysate was mixed with 1x reducing sample buffer and made up to total volume with RIPA buffer. Protein denaturation was then conducted by heating the samples at 95ºC for 5 minutes. Pre-cast gels (4-20% Mini-PROTEAN TGX Stain-Free Precast Gels, BioRad, Cat # 4568094) were used to separate proteins, run using a Mini-PROTEAN Tetra Vertical Electrophoresis Cell (BioRad) with Tris-Glycine-SDS running buffer. Electrophoresis was conducted at 120V for 30-45 minutes.

2.2.4.4. Protein Transfer

Proteins were transferred onto Amersham™ Protran® Premium Western blotting nitrocellulose membrane (pore size 0.45 µm) (Merck, Cat # GE10600003) using a Trans-Blot Turbo Transfer System (BioRad). Proteins were transferred for 11 minutes at a constant 2.5Amp in Trans-Blot Turbo transfer buffer (BioRad)

2.2.4.5. Protein Visualisation

The transfer membrane was checked for successful protein transfer using a Ponceau stain. The membrane would then be rinsed three times in TBS-T buffer, before blocking with 5% milk (made with TBS-T) for 1 hour with rocking. The membrane would then be rinsed three times in TBS-T on a rocker and placed within a 50ml centrifuge tube. 4ml of primary antibody at desired dilution in 5% milk would then be added, and the membrane rolled at room temperature for 2 hours. The membrane would then be removed from the tube, rinsed three times with TBS-T on a rocker, before being placed within a fresh 50ml centrifuge tube. 4ml of secondary antibody at desired dilution in 5% milk would then be added, and the membrane rolled at room temperature for 1 hour, or at 4°C overnight. For chemiluminescence-based detection, membranes were developed using Clarity Western ECL Substrate (BioRad, Cat # 1705061) according to manufacturer's instructions and imaged using a Chemidoc™ Touch (BioRad) imaging system.

2.2.5. Immunofluorescence

2.2.5.1. Coverslip Preparation

25mm coverslips (N1.5) were incubated in 1M HCl at 60°C for 4 hours, with occasional agitation. They were then vigorously washed in distilled water twice, and twice in double distilled water. The coverslips were then rinsed with 70% ethanol, before being dried between two sheets of whatman filter paper. Dried coverslips were stored in a clean, sealed container until use.

2.2.5.2. Coverslip Fixation and Staining

Culture medium was aspirated, and then the samples were incubated in 4% paraformaldehyde (w/v) solution (in PBS) at room temperature for 15 minutes. The PFA was then removed, the sample washed twice with PBS, and then permeabilised via treatment with 0.1% Triton X-100 solution (v/v) (in PBS) at room temperature for 15 minutes. The sample was then washed twice in PBS, and then blocked with 5% donkey serum for a minimum of 45 minutes at room temperature. Excess blocking solution was then removed, and the coverslip was inverted onto a 20µl drop of primary antibody solution and incubated for 1 hour at room temperature under humid conditions. The sample was washed three times with PBS, and then incubated with secondary antibody solution for 1 hour using the same procedure as for the primary. If phalloidin and/or Hoechst 33342 were used, they were included at this stage. The sample was washed three times with PBS, excess PBS was removed, and then the coverslips were mounted onto glass slides with ProLong™ Gold Antifade Mountant.

2.2.6. Light Microscopy

2.2.6.1. FRET Probe Imaging

Imaging of cells for determination of FRET was carried out on a Marianas spinning disk confocal microscope (Intelligent Imaging Innovations, Inc), with images captured using an EMCCD camera (Evolve, Photometrics). For imaging of the mN2-TS, three to five channels were captured; one channel detecting a 447-517nm range under a 445nm excitement with a 1000ms exposure (denoted ‘Donor’ channel), another detecting a 515-569nm range under 514nm excitement with a 200ms exposure (denoted ‘Acceptor’ channel), a third detecting a 515-569nm range under 445nm excitement with a 1000ms exposure (denoted ‘Transfer’ channel), and a further two channels consisting of a brightfield illumination of 100ms and a far-red channel (652-732nm range under 647nm excitement with a exposure of 500ms) for imaging fluorescent collagen if required. For singular images, the laser power was set to 100%; for time-lapse images, the power was set to 20%. Images were taken once every minute for time-lapse images. Single images were captured using a αPlan-Apochromat 63x/1.4NA oil objective lens (Zeiss), whilst timelapses were captured using a αPlan-Apochromat 40x/1.4NA oil objective lens (Zeiss).

For imaging of the Talin-TS, four channels were captured: one channel detecting a 495-555nm range under a 488nm excitement with a 100ms exposure (denoted 'Donor' channel), another detecting a 544-690nm range under 561nm excitement with a 100ms exposure (denoted 'Acceptor' channel), a third detecting a 544-690nm range under 488nm excitement with a 100ms exposure (denoted 'Transfer' channel), and a fourth channel consisting of a brightfield illumination of 100ms exposure. All images were captured using a αPlan-Apochromat 40x/1.4NA oil objective lens (Zeiss).

2.2.6.2. Laser Scanning Confocal Microscopy

All immunofluorescence images were captured using either a Zeiss LSM800 with a 63x/1.4NA oil objective, or a Zeiss LSM900 with either a 63x/1.4NA oil objective or a 40x/0.95NA water objective. For each fluorophore, the appropriate laser line chosen from 405nm, 488nm, 561nm and 647nm was selected, and a suitable detection range and channel set up was defined to prevent bleed-through between channels.

For nuclear morphology categorisation, tile scan images were taken using a 40x/0.95NA water objective, with a 5x5 grid of images being captured. Image overlap was set at 10%, and stitching conducted using Hoechst 33342 channel as the reference.

2.2.6.3. Spinning Disk Confocal Microscopy

All live cell imaging was captured using a Marianas spinning disk confocal microscope (Intelligent Imaging Innovations, Inc) with images captured using a CMOS camera (FLASH4.0 or ORCA-Fusion, Hamamatsu). For each fluorophore, the appropriate laser line chosen from 405nm, 488nm, 561nm and 647nm was selected, with a suitable emission band pass filter being selected (see table 2.6).

Table 2.6: Filters used for spinning disk confocal microscopy

Laser Emission	Filter Centre	Band Width	Product code
405	445	25	(FF01-445/45-25)
488	525	30	(FF01-525/30-25)
561	617	73	(FF01-617/73-25)
647	647	40	(FF01-692/40-25)

2.2.7. Traction Force Microscopy

2.2.7.1. Poly(acrylic acid) (PAA) Hydrogel Preparation

250µl of 0.1M NaOH solution was added to a 13mm glass-bottomed imaging dish (MatTek) and incubated at room temperature for 5 minutes. The NaOH was removed, and 200µl of (3-Aminopropyl)trimethoxysilane (APES) was added for 2½ minutes. After this time, PBS was added to the APES to halt the reaction, and then the APES was removed. The dishes were then washed twice in MilliQ water, before adding 200µl of 0.5% glutaraldehyde and incubating for 30 minutes. Dishes were washed twice with MilliQ water before being dried using an air duster.

Protogel (30% solution at 37.5:1 ratio of acrylamide:bis-acrylamide) (Geneflow) was diluted with PBS to a concentration of 9% (v/v). Fluorescent beads with an excitation wavelength of 488nm (Molecular Probes, Cat # F8811) were then mixed with the protogel solution at a ratio of 1:25 by vortex for ~2 minutes. The solution was then de-gassed at 400-500mbar for 15 minutes. Tetramethylethylenediamine (TEMED) and 10% ammonium persulfate (APS) were then added and mixed via pipetting, with care being taken to prevent the formation of air bubbles. 6µl of this solution was then added to each of the pre-prepared imaging dishes and then covered with a clean 13mm glass coverslip. The dish was then turned upside down and left to set for 15-30 minutes. The dishes were then righted, and the glass coverslip removed using forceps. The gel was washed twice with PBS and stored at 4ºC, immersed in PBS, until use.

2.2.7.2. PAA Hydrogel Functionalisation and Coating

A 0.2mg/ml solution of sulfo-SANPAH was prepared fresh, and 150µl of this was added to the PAA gels. The gels were then exposed to a 365nm UV light source for 10 minutes, before being rinsed three times with 50mM HEPES solution (pH 8.5). 10µg/ml fibronectin diluted in HEPES solution was added to the functionalised gels and incubated overnight at 4ºC. Following this, the gels were washed twice with PBS and sterilised by UV exposure for 20 minutes in a tissue culture flow hood.

2.2.7.3. Cell Seeding and Imaging

HGPS and healthy cell lines were seeded onto the coated PAA gels ~24 hours prior to imaging and immediately after dish disinfection. The gels were imaged using a Marianas spinning disk confocal microscope (Intelligent Imaging Innovations, Inc) and captured using a CMOS camera (ORCA-Fusion, Hamamatsu). Cells were identified by brightfield illumination, and a z-stack encompassing the gel (as indicated by the presence of fluorescent beads) captured under 488nm laser illumination. After initial acquisition, the dishes were treated with SDS to remove the cells from the gel and then re-imaged at the same positions. Images were captured using a αPlan-Apochromat 63x/1.4NA oil objective lens (Zeiss).

2.2.8. Atomic Force Microscopy

All atomic force microscopy was conducted using a JPK Nanowizard 3 (JPK BioAFM, Bruker) coupled to a Zeiss LSM880 confocal microscope. Correlative brightfield images were captured using a 40x/0.95NA air objective and aligned to AFM images using the JPK software's in-built optical image calibration function.

2.2.8.1. Cantilever and Surface Functionalisation

AFM cantilevers (Arrow^{TM} TL-2, NanoWorld) were functionalised with concanavalin A/fibronectin using the following protocol. Cantilevers were first placed within an oxygen plasma cleaner, operated at maximum power and 0.3mbar for two minutes, to clean and activate the surface of the cantilevers. Following this, cantilevers were immersed in a 2mg/ml concanavalin A and 1mg/ml fibronectin solution dissolved in PBS for one hour. Then, cantilevers were washed three times in PBS before being stored in PBS at 4ºC. Functionalised cantilevers were used no later than one week after coating. 24mm coverslips that were to act as the probed surface were functionalised as follows. The coverslips were placed into the well of a 6-well plate and washed with PBS. They were then immersed in a solution of 10µg/ml fibronectin at room temperature for one hour. They were then washed twice with PBS, before being stored in PBS at 4ºC until mounting. Coverslips were used within two days of functionalisation.

2.2.8.2. Cell Fishing and Stretching

Functionalised coverslips were mounted into a BioCell™ sample holder (JPK Instruments, Bruker), and 400µl of standard culture media supplemented with 20mM HEPES added into the holder. The holder was then mounted onto the CellHesion® stage for the Nanowizard 3, and the BioCell™ set to heat to a temperature of 37ºC. A functionalised cantilever was then mounted and lowered into the media. Cantilever calibration was then conducted using the contact-free thermal noise method provided by JPKs software package. Once the cantilever was calibrated, the coverslip surface was approached. After approach, a cell suspension was added into the holder. The extreme end of the cantilever was then moved above a candidate cell, and the cell approached. This was done repeatedly until the cell was seen to attach to the cantilever by brightfield observation. Once attached, the cell was retracted from the surface 100µm and left to settle for 15-30 minutes before being used to probe the surface. To stretch the cell, the attached cell was first brought into contact with the surface and left to adhere for 30 minutes. Once adhered, the cantilever was then raised/lowered at a speed of 0.5µm/s to the desired height using the 'Cell Capture' functionality of the CellHesion® module software.

2.2.8.3. Stiffness Measurement and Mapping

Stiffness measurements were conducted via JPKs QI™ mode to simultaneously gather data on sample height and young's modulus, using a MLCT-C probe (Bruker). Cantilever spring constant was calculated before each experiment, under experimental conditions, using the contact-based method provided by JPKs software package. All live cell experiments were conducted with appropriate culture media, supplemented with 25mM HEPES buffer, at 37°C without CO_2. Each sample was imaged for a maximum of 2 hours to avoid detrimental effects upon the cells influencing readings. QI™ mode imaging was conducted with a force setpoint of 0.5nN, and force curves were gathered over a z-length of 1-1.5µm and at a constant speed of 30µm/s. All images were set to a scan size of 128x128 readings, covering a square area of 40x40µm.

2.2.9. Image Analysis

2.2.9.1. FRET Index Calculation

Analysis of FRET images was conducted using the SlideBook 6 software (Intelligent Imaging Innovations, Inc) including the FRET module. Bleedthrough values for mTFP1 were determined using the 'Compute FRET Bleedthrough' functionality of the FRET module, imputing images of a mN2-TFP control construct taken under the same conditions as the mN2-TS experimental images. To analyse FRET readings at the NE, and exclude non-specific readings, a mask was manually drawn over the NE signal (as visualised by the Acceptor channel). All measurements and bleedthrough calculations were then conducted using pixels within the mask, subtracting for background intensity that was calculated from a region outside of the cell that showed no specific fluorescent signal.

2.2.9.2. Focal Adhesion Quantification

Analysis of immunofluorescence images was conducted using the FIJI image analysis software (Schindelin *et al.*, 2012). The image channel containing the focal adhesion marker (paxillin) was processed to generate adhesion ROIs as follows. The image was subtracted for background using the rolling ball method with a radius of 50. A Difference of Gaussians filter (GDSC ImageJ Toolsets) was then applied, with sigma radii of 10 and 3 for the first and second images respectively. The processed image was then used to generate an intensity threshold binary image, which was then used for object identification to define ROIs. For object identification, a minimum size threshold of 0.6μm^2 was used. These ROIs were then confirmed by visual observation and used to quantify adhesion area and shape factor (fit ellipse).

2.2.9.3. Young's Modulus Calculation

Analysis of force-distance curves was conducted using the JPKSPM data processing software (JPK Instruments, Bruker). The extension curve of the force-distance graph was used to calculate the surface stiffness as follows. The curve offset was first calculated in the Y and X axis and the trace shifted accordingly. The tip height was then corrected for cantilever bending by subtracting the cantilever deflection in units

of length from the piezo height. The corrected height curve was then fitted using a Hertz/Sneddon fit for a quadratic pyramid indenter, assuming a surface Poisson ratio of 0.5.

2.2.9.4. Traction Force Calculation

Analysis of PAA hydrogel images was conducted using the ImageJ macros developed by Martiel *et al.* (2015), following the protocol laid out within the supplementary information of that publication. Prior to analysis, gel images (taken as z-stacks) were maximum projected to generate a single plane image, using z-slices where the beads were in focus. Images before and after SDS addition, which were taken separately, were then combined into a single two channel image for each position. These images were then used to calculate the traction force following the protocol. In brief, the images were first aligned using the before image as a reference. The aligned images were then cropped to remove the image edges. The plugin then calculates the displacement vectors and force vectors and generates a false colour image displaying the vectors. The force measurements for the full image were averaged to yield the average traction force per image.

2.2.10. Data Presentation

The data within this work is presented in such a way as to make singular cell measurements the experimental unit. This was done to give a more comprehensive illustration of the variability within the measured cell populations. However, this method of data presentation requires that the distribution of the data be consistent between individual experimental repeats to convey an accurate overall result. To demonstrate the level of consistency within the data presented in this work, the experimental values have been plotted for an example experiment (data presented in Fig 3.11) (Fig 2.1).

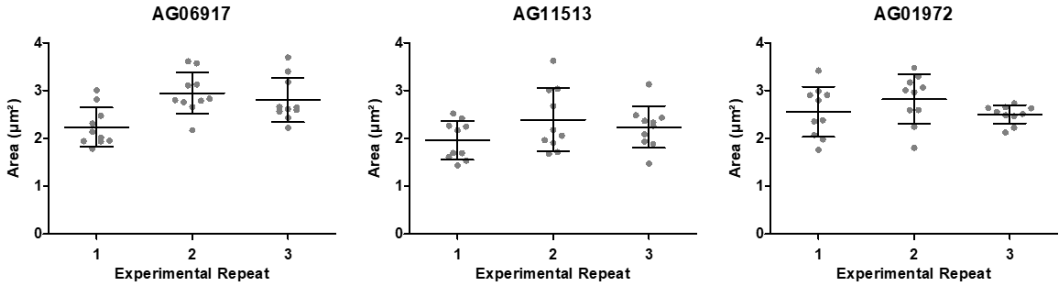

Fig 2.1. Plot of individual experimental repeats from example data sets. Individual experimental results for the measurement of average focal adhesion area in HGPS cell lines (Fig 3.11). Mean ± SD plotted.

3. Assessing Tension Across the Mechanotransduction Pathway in HGPS

3.1. Introduction

When considering the mechanotransduction pathway, two key junctions at which tensile forces are transmitted are the focal adhesion complex and the LINC complex, which either transmits forces to or receives forces from the actin cytoskeleton respectively (Arsenovic *et al.*, 2016; Kumar *et al.*, 2016). Therefore, if one wishes to assess the ability of the cell to transmit forces from the extracellular environment to the nuclear interior, these structures can be key barometers in gauging force transmission along the pathway. One way in which tensile forces across proteins can be assessed *in situ* is to use FRET based tension biosensors. These sensors employ two fluorophores whose excitation and emission spectrums overlap and places them either side of an elastic linker sequence. Such sensors have been used previously to measure tensile forces across focal adhesion proteins such as vinculin and talin (Grashoff *et al.*, 2010; Kumar *et al.*, 2016).

The nesprin-2 based tension biosensor that will be used within this work (termed mN2-TS) (Woroniuk *et al.*, 2018) was developed within the lab and is based upon the previously published tension sensing module TSMod (Grashoff *et al.*, 2010) (Fig 3.1A). The sensor was placed between the two halves of mini-nesprin-2, a truncated form of nesprin-2 (Ostlund *et al.*, 2009) that has been widely used to study nesprin-2 function. This truncated form of nesprin-2 lacks the majority of the spectrin repeat domains found within the rod of full length nesprin-2 (Fig 3.1A), thus losing many of the full-length protein's binding sites. However, the construct still possesses nesprin-2's actin binding CH domain, allowing it to engage with filamentous actin. When subjected to tensile forces, the elastic region within the sensor module will be stretched, separating the two fluorophores (Fig 3.1B). This separation of the fluorophores will reduce the efficiency of photon transfer between the two, which is observable as a reduction in the measured FRET index (Fig 3.1B). As such, an increase in tensile force at the LINC complex (where the mN2-TS is situated) will result in a lower measured FRET index at the NE. A version of the sensor that lacks the CH

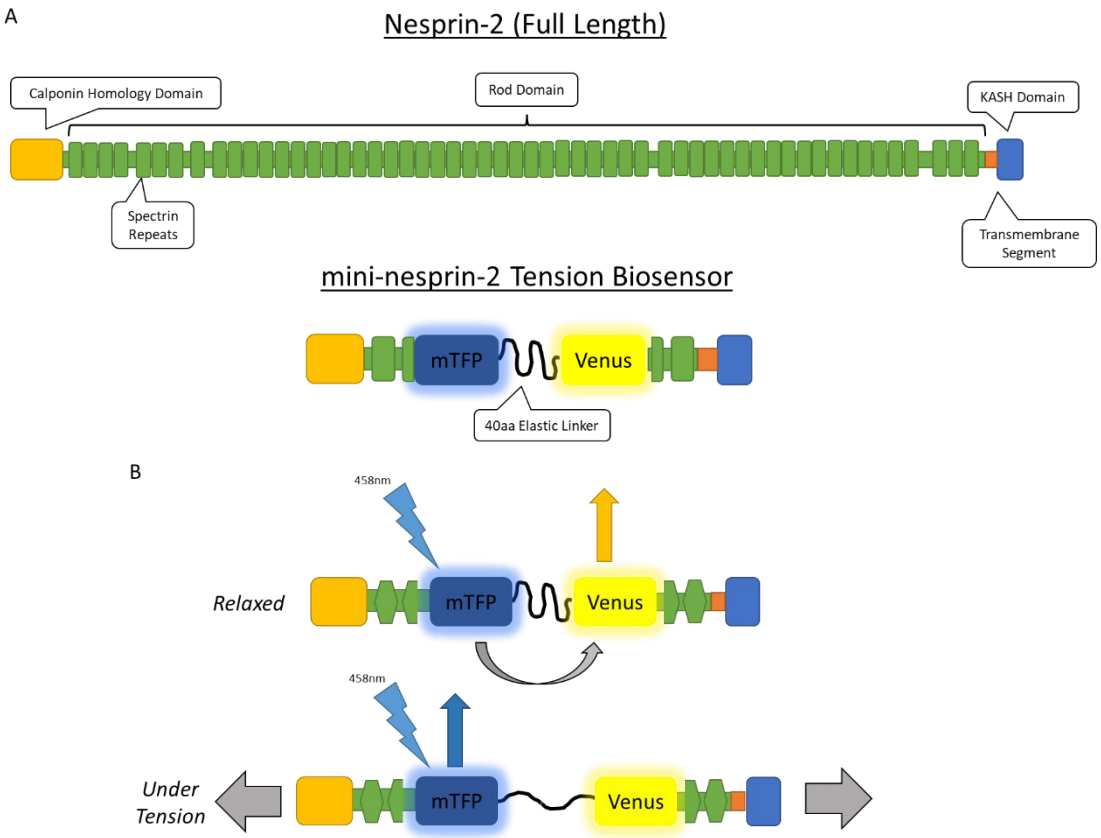

Figure 3.1. Schematic of FRET based tension biosensor, mN2-TS. (A) The full length nesprin 2 consists of an N-terminal calponin homology domain, a rod domain consisting of 56 spectrin repeats, and a C-terminal KASH domain. To study tensile forces applied at the NE the FRET based mini-nesprin-2 tension biosensor (mN2-TS) was developed, consisting of the terminal ends of the full-length protein placed either side of the TSMod tension biosensor. (B) When in a relaxed state, photon transfer between the donor (mTFP) and acceptor (mVenus) fluorophores is at its highest, resulting in increased acceptor fluorescence on donor excitation. When the sensor is placed under tensile stress, the elastic region extends, separating the two fluorophores. This reduces the efficiency of photon transfer, resulting in reduced FRET and increased direct photon emission by the donor fluorophore.

domain was also developed to act as a negative control, as this version of the sensor will not be able to experience any tensile force due to its inability to bind actin.

Employing the mN2-TS and talin-TS (Kumar *et al.*, 2016) together provides oversight of the forces being transmitted along the mechotransduction pathway. One context in which this could prove valuable is within the premature ageing disease HGPS. Cells expressing a mutant form of lamin A, termed progerin, have been demonstrated to be particularly sensitive to mechanical stresses, potentially contributing to the pathology and death of HGPS patients via atherosclerosis in mechanically damaged vascular

tissues (Kim *et al.*, 2018; McClintock *et al.*, 2006). The movement of chromatin within the nucleus in response to shear stress is also reduced in HGPS cells (Booth *et al.*, 2015), raising the possibility that there is a change in the tensile forces that are transmitted to the NE. This raises the important question of why these tissues become sensitive to mechanical stresses, and where within the mechanotransduction pathway between the focal adhesions and the nuclear interior are force stimuli diminished?

3.2. Chapter Aims

There is mounting evidence that sensitivity to force stresses plays a pivotal role in the pathology of HGPS. As such, understanding how the various components of the mechanotransduction pathway are affected by progerin expression in cells is important for our understanding of the disease and its effects. As such, this project aimed to provide an overarching assessment of mechanotransduction from the ECM to the nucleus in HGPS, thereby building up an overall picture of the changes in the mechanotransduction pathway for future assessment and exploration. In this chapter, the aims were to decide upon a model system and develop the protocols necessary to assess mechanotransduction within that chosen model.

3.3. Results

3.3.1. Establishment of mN2-TS as a Dynamic Measure of Force Application onto the Nuclear Envelope

To test the use of the mN2-TS, I decided to investigate the effects of matrix dimensionality on nuclear tension. Initial experiments were conducted using the triple negative breast cancer cell line MDA-MB-231 (Cailleau *et al.*, 1978), which are a highly invasive and metastatic cell line. These MDA-MB-231 cells were transfected via electroporation with the mN2-TS construct, and then cultured on either plastic coated with 10μg/ml collagen, or suspended in a collagen I matrix of either 0.5mg/ml or 2mg/ml concentration (Fig 3.2A, B). The concentrations of the collagen matrix were chosen to present the cells with either a sparse (0.5mg/ml) or dense (2mg/ml) matrix. Collagen I, from the same source, was also used to coat the 2-D plastic surface. The

nuclei of the cells were imaged at their central plane to maximise the signal-to-noise ratio for the sensor. The background signal of the images was subtracted, and the FRET index of each pixel calculated (Fig 3.2A). The average FRET index across the NE per cell was calculated by averaging all pixel values underneath a manually drawn mask, using the strongest signal (in this case, the 'Acceptor' channel) as a reference (Fig 3.2B). MDA-MB-231 cells suspended within a dense 3D matrix demonstrated a greater level of tension across the LINC complex than those cultured upon 2D surfaces, as evidenced by a reduced FRET index (Fig 3.2A, B). Interestingly, this increase in tension appeared to increase with substrate density, as the cells within a low-density 3D matrix appeared to fall between the 2D and dense 3D conditions (Fig 3.2A, B). To confirm the role acto-myosin contractility in this tension differential cells embedded within a 2mg/ml matrix were treated with either 20µM Y-27632 and ML-7, a ROCK and MLC kinase inhibitor respectively, for 2 hours or an equivalent volume of vehicle control (DMSO). These concentrations were used for a previous study within the lab (work by Daniel Newman, unpublished) and found to effectively reduce acto-myosin contractility in this cell line. Inhibitor treatment significantly reduced the tension across the mN2-TS, with the FRET index returning to levels seen in cells upon the 2D substrate (Fig 3.2B). To investigate the possibility that FRET index values were influenced by signal intensity, average FRET index values from all three experimental repeats were plotted against the average pixel intensity for the pixels analysed (Fig 3.2C). Based upon the linear regression calculated, there was no obvious or significant trend between the intensity and the measured FRET index. This was true both for the cells seeded on 2D collagen and the cells suspended within the 3D collagen gels.

To assess the potential use of the mN2-TS as a readout of temporal tension changes, MDA-MB-231 cells were seeded into dense (2mg/ml) collagen matrices and their migration through the matrix was imaged (Fig 3.3). The FRET imaging setup was maintained, though the laser power was reduced to 20% (from 100%) to minimise photobleaching whilst also providing enough signal for FRET calculation. Images were taken at a rate of 1 frame/minute on a single Z-plane, again at the central plane of the nucleus (at the start of the timelapse) to maximise signal-to-noise ratio. The resulting timelapses were then analysed as described previously to calculate the FRET index per pixel (Fig 3.3A).

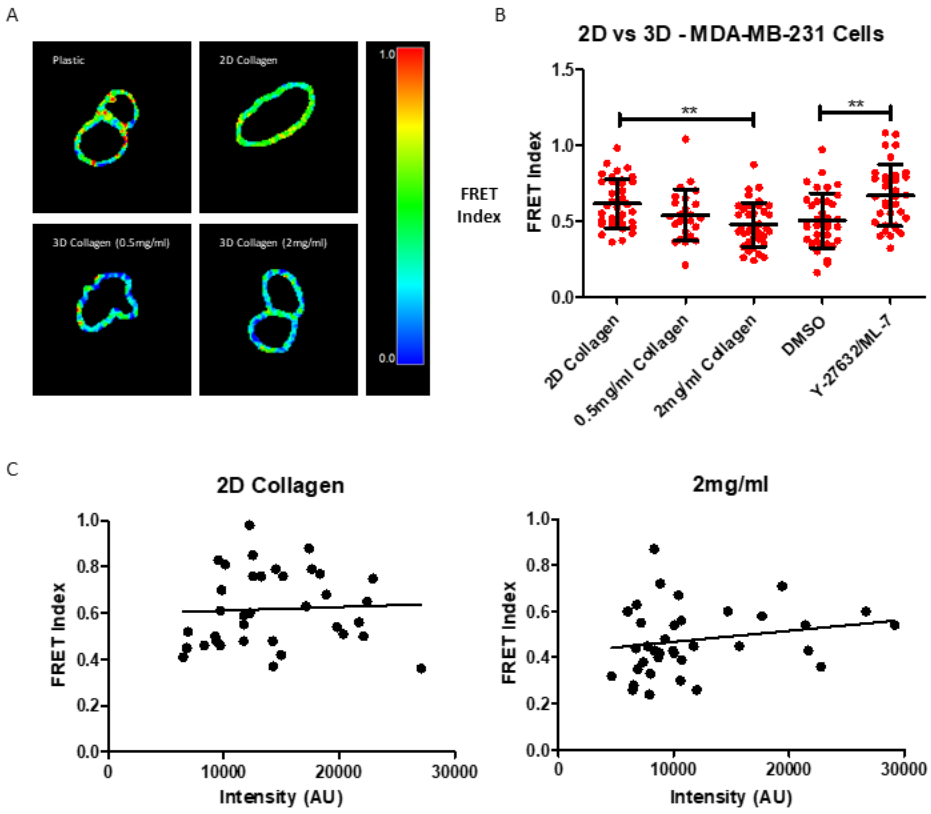

Figure 3.2. 2D vs 3D environment effect on nuclear tension. (A) MDA-MB-231 cells were cultured on either 2-D surfaces or within a 3-D matrix. False colour images show the pixel-by-pixel FRET index across the NE (B) The average FRET index across a central cross-section of the NE (in the horizontal plane) was calculated for each cell. Drug treatment used 20µM Y-27632/ML-7 and was compared to cells treated with an equivalent volume of DMSO. (C) Scatter plot of average pixel intensity (acceptor) vs average FRET index across all three experimental repeats. Linear trend line shown. Mean ± SD plotted. Statistical significance tested via one-way ANOVA with Tukey's Multiple Comparison Test (Significance = $p < 0.05$), slope significance tested by linear regression (2D Collagen: $p = 0.7695$, $R^2 = 0.002559$. 2mg/ml Collagen: $p = 0.2301$, $R^2 = 0.04088$). N = 3, $n \geq 24$.

The nucleus of the migrating cells was then divided into two halves, split along the centre line perpendicular to the direction of migration (Fig 3.3B). Two masks, corresponding to these two halves, were then manually drawn along the NE again using the 'Acceptor' channel as a reference. The average FRET index of all pixels within these masks was then calculated for each time point, and the FRET index at each timepoint plotted against time (Fig 3.3C). Plotting of the data indicated that the sensor readings over time, with the imaging setup used, were subject to a degree of noise that made precise observations over time difficult; however, it was possible to detect general trends. It was observed that in some instances a cell would pause in its migration before then continuing to migrate, possibly due to encountering a difficult

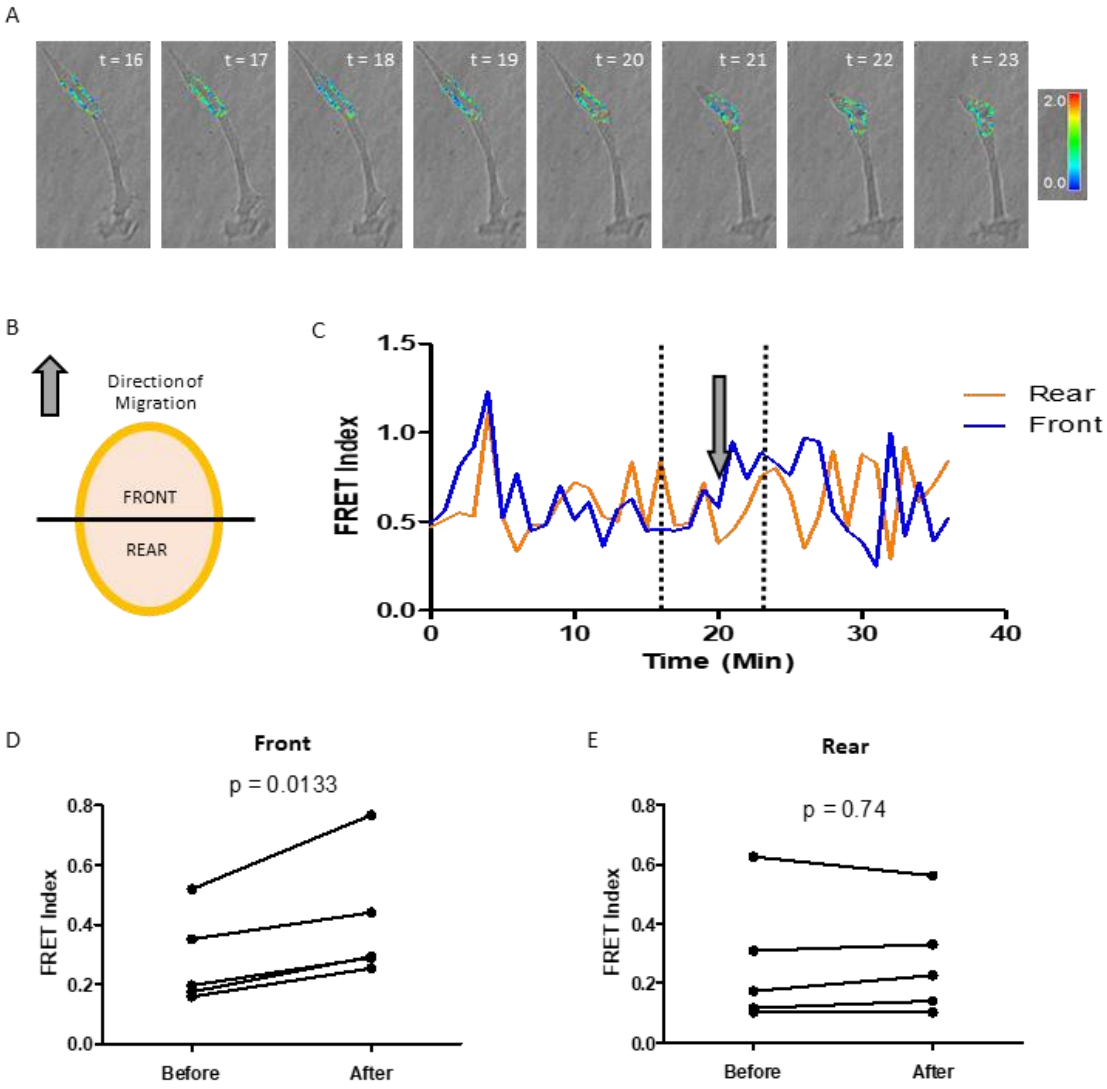

Figure 3.3. Dynamic tension measurements during 3-D migration. (A) False colour images of the NE, showing the FRET index values, overlaid onto a Brightfield image. Images correlate to the time point range highlighted in C (dotted lines). (B) Schematic demonstration of the definition of front/back. (C) Trace of the FRET index measured for the front and rear halves of the nucleus shown in A. (D) Average FRET index of the front half of the NE before and after (t ± 10min) translocation event for 5 cells. (E) Corresponding result for the rear half of the nucleus before and after translocation. Statistical significance tested using a paired t-test (Significance = $p < 0.05$).

to navigate constriction within the matrix. By correlating the FRET plots to the images, it was found that in these instances the front of the nucleus experienced a loss of tension on the mN2-TS upon the resumption of migration (Fig 3.3C, D), whilst the tension at the rear of the nucleus was unchanged (Fig 3.3E).

As the mN2-TS had shown itself to be capable of measuring dynamic changes in nuclear tension, the next step was to assess whether the sensor could register actively applied tensile stresses. To this end, an attempt was made to establish an experimental setup which could then be used to apply known tensile forces to cells expressing the mN2-TS. Tipless cantilevers (Arrow^{TM} TL-2, Nanoworld) were primed (via plasma cleaning) and coated with a mixture of 1mg/ml fibronectin and 2mg/ml concanavalin A. Conanavalin A is a member of the legume family of lectins and binds to glycosylated proteins and lipids (Goldstein *et al.*, 1965). This allows concanavalin A to bind to glycolipids within the cell membrane and capture cells without the need for specific receptor mediated adhesions to form; a factor intended to aid in the initial cell capture phase. These functionalised cantilevers were then mounted onto an JPK Nanowizard 3 fitted with a CellHesion module; this module acts to increase the effective z-piezo motor operational range of the AFM from 15µm to 100µm. The CellHesion module requires coverslips to be mounted, which act as the bottom of the imaging chamber; these coverslips were coated with 10µg/ml fibronectin prior to mounting. A cell suspension of freshly trypsinised MDA-MB-231 was then added to the chamber and allowed to settle to the bottom. The functionalised cantilever was then used to "fish" the cells from the coverslip surface before being raised away. The cells were then left to adhere to the cantilever surface, before being brought back into contact with the coverslip. After the cell was given time to adhere to the coverslip surface, the cantilever was then raised. This raising would stretch the cell between the two surfaces and apply a tensile force (Fig 3.4A). This stretching could be done in combination with confocal imaging to simultaneously apply a tensile force and image the mN2-TS present in the cell. A couple of attempts at this were made using MDA-MB-231 cells (Fig 3.4B), and a correlation between the applied tensile force and the FRET index was seen. However, the technique proved to be low throughput due to the difficulty of finding and fishing transfected cells during the window of opportunity prior to the cells adhering to the coverslip surface. This difficulty was further compounded when the setup was tested on a fibroblast cell line (in this case, MEFs). As such, this experimental setup was ultimately not followed up further. However, the results gathered do indicate that the mN2-TS sensor is capable of detecting dynamically applied force stimuli at the NE.

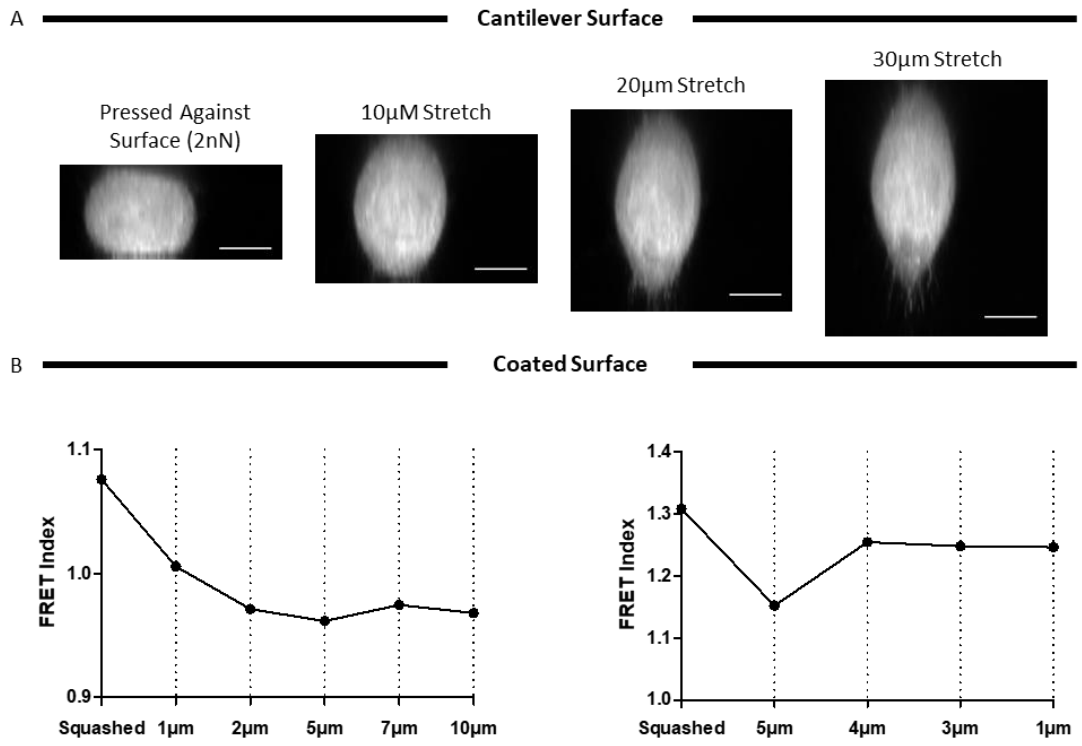

Figure 3.4. Cell stretching via atomic force microscopy. (A) A re-sliced and interpolated z-stack of an MDA-MB-231 cell, transfected with GFP-Lifeact, stretched between a cantilever (top of image) and the coverslip (bottom of image). Scale bar = 10µm. (B) FRET index measurements of MDA-MB-231 cells stretched to the stated heights. Cantilever movement was conducted in order of left-to-right on the graph. FRET index calculated from intensity ratio of donor/FRET channels.

3.3.2. Cloning of Progerin Expressing Cell Lines

With protocols for the use of the mN2-TS in place, a model system was needed to conduct investigations into HGPS. There are three main options that are used regularly within the literature for the study of HGPS. These options are to use a mouse model or mouse model derived cell lines (Hale *et al.*, 2008; Mounkes *et al.*, 2003; Sagelius *et al.*, 2008), to use primary fibroblasts taken from biopsies of HGPS patients, or to use fibroblast cell lines that are transfected, transiently or stably, with progerin. I decided that initial attempts should be made to conduct the experiments within a transfected fibroblast cell line, rather than a primary cell line or mouse model, due to the requirement for effective transfection of the tension biosensors; a task that is difficult to achieve in primary HGPS lines. In service of this, plasmids were developed which contained either the WT lamin A gene or a form of the gene lacking 50 base pairs, corresponding to those which are removed via splicing in the G608G mutant of

HGPS (termed Δ50 progerin), tagged with the fluorophore mRuby2 (Lam *et al.*, 2012). Plasmids containing the required sequences were kindly provided by Iakowos Karakesisoglou (University of Durham, The School of Biological and Biomedical Sciences). These sequences were then cloned into a pcDNA3.1 backbone which contained the mRuby2 sequence, in such a way as to place the mRuby2 tag at the N-terminal end of the lamin A/Δ50 progerin sequence. Validation of correct labelling and localisation was confirmed by immunofluorescence of transiently transfected NIH-3T3 fibroblasts labelled with α-lamin A/C antibody.

Whilst it would be possible to conduct the study using transient transfection, it is worth considering that lamin A expression level is known to influence nuclear behaviour and be tied into the response of cells to mechanical cues (Swift *et al.*, 2013). As such, it's possible that overexpressing lamin A will have an impact on the mechanotransduction pathway, which would make elucidating the role of progerin expression specifically more difficult. I therefore decided that a stable transfection, with only a single integration, would provide a more suitable platform for studying the effects of progerin expression. This was accomplished using the Flp-In^{TM} system (Thermo Fisher Scientific); a DNA recombination method for gene integration and expression based upon the site-specific recombinase Flp (O'Gorman *et al.*, 1991). NIH-3T3 fibroblasts containing a single FRT sequence are commercially available (Thermo Fisher Scientific), and these were chosen for use in this study due the prevalence of NIH-3T3 cells in previous HGPS studies. The mRuby2-lamin A/Δ50 progerin sequences were cloned into the pcDNA5/FRT expression vector (3.5A), which were then co-transfected with the pOG44 plasmid (which constitutively expresses Flp) to integrate them into the genome of the NIH-3T3 cells. Successful stable clones were selected via continuous treatment with 200μg/ml hygromycin, which continued until cell colonies were clearly visible (and all negative control cells had perished). Colonies were then

pooled into mixed populations, and expression of the mRuby2 tagged lamin A/Δ50 progerin within the populations confirmed via western blotting for lamin A/C (Fig 3.5B) and immunofluorescence imaging alongside α-lamin A/C antibodies (Fig 3.5C).

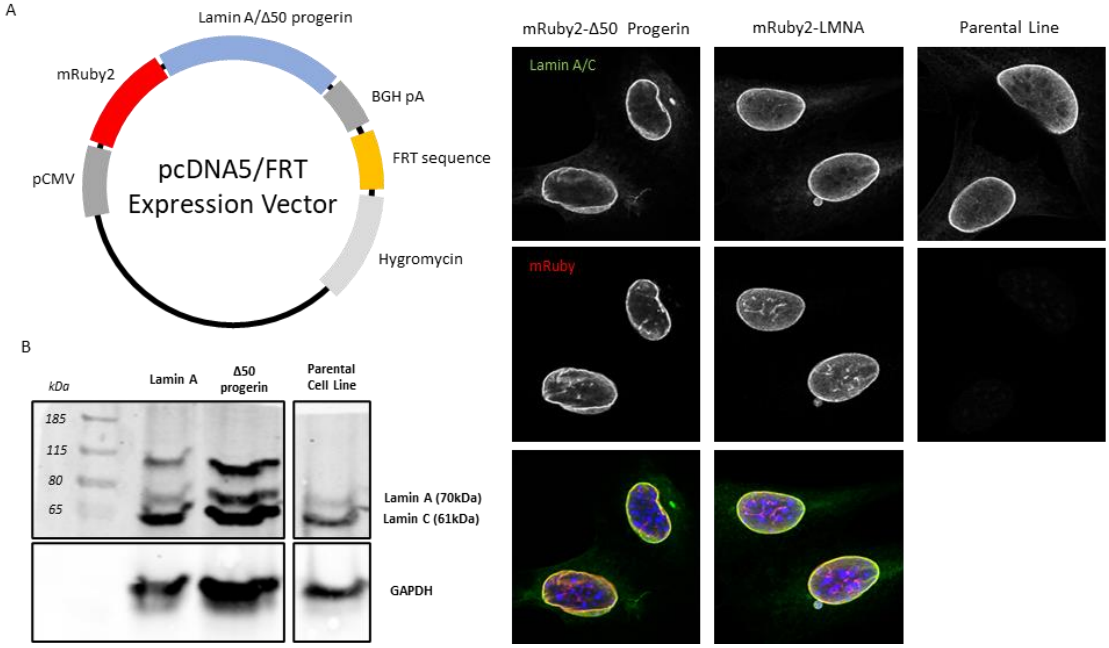

Figure 3.5. Generation and validation of stable NIH-3T3 cell lines. (A) Schematic showing the pcDNA/FRT vector cloned with either lamin A or the mutant Δ50 progerin used to generate the NIH-3T3 FlpIn^{TM} cell lines. (B) Western blot of mixed cell population lysate, probed for lamin A/C, demonstrating the expression of the gene of interest (top band). (C) Immunofluorescence staining of lamin A/C (green) alongside imaging of mRuby2 (red), with a merge of the two channels including Hoechst 33342 (blue, bottom).

3.3.3. Assessment of tensile forces in NIH-3T3 Flp-In^{TM} Cell Lines

With these stable expression cell lines in hand, the investigation of tensile forces and mechanotransduction in this HGPS model could begin. Lamin A and Δ50 progerin cells, as well as the parental NIH-3T3 Flp-In^{TM} cell line, were transfected with the mN2-TS and seeded onto fibronectin (Fig 3.6A). The average FRET index at the central nuclear plane for each cell line was then calculated (Fig 3.6B). No significant differences were observed between the three cell lines, suggesting that in this model there was no major alterations in overall force experienced at the NE. However, treatment of these cells with Y-27632/ML-7 inhibitors also did not seem to influence the FRET index (Fig 3.6C), despite the previously seen effect in MDA-MB-231 cells. Given that this inhibitor combination also increased the measured FRET index in a different fibroblast cell line, MEFs (Woroniuk *et al.*, 2018), the lack of response in the

NIH-3T3 cells is concerning. Higher concentrations of inhibitors were tested, however these resulted in significant cell death within the population, preventing meaningful observation. This unfortunately makes it difficult to draw any conclusive answers from these experiments.

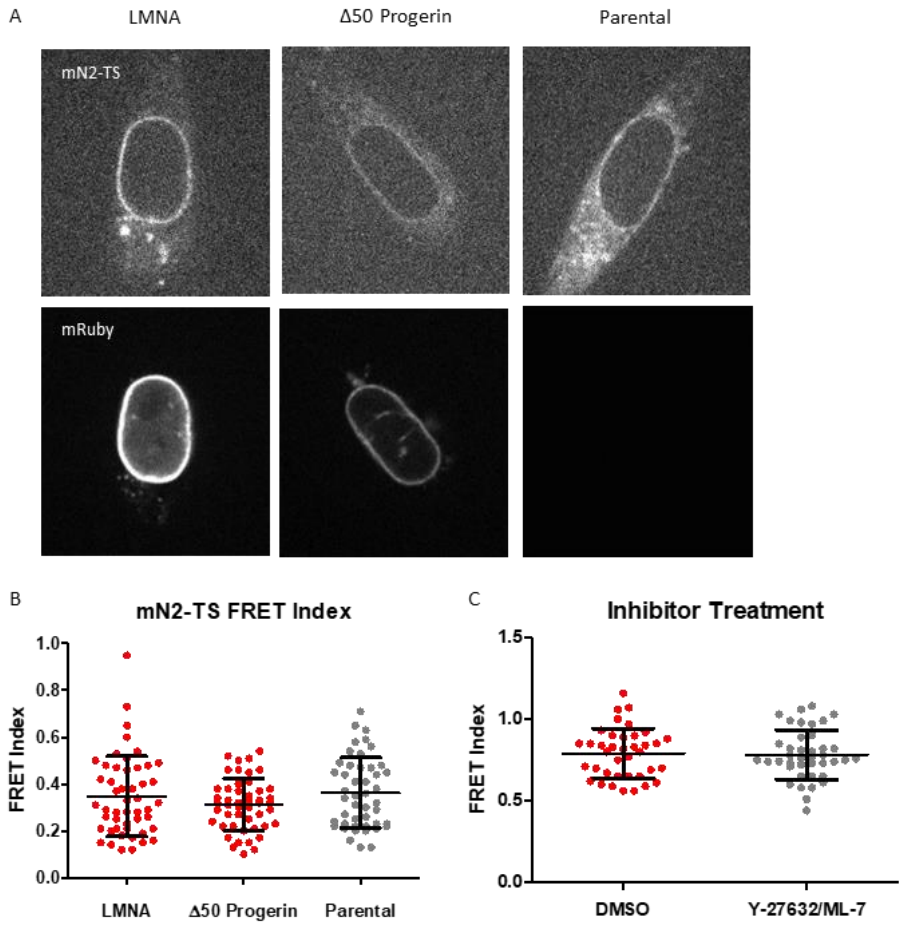

Figure 3.6. Tension at the NE in progeria expressing NIH-3T3 cell line. (A) Confocal imaging of NIH-3T3 Flp-In cell lines transiently expressing mN2-TS. Fluorescence images show acceptor (mVenus) channel, as well as images of the mRuby tag. (B) The average FRET index across a central cross-section of the NE (in the horizonal plane) was calculated for each cell. (C) FRET index calculated for cells treated with a combination of Y-27632/ML-7 inhibitors, or an equivalent volume of DMSO. Mean ± SD plotted. Statistical significance tested using a one-way ANOVA with Tukey's multiple comparison test (Significance = $p < 0.05$). N = 3, $n \geq 34$.

To investigate forces at the focal adhesions, a tension biosensor based upon talin (termed talin-TS) was used, which was previously developed by the Schwartz lab to demonstrate that talin is subject to tensile forces within adhesions (Kumar *et al.*, 2016). This sensor uses the fluorophores EGFP and tagRFP as the donor and acceptor respectively, with the same elastic linker separating them as used by the mN2-TS. A

force negative variant of the construct whose sensor is placed at the C-terminal end of the protein, rather than within the sequence, is used as a negative control; since placing the sensor at the end will result in no tension being applied to it (Kumar *et al.*, 2016). These constructs were transfected into the cell lines, which were then seeded onto 10μg/ml fibronectin and imaged (Fig 3.7A). For the analysis a mask of the focal adhesions was drawn via intensity thresholding, using the direct GFP excitation/emission images as a reference. For this purpose a focal adhesion was defined as any object with an area larger than 0.6μm^2, as this size threshold ensured that the majority of background signal identified by the threshold was excluded. In the context of this analysis, the use of the talin-TS does come with one issue; this being that the acceptor, tagRFP, has overlapping emission spectra with mRuby2 (as can be seen in Fig3.7A). Therefore, to remove the influence of mRuby2 bleedthrough on the FRET index calculations, adhesions that lay under the nucleus were excluded from the mask via manual removal. In parental cells, brightfield images were used as a reference for this purpose. Once the mask had been finalised, the FRET index of all pixels within the mask were averaged and plotted (Fig 3.7B). There was no significant difference in the FRET index between the lamin A/Δ50 progerin cell lines and the parental line, though the cells expressing lamin A had significantly reduced FRET index in comparison to the progerin expressing cell line. All conditions were significantly lower than the force negative control, demonstrating that in all cell lines talin was subjected to some tensile forces.

In parallel to the talin-TS experiments, an assessment of the focal adhesion morphology was also conducted. Immunofluorescence staining for paxillin was used to label the focal adhesions in the NIH-3T3 cell lines, alongside phalloidin to stain the actin cytoskeleton. These cells were then imaged using a laser scanning confocal microscope, taking a single plane image along the bottom surface of the cells (Fig 3.8A). A macro developed in ImageJ was then used to identify the adhesions via intensity thresholding and measure the individual adhesion area and shape factor (major/minor axis length of a fitted ellipse), and the number of identified ROIs used as a measure of adhesion count. The average area of all adhesions within each cell was then calculated and plotted (Fig 3.8B). The average adhesion area within the Δ50 progerin expressing cells was significantly larger than those in the parental cells (Fig 3.8B); an increase that was the result of increases in both the length and width of

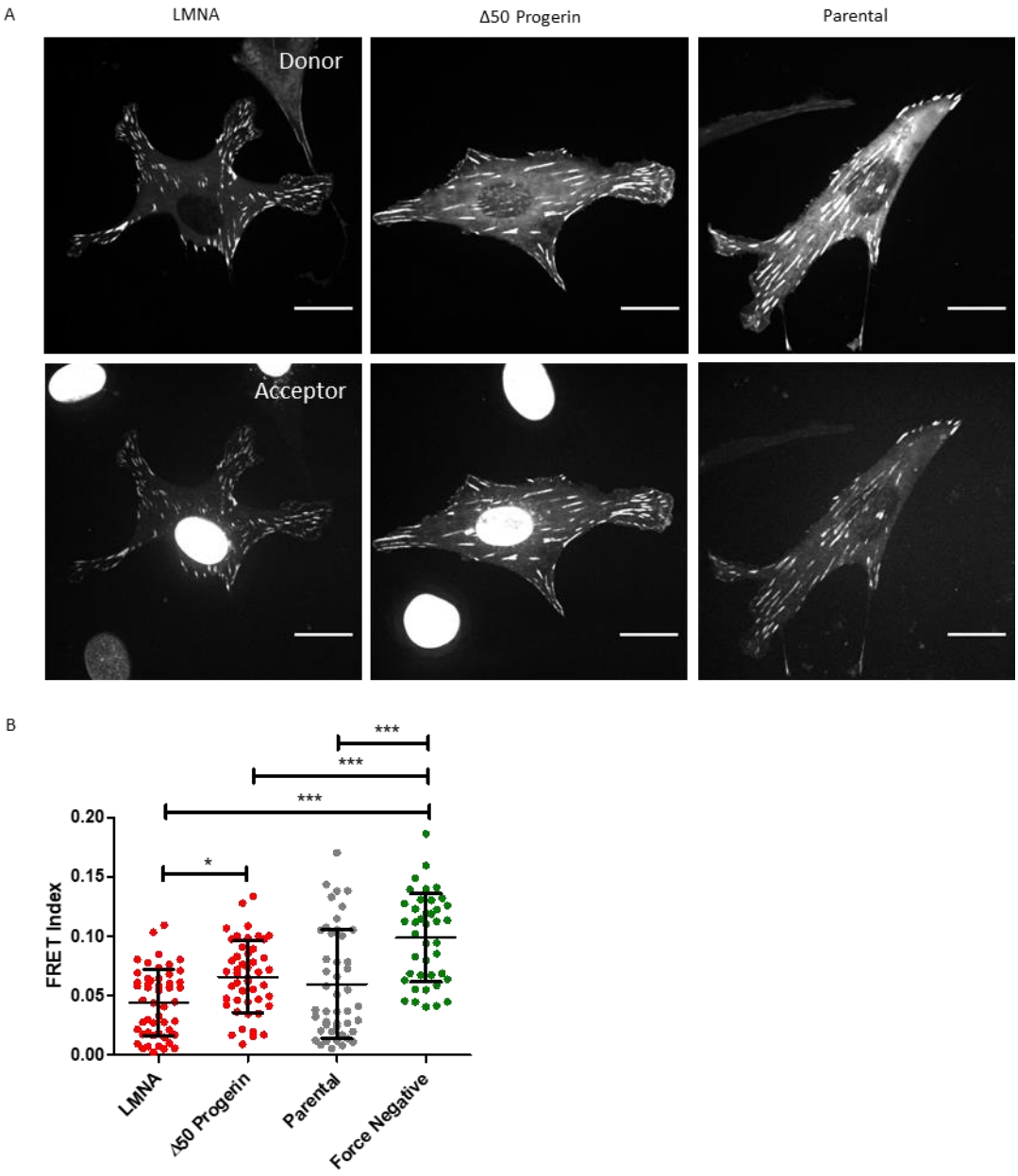

Figure 3.7. Tension at the focal adhesions across Talin in progeria expressing NIH-3T3 cell line. (A) Confocal imaging of NIH-3T3 Flp-In cells transiently expressing Talin-TS. Fluorescence images show donor (eGFP) and acceptor (tagRFP) channels. Nuclear signal from mRuby-tagged proteins is visible in the acceptor channel. Scale bar = 20µm. (B) The average FRET index for each focal adhesion within a cell was calculated, and then averaged together to give a cell-wide FRET index average. All adhesions that overlapped with the nucleus were excluded in all conditions to prevent false readings caused by mRuby signal. Mean ± SD plotted. adhesions, as suggested by the change in both major and minor axis lengths (Fig 3.8C). Statistical significance tested using a one-way ANOVA with Tukey's multiple comparison test (Significance = $p < 0.05$). N = 4, $n \geq 41$.

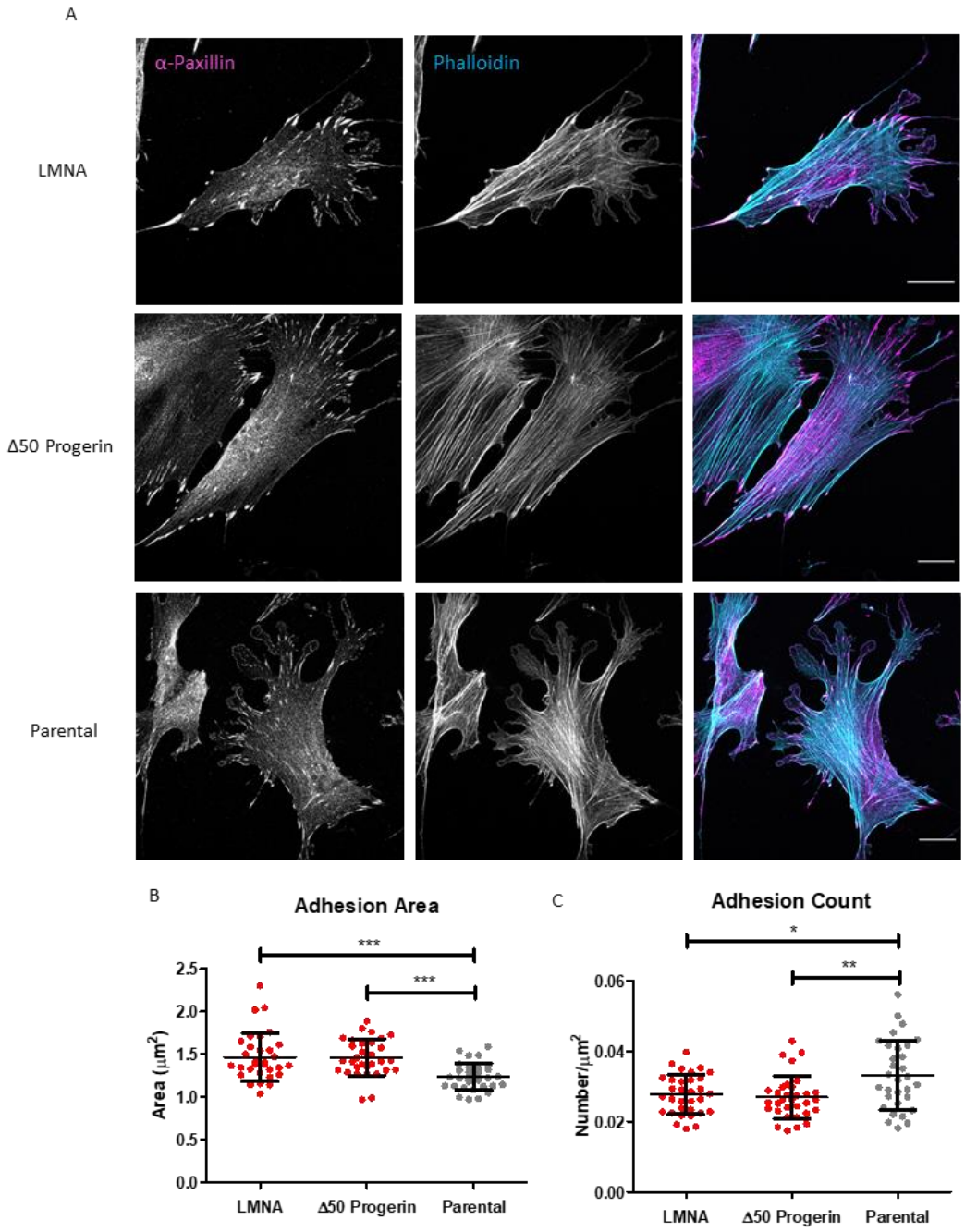

Figure 3.8. Assessment of focal adhesion morphology in progeria expressing cells. (A) Immunofluorescence images of NIH-3T3 Flp-In cell lines, with antibody staining against paxillin (magenta) and phalloidin (cyan) staining for filamentous actin. Scale bar = 20μm. (B) Individual focal adhesion areas were calculated for all adhesions within a cell, and then averaged to give an average adhesion area per cell. (C) The number of identified focal adhesions in a cell was divided by the total cell area (as defined by actin) to obtain the number of adhesions per μm^2. Mean ± SD plotted. Statistical significance tested using a one-way ANOVA with Tukey's multiple comparison test (Significance = $p < 0.05$). N = 3, $n \geq 30$.

This increase in adhesion area was accompanied by an increase in the number of adhesions per cell (Fig 3.8D). To account for differences in cell area in the counting, all adhesion counts were first normalised to their respective cell area (calculated using phalloidin as the reference) before being plotted.

It was noted that the cell line expressing the wild type lamin A also demonstrated an increase in adhesion area/number in line with the Δ50 progerin expressing cells. This raised the possibility that the phenotype observed were a result of *LMNA* overexpression, rather than solely the result of Δ50 progerin expression. To try and eliminate this possibility, mRNA knockdown of endogenous *LMNA* was attempted in the NIH-3T3 cell lines, followed by paxillin/phalloidin staining. However, the results of these experiments were inconclusive, as the values obtained were highly variable; likely as a result of inconsistent knockdown efficiency as observed via western blotting (data not shown).

3.3.4. Assessment of tensile forces in Primary Patient Fibroblasts

Due to the observed complications in the NIH-3T3 cell lines, I decided to assess the same factors in primary patient fibroblasts. Inspired by the work of Chang *et al.* (2019), three pairs of cell lines were selected for use in this study (Table 3.1). Each pair consists of a fibroblast cell line derived from a HGPS patient (denoted as AG) and an age-matched healthy individual (denoted as GM). These cell lines were obtained from the Coriell Institute's NIA Aging Cell Culture Repository (https://www.coriell.org/1/NIA). Three separate pairs of cell lines were used to account for potential variations between individuals and allow for universal differences brought about by progerin expression to be elucidated. Normalising each HGPS cell line to its respective healthy cell line allows the observations from each pair to be grouped, and the overall trend plotted.

Using these cell pairs, the previous assessment of the mN2-TS in the NIH-3T3 lines was repeated. Primary cells were seeded into glass bottomed imaging dishes coated with fibronectin and transiently transfected with the mN2-TS. The cells were then imaged, and the average FRET index calculated for each cell (Fig 3.9A). There was no change in FRET index for two of the three HGPS cell lines, whilst one cell line

showed an increase in FRET index (Fig 3.9B). This demonstrates that tension across nesprin-2 in HGPS cells is at the very least unchanged relative to their healthy counterparts, if not reduced.

Table 3.1. Primary cell lines obtained for use in this study. Cells were obtained from the Coriell Institutes NIA Aging Cell Culture Repository. Each pair consists of a HGPS patient derived cell line (AG06917, AG11513, AG01972) and a cell line derived from a healthy individual of similar age and same sex (GM00498, GM00038, GM01652).

	Name	Age	Sex	Source
Pair 1	AG06917	3	M	Skin, Arm
	GM00498	3	M	Skin, Unspecified
Pair 2	AG11513	8	F	Skin, Leg
	GM00038	9	F	Skin, Unspecified
Pair 3	AG01972	14	F	Skin, Thorax
	GM01652	11	F	Skin, Arm

Next, the assessment of tensile forces at the focal adhesions was repeated using the talin-TS (Fig 3.10), as had been done previously for the NIH-3T3 cell lines and using the same methodology as used for the mN2-TS transfection. The FRET index of the adhesions for two of the three pairs was significantly lower in the HGPS cell line than the healthy counterpart (Fig 3.10B). This shows that talin is under increased tensile stress in the HGPS cell lines. To investigate whether this difference in talin tension could be related to differences in cell area, the average adhesion FRET index per cell was plotted against the total cell area (Fig 3.10C). These plots demonstrate that the elevated adhesion tension in the HGPS was not related to the increased area of these cells. Parallel assessment of focal adhesion morphology via paxillin immunofluorescence imaging showed that focal adhesion area was increased in the HGPS cell lines (Fig 3.11); which is seen consistently across all three pairs (Fig 3.11B). As was the case in the NIH-3T3 cell lines, this increase in area is seen as an increase in both the adhesion width and length. Measurement of the adhesion count showed that one of the HGPS cell lines had a large increase in the number of adhesions. In the other two lines, adhesion count differences were small and the differences were not statistically significant at type I error rate of 0.05 (Fig 3.11C).

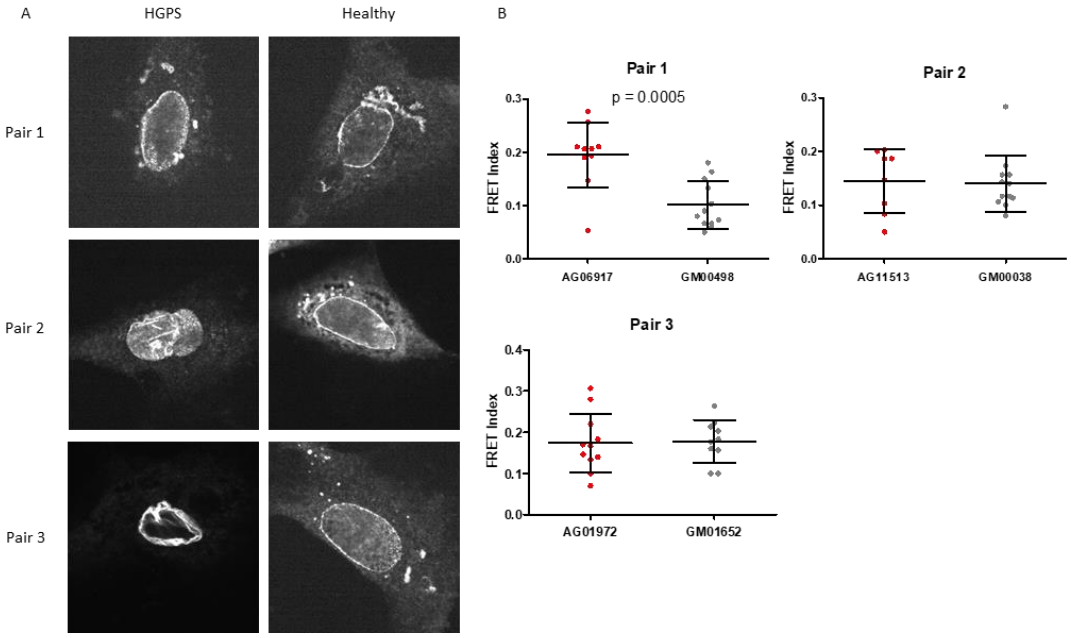

Figure 3.9. Tension at the NE in primary cell line pairs. (A) Confocal imaging of HGPS/Healthy primary cell lines transiently expressing mN2-TS. Fluorescence images show acceptor (mVenus) channel. (B) The average FRET index across a central cross-section of the NE (in the horizonal plane) was calculated for each cell, and the FRET index for each pair plotted. Mean ± SD plotted. Statistical significance tested using an unpaired t-test (Significance = $p < 0.05$). $N = 2$, $n \geq 8$.

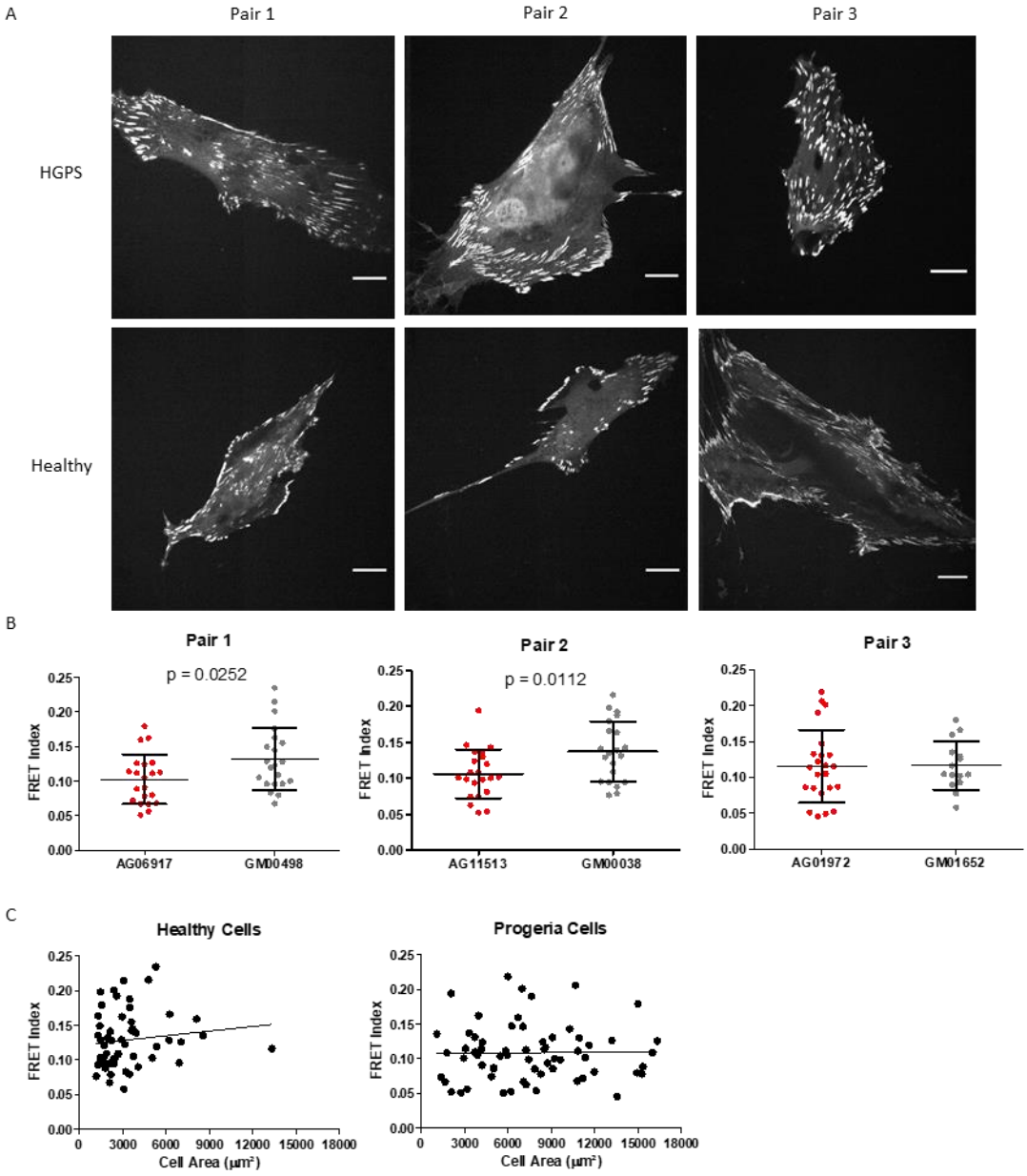

Figure 3.10. Tension at the focal adhesions across Talin in progeria patient cell lines. (A) Confocal imaging of NIH-3T3 Flp-In cells transiently expressing Talin-TS. Fluorescence images show donor (eGFP) channel. (B) The average FRET index for each focal adhesion within a cell was calculated, and then averaged together to give a cell-wide FRET index average. (C) Scatter plots of average FRET index vs cell area, showing linear trend line. Mean ± SD plotted. Statistical significance tested using an unpaired t-test (Significance = $p < 0.05$), slope significance tested by linear regression (Healthy cells: $p = 0.3729$, $R^2 = 0.01530$. HGPS cells: $p = 0.8971$, $R^2 = 0.0002716$). N = 3, $n \geq 15$.

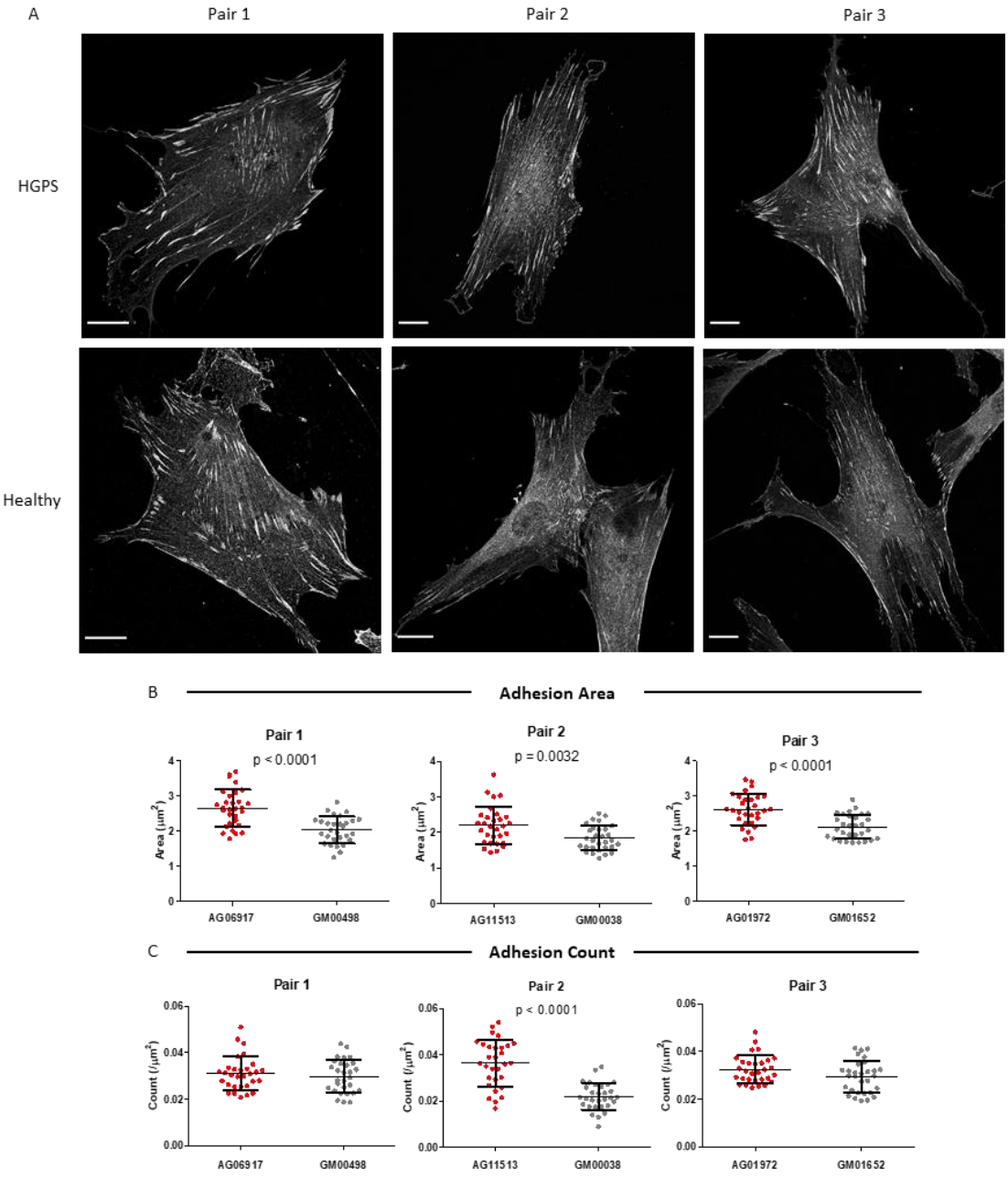

Figure 3.11. Assessment of focal adhesion morphology in progeria patient cell lines. (A) Immunofluorescence images, with antibody staining against paxillin. Scale bar = 20μm. (B) Individual focal adhesion areas were calculated for all adhesions within a cell (adhesion defined as objects > 0.6μm^2, to exclude background), and then averaged to give an average adhesion area per cell. (C) The number of identified focal adhesions in a cell was divided by the total cell area (as defined by actin) to obtain the number of adhesions per μm^2. Mean ± SD plotted. Statistical significance tested using an unpaired t-test (Significance = $p < 0.05$). N = 3, n ≥ 29.

3.4. Discussion

The first aim of this chapter was to establish the use of the mN2-TS as a readout of force transmission to the nucleus, and then apply this sensor to the study of HGPS. Considering this, MDA-MB-231 cells were used to assess the influence of matrix dimensionality on the forces experienced at the NE. These results suggest that cells within a dense 3-D matrix experience increased forces at the NE, in a manner dependant on the actin cytoskeleton. Increased confinement has been shown to facilitate the alignment of stress fibres, resulting in more effective cell migration (Pathak and Kumar, 2012). This alignment of stress fibres also aligns the NMII-dependant contractile forces (Pathak and Kumar, 2012), which would likely increase the cumulative force exerted on the NE via the LINC complexes. This would account for the increased tensile force applied to the mN2-TS in the dense matrix, as well as explain why the sparser matrix did not show the same level of force application at the NE. However, varying the concentration of the collagen hydrogel will not only increase the confinement of the cell. Increasing the concentration of collagen used to form the hydrogel also increases the stiffness of the gel (Roeder *et al.*, 2002) due to increased cross-link density between the fibres (Lin & Gu, 2015). As increased stiffness within 3D collagen gels promotes the maturation of focal adhesions (Doyle *et al.*, 2015), it's possible that increasing substrate stiffness is responsible for the increased tensile forces at the NE by promoting a stronger and more stable connection between the ECM and the NE. Further experiments in which each of these factors is varied independently would need to be conducted to elucidate the exact cause.

Migration through dense 3-D matrices is reliant upon NMII activity (Pathak and Kumar, 2012; Thomas *et al.*, 2015), and this NMII dependence also relies upon the presence of nesprin-2 (Thomas *et al.*, 2015). Nesprin-2 has also recently been observed to accumulate at the leading edge of the nucleus during nuclear translocation through narrow apertures (Davidson *et al.*, 2020). This, in combination, would suggest that forward motility of the nucleus through restrictive apertures would be the result of acto-myosin generated forces pulling the nucleus forwards. This hypothesis is validated by the findings of the migration assays conducted with the mN2-TS within this project, which showed increased tensile forces across nesprin-2 during nuclear

translocation events in dense 3D matrices. These findings, alongside practical applications in a published work that lies beyond the scope of this project (Woroniuk *et al.*, 2018), firmly establish the usefulness and validity of the mN2-TS.

With this in hand, the next aim of this chapter was to establish the model system that would be used for the study of HGPS and apply the mN2-TS to this model. Initially, the use of a NIH-3T3 Flp-In^{TM} cell line was explored, with the FlpIn^{TM} system being used to stably express the mutant form of lamin A, progerin. Whilst the generation of this clonal cell line was successful, and some intriguing observations made surrounding focal adhesion morphology, ultimately the usefulness of this model was limited by the complications associated with potential lamin A overexpression phenotypes, as well as the lack of responsiveness for the mN2-TS. The fact that lamin A overexpression resulted in an increase in adhesion area and number is an interesting observation in and of itself. Cells are known to regulate their lamin A expression levels in response to substrate stiffness (Swift *et al.*, 2013), and the loss of lamin A expression has been shown to reduce adhesion size and number (Corne *et al.*, 2017). This suggests that lamin A expression is linked to the formation and maturation of adhesions, and that this link is important for regulating the cell's ability to sense and respond to the mechanical properties of their environment. As this question falls outside the scope of this project, the hypothesis is not explored further here. However, future work exploring the mechanism and importance of this link between lamin A expression and cellular regulation of mechanosensitivity may yield interesting and important insights into how cells respond to the mechanics of their environment.

As a result of these complications with the NIH-3T3 cell lines, I decided to switch from this model to a model based around primary patient fibroblasts. The use of three HGPS derived cell lines, rather than a singular example, was established to identify and reduce the impact of individual genetic variations in the final observations. Applying the mN2-TS into this model showed that there was at least no change in nuclear tension between the HGPS cell lines and their healthy counterparts, if not a reduction as seen in one of the pairs (AG06917/GM00498). Low cell numbers, resulting from a poor transfection efficiency, makes definitive conclusions difficult; however, these data would suggest that there is a reduction, or at the very least no change, in tension at the NE mediated by nesprin-2.

Moving to the other end of the force propagation pathway, expression of the talin-TS in the HGPS derived cell lines showed that a majority of the HGPS lines had increased tensile force at the focal adhesions. This was accompanied by an increase in focal adhesion area, as seen by observation of immunofluorescence labelling of paxillin. As force application on talin is a key factor controlling focal adhesion stabilisation and maturation (Rahikainen *et al.*, 2019), one would expect that talin being subjected to greater tensile force would result in stabler, and therefore larger, adhesions. This raises the question of why these HGPS cells display this adhesion phenotype? Is the cell's ability to sense the substrate properties affected, resulting in increased adhesion growth? Or are the adhesions being subjected to increased tensile forces from elevated acto-myosin contractility? And in either case, another question is why is the NE not experiencing the same increase in tensile force as the adhesions? If the adhesions and the NE are linked directly via the stress fibres, then one would expect changes in tensile forces to be propagated through the entire mechanotranductory pathway; but this does not seem to be the case in these HGPS cell lines.

4. Investigating Changes in Mechanically Induced Signalling

4.1. Introduction

The cell's ability to respond to external mechanical stresses relies upon its ability to sense those changes and alter its gene expression and morphology accordingly. This sensing of external force stimuli can be accomplished via two means; either direct channelling of forces into the nuclear interior to alter chromatin structure (Heo *et al.*, 2016; Iyer *et al.*, 2012; Tajik *et al.*, 2016) or by activating biochemical signalling pathways that regulate alterations in focal adhesion and actin structure (Boutahar *et al.*, 2004; Humphries *et al.*, 2007; Stutchbury *et al.*, 2017; Wang *et al.*, 2005; Webb *et al.*, 2004; Zhao *et al.*, 2010).

The channelling of forces through the cell and into the nucleus relies upon the actin cytoskeleton and stress fibres, and an important factor that facilitates this function of the actin cytoskeleton is pre-stress (Hu *et al.*, 2003; 2005). Using acto-myosin contractility, the actin cytoskeleton is subjected to a base level of force stress that places the system under tension (Guolla *et al.*, 2012). This tension makes the system more sensitive to external force stresses (Hu *et al.*, 2005), and allows force propagation over greater distances (Hu *et al.*, 2003), than would otherwise be possible in the absence of pre-stress. Acto-myosin contractility can be increased via the phosphorylation of myosin light chain (MLC) by ROCK, which acts to increase NMII ATPase activity (Amano *et al.*, 1996). Therefore, observing the base level of pMLC phosphorylation would provide an indicator for acto-myosin contractility within HGPS cells, and give insights into potential changes in cellular pre-stress. Another way in which cytoskeletal tension can be assessed is via the use of AFM. Higher cytoskeletal tension results in increased cellular stiffness, and vice versa (Wang *et al.*, 2002), making cellular stiffness measurements a good indicator of underlying cytoskeletal tension/pre-stress. Indeed, increased MLC activity is known to be accompanied by an increase cellular stiffness (Cai *et al.*, 1998). Due to the importance of pre-stress in force propagation, any change in actin cytoskeletal tension would likely influence the cell's ability to respond effectively to mechanical stresses. Given that the mechanically loaded tissues of the body are heavily affected in HGPS, it is worth

investigating whether there is any change in acto-myosin contractility and tension in these cells that could contribute to the disease pathology.

The activation of biochemical signalling upon mechanical stimulation is controlled by a variety of signalling proteins. One of the more prominent proteins within this group is FAK, whose interactions with other signalling proteins, such as Src, triggers the activation of various downstream signalling pathways that control a host of different cell behaviours (Boutahar *et al.*, 2004; Humphries *et al.*, 2007; Stutchbury *et al.*, 2017; Wang *et al.*, 2005; Webb *et al.*, 2004; Zhao *et al*., 2010). FAK is activated via tyrosine phosphorylation (Toutant *et al.*, 2002; Calalb *et al*., 1995), and can be activated in response to a variety of force stimuli (Zebda *et al.*, 2012). Mechanical stimuli do not only influence signalling at the focal adhesions but can also regulate the nuclear localisation of transcription factors. YAP is a prominent example of one such transcription factor, whose localisation to the nucleus can be stimulated by external force stimuli (Dupont et al., 2011; Elosegui-Artola et al., 2017) where it facilitates the transcription a wide range of genes (Zanconato *et al.*, 2015; Zhao *et al.*, 2008). Observation of YAP localisation is therefore an indicator of potential changes in mechanically regulated signalling.

YAP and FAK are among the primary initiators of a cell's mechanical signalling and response, but another protein that plays an important role in controlling the necessary alterations in adhesion/cytoskeletal structure is RhoA (Ridley & Hall, 1992). This Rho family GTPase coordinates the formation and polarisation of actin stress fibres in response to mechanical stimulation (Kaunas *et al.*, 2005), as well as promoting the maturation of focal adhesions by increasing acto-myosin contractility via the phosphorylation of MLC (Amano *et al.*, 1996; Chrzanowska-Wodnicka & Burridge, 1996).

The focal adhesions and stress fibres play an important role in transmitting forces from the extracellular environment to the nuclear interior, as previously discussed. However, they can also act to exert forces on the extracellular environment from the cell interior. These forces, referred to as traction forces, play an important role in cell migration (Fournier *et al.*, 2010), substrate stiffness sensing (Ghassemi *et al.*, 2012; Giannone *et al.*, 2004) and cell polarisation (Prager-Khoutorsky *et al.*, 2011). These

traction forces are applied through the connection between the matrix and focal adhesions and generated by the contraction of the acto-myosin cytoskeleton. The loss of traction forces can have profound effects upon the cells ability to sense and react to its local mechanical environment. The traction forces that a cell generates upon a 2-D substrate can be measured using traction force microscopy (TFM) (Wang & Lin, 2007). This methodology uses fluorescent beads embedded within a hydrogel of defined stiffness as markers, whose displacement by the action of cell traction forces can be tracked. The tracking of these markers can then be used to calculate the forces exerted by the cell on the underlying gel.

4.2. Chapter Aims

The HGPS cell lines have been observed to have enlarged focal adhesions, and talin within these adhesions is subject to increased tensile forces. This increase in tension and change in adhesion phenotype may be accounted for by increased acto-myosin contraction within the stress fibres. As such, this chapter aims to assess the stress fibres and wider cytoskeleton to determine whether there is increased acto-myosin activity in the HGPS cell lines. An assessment of the cellular localisation of YAP will be used to identify if there are any changes in mechanically regulated transcription in the HGPS cell lines. The effect of substrate stiffness on the HGPS phenotype will also be investigated to determine whether the observed changes in adhesion morphology are tied to substrate stiffness. The altered adhesion phenotype may also influence the ability of the cell to exert forces upon the extracellular matrix, a process important for focal adhesion formation as well as various cellular processes such as polarisation and migration. Traction force microscopy (TFM) will be employed to investigate whether the HGPS cell lines have an altered ability to exert forces on their environment.

4.3. Results

4.2.1. Changes in Cytosketetal Stiffness

As increased cytoskeletal stiffness is linked to increased acto-myosin activity (Wang *et al.*, 2002), one can use measurements of cellular stiffness as an indicator of acto-myosin contractility. As such, AFM was employed to measure cellular stiffnesses for the primary cell lines to determine whether there are any changes in cellular stiffness between the HGPS and healthy cell lines (Figure 4.1). MLCT-C cantilevers were used to probe a 40μm^2 area of the cell body that incorporated the nucleus via Quantitative Imaging mode. This imaging modality generates an image in which each pixel of that image represents a single force-distance curve. Analysing each of these force-distance curves then allows an image to be generated in which each pixel has a value equal to the Young's modulus calculated for that area (Figure 4.1A). In this case, a 128x128 pixel image was used to cover the 40x40µm area of the cell that was selected, for a total of 16,384 force-distance curves. The slope of these force-distance curves was then calculated using a Hertz/Sneddon fitting model, which yielded the Young's modulus value for each pixel. A maximum stiffness threshold of 500kPa was used during the analysis step to exclude any readings taken from the glass surface, which exceeded this value. The remaining pixels were then averaged to generate an average Young's modulus for the cell region (Figure 4.1B). Two of the pairs (Pair 1 and 3) showed a general trend towards increased stiffness in the HGPS cell lines (Figure 4.1B). To accompany this data, attempts were made to assess the levels of phosphorylated MLC to further investigate whether there was increased activation of acto-myosin contractility. Western blotting for pMLC was conducted, however these efforts ultimately proved unsuccessful in labelling pMLC within the experiments conducted.

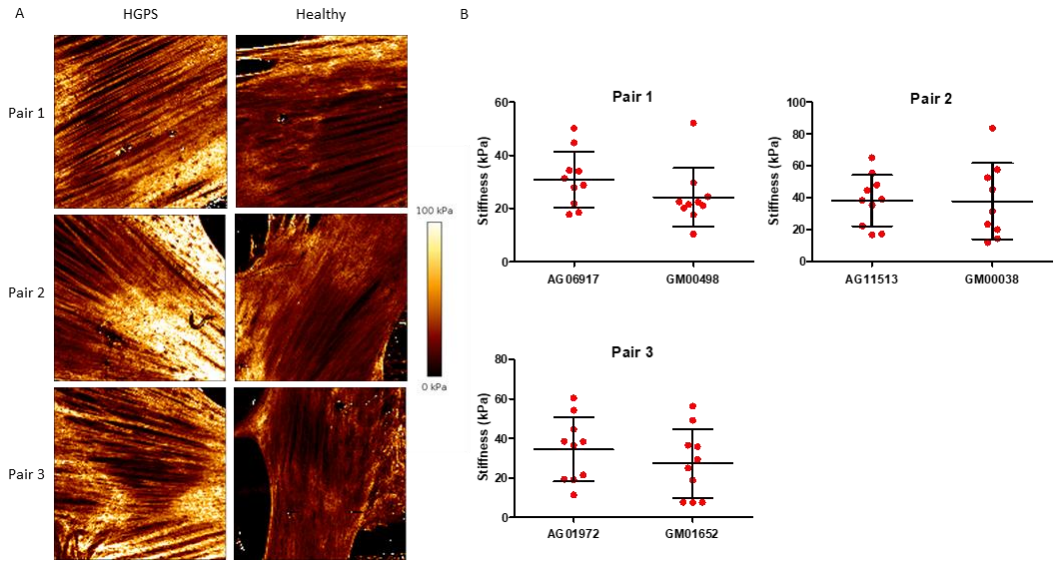

Figure 4.1. Measurement of cytoskeletal stiffness in patient cell lines using atomic force microscopy. (A) A 40x40µm area of the cell body, encapsulating the nucleus, was imaged via Quantitative Imaging mode with an image size of 128x128 pixels. Force-distance curves were then analysed via a Hertz/Sneddon fitting model, and Young's modulus images generated. Image colour scale shown right of images. (B) The Young's modulus of all pixels within the scanned area, below a 500kPa threshold, were averaged to give a cell area average. Mean ± SD plotted. Statistical significance tested using an unpaired t-test (Significance = $p < 0.05$). N = 3, $n \geq 9$.

4.2.2. Investigating Changes in Key Mechanotransduction Signalling Activity

Mechanical forces do not only trigger signalling at the focal adhesions, but also regulates the nuclear localisation of multiple transcription factors. The most prominent of these is YAP, which localises to the nucleus upon force application (Elosegui-Artola *et al.*, 2017), as well as on higher substrate stiffnesses (Dupont *et al.*, 2011). This nuclear localisation aids in the regulation of the cell's response to substrate stiffness (Calvo *et al.*, 2013; Dupont *et al.*, 2011; Elosegui-Artola *et al.*, 2016), as well as in the adaptation to force stresses (Aragona *et al.*, 2013; Benham-Pyle *et al.*, 2015; Nakajima *et al.*, 2017). To investigate whether there were any changes in YAP localisation within the HGPS cells, immunofluorescence imaging of endogenous YAP was conducted on cells seeded onto glass coverslips coated with fibronectin (Figure 4.2A). Staining with Hoechst 33342 and phalloidin-alexafluor-670 was conducted alongside antibody labelling of YAP to act as markers for the nucleus and cell body respectively. These were then imaged via confocal microscopy, capturing a single plane where the nuclear cross section was largest. ImageJ was then used to define ROIs of either the nucleus

or the whole cell excluding the nucleus, and these ROIs used to measure the mean intensity of YAP labelling in each area. The ratio of these intensities (Nuclear/Cytosolic) was then calculated (Fig 4.2B). Curiously, there appeared to be no consistent behaviour between the three cell line pairs, with each pair showing a distinct behaviour. Under these conditions, YAP should predominantly be localised to the nucleus due to the very high stiffness of glass as a substrate (in the GPa scale). It would therefore appear that at very high stiffnesses, the HGPS cell lines display a varied ability to localise YAP to the nucleus.

While this initial assessment has some use, the excessively high stiffness of glass as a substrate makes it difficult to directly relate these findings to a physiological context. As such, the next step was to assess whether the localisation of YAP in the HGPS cell lines differed at substrate stiffnesses found within human tissues. For this, cells were grown in imaging dishes that contained a PDMS hydrogel which was either "soft" (1.5kPa) or "stiff" (28kPa). As most tissue stiffnesses lie between these two values (Guimarães *et al.*, 2020), these substrates should provide a snapshot of the HGPS phenotype at either end of the tissue stiffness scale. These substrates were coated with fibronectin and the YAP immunofluorescence imaging repeated, using the same methodology and analysis as used for the glass substrate (Fig 4.3). Two of the three cell pairs (Pair 1 and 3) showed a clear reduction in nuclear/cytosolic YAP ratio on these substrates, while the remaining pair (Pair 2) demonstrated the inverse behaviour on the PDMS substrates, as was seen on the glass substrate (Fig 4.3B, C). This difference in the localisation of YAP could be related to changes in YAP expression within the cell, as much as it could be related to perturbations in mechanical signalling. Therefore, the expression levels of YAP within the HGPS/healthy cell lines needed to be established to determine which may be the primary factor. Western blotting of whole cell lysates labelled for YAP was used to observe the endogenous expression of YAP in these cells. The intensity of the bands was then measured and plotted (Fig 4.4). One of the cell pairs (Pair 2) demonstrated a reduced level of YAP expression in the HGPS cell line, but this was not seen in the other two cell line pairs. This difference was also observed in the mean intensity of YAP staining within the cell body of this cell line when imaging the immunofluorescence labelling of endogenous YAP. Interestingly, this pair was the one that demonstrated a differing YAP localisation

phenotype relative to the other two cell line pairs, suggesting a possible link between the YAP expression and its localisation in the HGPS cell lines.

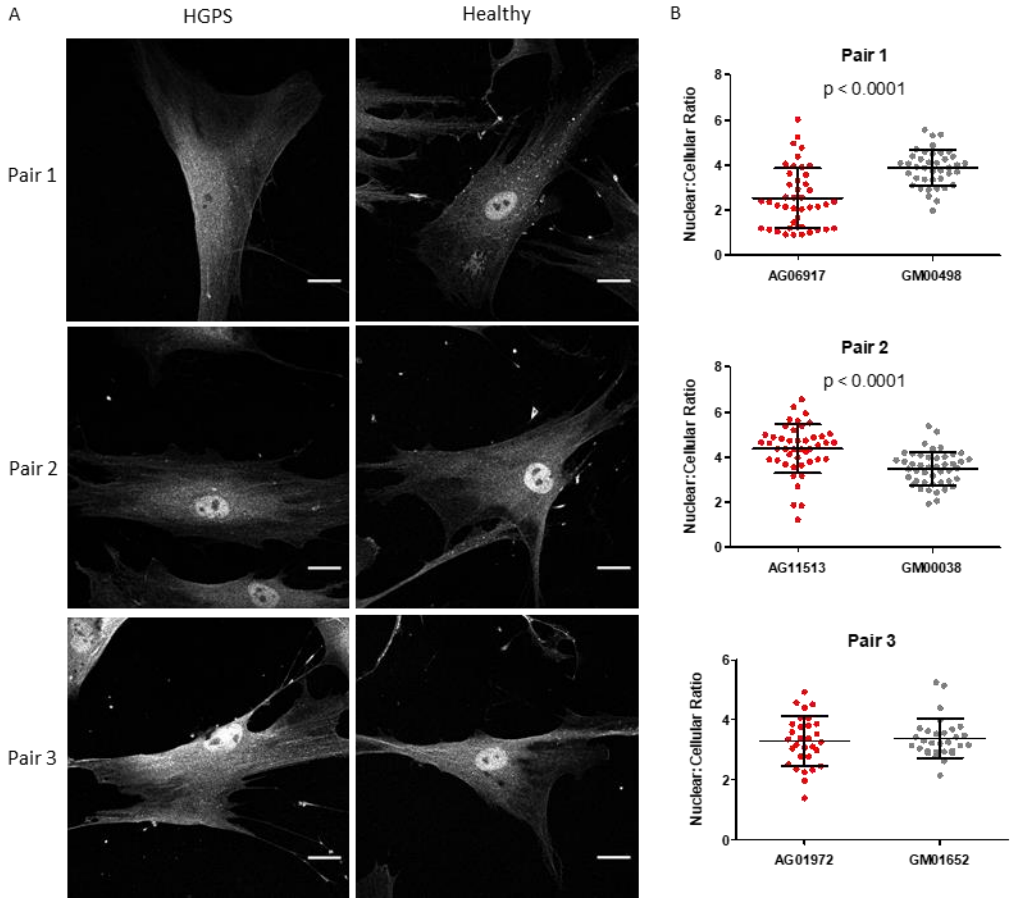

Figure 4.2. Localisation of YAP in patient cell lines on an ECM coated glass substrate. (A) Immunofluorescence imaging of HGPS and healthy cell lines labelled for endogenous YAP. Scale bar = 20µm. (B) The intensity of YAP labelling within the nucleus and cell body (excluding the nucleus) was measured and the ratio of nuclear : cytoplasmic intensity calculated. Mean ± SD plotted. Statistical significance tested using an unpaired t-test (Significance = $p < 0.05$). N = 3, $n \geq 30$.

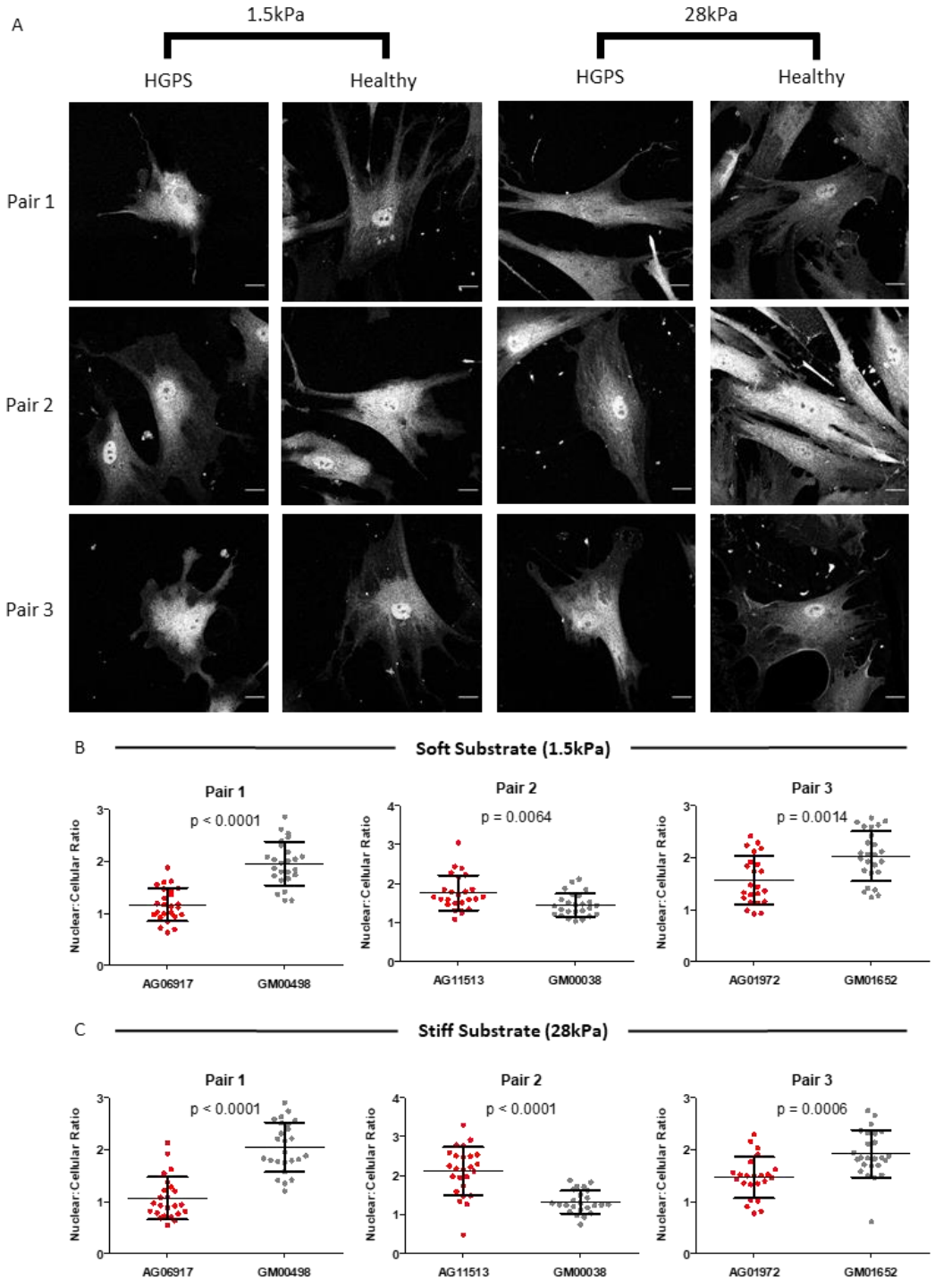

Figure 4.3. Localisation of YAP in patient cell lines on differing stiffness PDMS substrates. (A) Immunofluorescence imaging of HGPS and healthy cell lines labelled for endogenous YAP, seeded onto either "soft" or "stiff" PDMS substrates coated with fibronectin. Scale bar = 20µm. (B+C) The intensity of YAP labelling within the nucleus and cell body (excluding the nucleus) was measured and the ratio of nuclear : cytoplasmic intensity calculated. Mean ± SD plotted. Statistical significance tested using an unpaired t-test (Significance = $p < 0.05$). N = 2, $n \geq 23$.

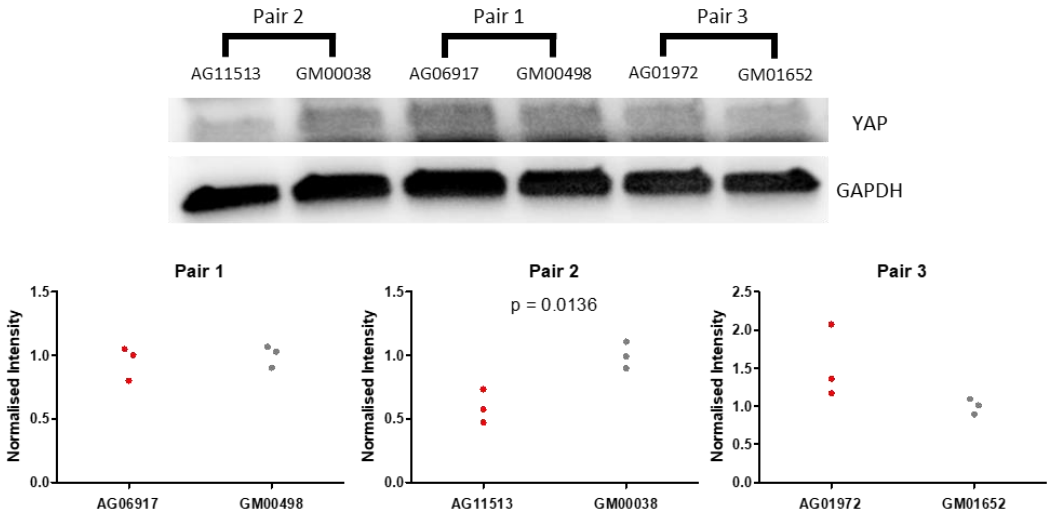

Figure 4.4. Protein level of YAP in HGPS and healthy cell lines. Western blotting of whole cell lysates from either HGPS or healthy cell lines was conducted, labelling with antibodies targeting YAP. GAPDH was also labelled to act as a loading control. YAP band intensities were measured and normalised to GAPDH band intensities. For each pair, these values were then normalised to the corresponding healthy pair average. Mean values plotted. Statistical significance tested using an unpaired t-test (Significance = $p < 0.05$).

4.2.3. Effect of Substrate Stiffness on Adhesion Phenotype

The HGPS cell lines have consistently displayed a larger average adhesion area on a rigid glass substrate, however it was worth investigating whether this difference was maintained on a PDMS substrate with a more physiological stiffness. To this end, the primary cell lines were grown in dishes with a PDMS substrate of 15kPa stiffness coated with fibronectin. This value was chosen as it is close to the stiffness of many tissues (Guimarães *et al.*, 2020) and is compatible with the TFM experiments conducted later in this work. These cells were then fixed, labelled for paxillin and imaged (Fig 4.5A), as was done previously. The mean adhesion area was calculated for each cell, following the same analysis protocol as used for the previous adhesion quantification, and these results were then plotted for each cell pair (Fig 4.5B). The average adhesion area within the HGPS cell lines was still larger than their healthy counterparts, though the extent of the difference appeared to be reduced when compared to the cells plated on a glass substrate (Fig 3.11B).

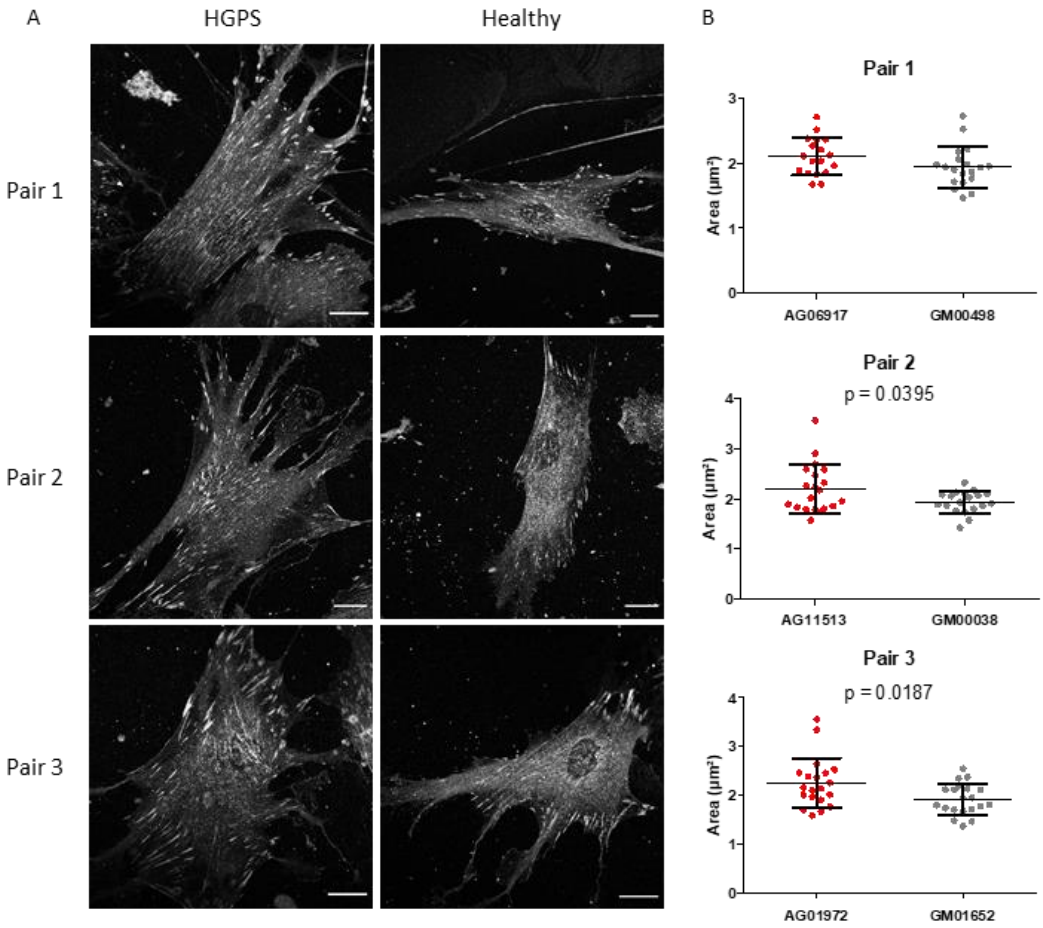

Figure 4.5. Assessment of focal adhesion morphology in patient cell lines on 15kPa PDMS substrate. (A) Immunofluorescence imaging of HGPS and healthy cell lines labelled for paxillin, seeded onto a 15kPa PDMS substrate coated with fibronectin. Scale bar = 20µm. (B) Individual focal adhesion areas were calculated for all adhesions within a cell (adhesion defined as objects > 0.6µm^2, to exclude background) and then averaged to give an average adhesion area per cell. Mean ± SD plotted. Statistical significance tested using an unpaired t-test (Significance = $p < 0.05$). N = 2, n ≥ 29.

4.2.4. Influence of Adhesion Phenotype on Cell Traction Forces

The ability of a cell to respond to the mechanical properties of its environment relies on the cell being able to probe the surrounding matrix and ascertain the local stiffness. This probing is accomplished through the application of traction forces, which allows the cell to judge the stiffness of the matrix via deformation of said matrix (Ghassemi *et al.*, 2012; Giannone *et al.*, 2004). Given that the focal adhesions are critical for the application of these forces, and the magnitude of these forces is controlled by acto-myosin contractility, it's possible that the changes in these structures observed in the

HGPS cell lines would also affect the ability of these cells to exert traction forces on the surrounding matrix. To test this possibility, traction force microscopy (TFM) was employed. Patient and healthy cell lines were seeded onto poly(acrylic acid) (PAA) hydrogels that contained embedded fluorescent beads (488nm excitation). These gels were made from a 9% protogel solution (Geneflow), which would yield a gel with a measured stiffness of 10-15kPa. The gels were imaged with the cell being present, then the cells were removed from the gel surface using SDS treatment. The gels were then re-imaged at the same positions. An ImageJ macro set (Martiel *et al.*, 2015) was then used to identify the beads and track their movement between the two images. Since the mechanical properties of the gel are known, the distance that the beads are displaced prior to the cell being removed (relative to their resting position) can be used to calculate the amount of force that was being exerted by the cell on that area of the gel (Fig 4.6). These forces, and their vector, can be mapped for each cell (Fig 4.7A). The magnitude of the traction forces within each image were then averaged to give an average traction force per cell (Fig 4.7B). One of the three pairs (AG01972/GM01652) showed a significant, though variable, increase in cell traction force, whilst the other two pairs demonstrated no change in traction forces.

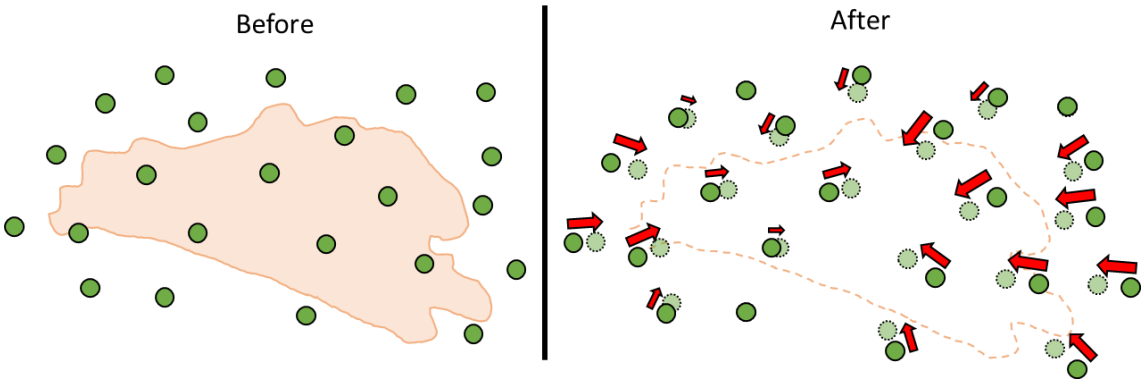

Figure 4.6. Diagram demonstrating traction force microscopy technique. (Left) Cells are seeded onto PAA hydrogels, which contain fluorescently labelled beads (green circles). The gels are then imaged prior to SDS treatment. (Right) SDS treatment is used to remove the cell, and the gel is imaged again at the same position. The position of the beads before (dotted circle) and after (solid circle) treatment is compared, and the distance between the two used to calculate the force vector (red arrow).

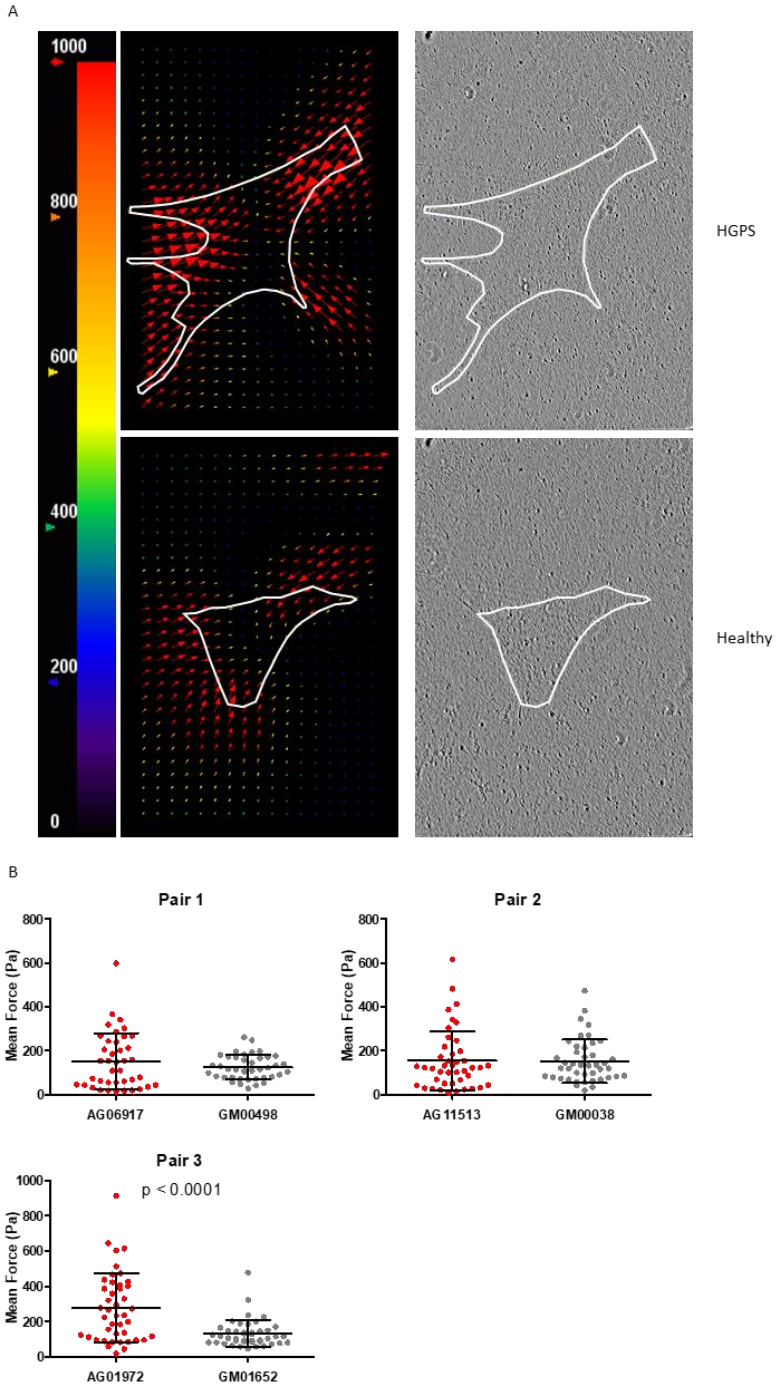

Figure 4.7. Quantification of cell traction forces using Traction Force Microscopy. (A) False colour force vector images of two example cells taken from Pair 2 (AG11513/GM00038). Arrow colour denotes force intensity, on a scale of 0-1000Pa, whilst arrow direction denotes force vector. The cell within the image is outlined in white, based on the corresponding brightfield image. (B) The average traction force per cell was calculated by averaging the individual force vector magnitudes within each image. Mean ± SD plotted. Statistical significance tested using an unpaired t-test (Significance = $p < 0.05$). N = 3, $n \geq 40$.

4.4. Discussion

The aims of this chapter were to assess acto-myosin contractility and observe whether there were any changes in mechanically sensitive signalling pathways within the context of HGPS. To this end, AFM was employed to measure the cellular stiffness of the primary cell lines and provide a comparison between the HGPS and the healthy cell lines. There was a trend toward increased stiffness within two of the three cell line pairs studied, which would suggest there may be increased acto-myosin contractility. When considering the individual images, it also appears that there are cytoskeletal fibres (presumed actin fibres by their morphology) that are more prominent in the HGPS cell lines than in the healthy cell lines. This suggests that whilst the average stiffness is not significantly higher for the individual HGPS cell lines, there is a visible increase in stiffness within the actin filaments themselves, further suggesting that acto-myosin contractility is increased in the HGPS cell lines. Mu *et al.* (2020) also recently observed increased cellular stiffness in a Zmpste24$^{-/-}$ mouse cell line model, though these measurements were only taken from a single point within the cell body. A further examination of the individual fibre stiffnesses would be warranted to confirm the observations made here. Increased acto-myosin contractility would be accompanied by increased levels of MLC phosphorylation, and as such an attempt was made within this work to directly observe the levels of pMLC within the cell lines via western blotting. Despite best efforts, this proved unsuccessful. As such, it isn't possible to use this information to supplement the data obtained via AFM. For future studies, alternative ways of assessing acto-myosin activation would need to be explored.

Another prominent response to mechanical stimulation is the nuclear localisation of the transcription factor YAP (Elosegui-Artola *et al.*, 2017). The localisation of YAP within the HGPS cell lines was first assessed upon glass, followed by an assessment upon "stiff" (28kPa) and "soft" (1.5kPa) PDMS substrates. These experiments suggested that the nuclear localisation of YAP was reduced in the HGPS cell lines when grown on the PDMS substrates, though not when grown on a glass substrate. This may reflect a defect in the cell's ability to activate mechanically regulated gene transcription, which would negatively impact the cell's ability to respond to external force stimuli. This also indicates that the potential increases in force transmission

across the adhesions and stress fibres in the HGPS phenotype is not reflected in the localisation of YAP. The question this raises is why is YAP nuclear localisation reduced in the HGPS cells? One potential explanation lies in the observation that force application can directly trigger the import of YAP into the nucleus (Elosegui-Artola *et al.*, 2017). Perhaps the lack of force at the NE prevents this mechanism of triggering YAP import into the nucleus?

Given the changes in the focal adhesions seen in the HGPS cell lines, one question was whether this alteration in the adhesions affected the cell's ability to exert forces upon the surrounding matrix. Given the importance of traction forces in the cell's ability to sense matrix stiffness (Ghassemi *et al.*, 2012; Giannone *et al.*, 2004), any changes in these forces could have a detrimental impact on the cell's ability to sense and adapt to mechanical changes in its environment. To investigate this possibility, TFM was used to assess the traction forces exerted by the HGPS cell lines on a PAA hydrogel with a stiffness of 10-15kPa. The data from these experiments suggests that there is a change in the traction forces exerted by the HGPS cell lines, in line with the changes in adhesion area. One might have expected this, as an increase in focal adhesion area would have resulted in increased traction forces in healthy contexts (Balaban *et al.*, 2001; Tan *et al.*, 2003).

5. Investigating the Causal Factor for HGPS Adhesion Phenotype

5.1. Introduction

The RhoA signalling pathway is important for mechanotransduction, as it plays a role in regulating the structure and organisation of actin stress fibres in response to mechanical stresses (Lessey *et al.*, 2012). RhoA can exist in two states: either an active GTP bound state, or an inactive GDP bound state. The movement of RhoA between these states is controlled by three groups of proteins: guanine nucleotide-exchange factors (GEFs), GTPase-activating proteins (GAPs) and guanine nucleotide-dissociation inhibitors (GDIs). GEFs promote the active state of RhoA by catalysing the exchange of bound GDP for GTP, while GAPs promote the inactive state by inducing GTP hydrolysis (Bos *et al.*, 2007). RhoA can also be sequestered within the cytoplasm by GDIs in an inactive state, both controlling its activity and allowing it to be shuttled between membranes (Garcia-Mata *et al.*, 2011). Active RhoA exerts its control over the actin cytoskeleton through two main downstream effectors, RhoA kinase (ROCK) and mDai1. ROCK acts to increase acto-myosin contractility via two main mechanisms. It firstly increases the activity of NMII isoforms via phosphorylation of MLC, which enhances NMII ATPase activity (Amano *et al.*, 1996). It also phosphorylates MLC phosphatase, inhibiting its activity and thereby preventing inactivation of MLC (Kimura *et al.*, 1996). ROCK also acts to stabilise the actin cytoskeleton via phosphorylation and activation of LIM kinase, which in turn phosphorylates and deactivates cofilin, an actin filament severing protein (Maekawa *et al.*, 1999). mDia, meanwhile, promotes the formation of new actin filaments via its ability to act as an actin nucleation factor (Watanabe *et al.*, 1999). Together, these effectors act to promote the formation and reinforcement of actin stress fibres.

The transmission of forces to the nucleus along actin stress fibres plays an important role in regulating the activation/deactivation of key genes involved in the response to mechanical stresses (Li *et al.*, 2014; Shiu *et al.*, 2018; Wei *et al.*, 2020). This can be directly via changes in chromatin structure (Heo *et al.*, 2016; Iyer *et al.*, 2012; Tajik *et al.*, 2016; Wei *et al.*, 2020), but it can also be indirectly via the localisation of

transcription factors (Shiu *et al.*, 2018). YAP is an example of one such transcription factor, which localises to the nucleus in response to mechanical stimulation (Dupont et al., 2011; Elosegui-Artola et al., 2017). This change in localisation can be directly controlled by the application of force to the nucleus (Elosegui-Artola et al., 2017). The nuclear pore complexes (NPC) act as the gateway between the cytoplasm and the nucleoplasm, through which all nuclear-bound cargo must travel. The NPC is a large protein complex of ~125MDa (Reichelt et al., 1990), however despite being one of the largest protein complexes in the cell the entire structure is constructed using a limited number of proteins (~30) (Rout et al., 2000), which are collectively referred to as nucleoporins (Nups). The overall structure of the NPC consists of three rings; a central ring, which anchors the NPC within the NE, a nucleoplasmic ring and a cytoplasmic ring. The cytoplasmic and nucleoplasmic rings have eight filaments attached to them, with the cytosolic filaments having loose ends whilst the nucleoplasmic filaments form a structure termed the nucleoplasmic 'basket' (Ris, 1989, 1991; Goldberg & Allen, 1992). Force application onto the nucleus, and resulting stretching of the NE, can open the NPCs and facilitate the increased import of YAP into the nucleus (Elosegui-Artola et al., 2017). One of the Nups that constitutes the nucleoplasmic basket, Nup153, may facilitate direct alteration of the state of NPCs by mechanical forces transmitted via interaction with the LINC complex protein SUN1 (Donnaloja *et al.*, 2019).

Another important regulator of nuclear import is the small GTPase Ran. Ran is important for both the import (Melchior *et al.*, 1993) and export (Moroianu & Blobel, 1995) of cargo to/from the nucleoplasm. Control of import/export is facilitated via a gradient of RanGTP concentration, with RanGTP being concentrated within the nucleoplasm via transport of RanGDP back into the nucleus by NFT2 (Ribbeck *et al.*, 1998). As such, any change in the localisation of Ran will have profound effects upon the movement of cargo both into and out of the nucleus that is not small enough to passively move through the NPC via diffusion, including many transcription factors. A loss of nuclear localisation of both Ran and Nup153 have recently been reported and shown to play a direct role in the HGPS phenotype (Larrieu *et al.*, 2018). A loss of the Ran gradient had been previously reported in HGPS cell lines (Kelly *et al.*, 2011; Snow *et al.*, 2013), though this work reported that Nup153 was properly localised within the nucleus (Snow *et al.*, 2013).

The adhesion phenotype displayed by the HGPS cell lines has been shown to be consistent in all three of the individual cell lines observed, as well as maintained on both a rigid and softer, more physiologically relevant, substrate. This alteration in adhesion phenotype may be the result of increased RhoA activity, however the question remains as to whether this change in the adhesions is directly related to the accumulation of progerin, the mutant form of lamin A responsible for the disease (Goldman et al., 2004), within the NE. One way in which this can be tested is by treating the HGPS cell lines with a farnesyltransferase inhibitor and observing the adhesion phenotype post treatment. As it is the accumulation of the permanently farnesylated progerin within the NE that results in the disease phenotype, preventing that farnesylation from taking place can mitigate some of the toxicity of its accumulation (Capell *et al.*, 2005; Glynn & Glover, 2005; Toth *et al.*, 2005). One such inhibitor, called lonafarnib, has been used in human clinical trials as a potential treatment for HGPS, resulting in increased lifespan (Gordon *et al.*, 2014; 2018).

5.2. Chapter Aims

The HGPS cell lines have displayed enlarged focal adhesions and elevated acto-myosin contractility but show no increase in tensile force at the NE, which may hamper their ability to respond to external force stimuli. This altered phenotype could be caused by numerous factors, including RhoA signalling pathways and abrogated nuclear import rates. As such, this chapter aims to explore some of these possible causative factors and provide an avenue for future research that could explore the causative factors for the increased sensitivity of progerin expressing cells to mechanical stresses.

Nuclear import defects will be investigated via observation of the localisation of two key proteins, Ran and Nup153. Changes in the levels of these proteins within the nucleus would be an indicator of defective nuclear import and may provide evidence for a loss of mechanically regulated import.

HGPS is caused by the accumulation of the farnesylated form of pre-lamin A, termed progerin. Many treatments for HGPS therefore employ fanesyltransferase inhibitors to

prevent the farnesylation and alleviate the negative effects of progerin accumulation. The final aim of this chapter will be to treat the HGPS cell lines with one such inhibitor, lonafarnib, and observe the effect of this treatment upon the focal adhesion phenotype. This will provide insight on whether progerin accumulation by itself is sufficient to bring about the altered focal adhesion phenotype.

5.3. Results

5.3.1. Investigating Changes in RhoA Activity

Given the increased focal adhesion area that is observed in the HGPS cell lines, one of the likely candidates that could regulate this change is the small Rho-GTPase RhoA. RhoA plays a prominent role in the regulation of both stress fibre formation and focal adhesion maturation (Ridley & Hall, 1992, Watanabe et al., 1999). Changes in RhoA activity would therefore provide a potential mechanism via which the adhesions of HGPS would become larger and experience increased talin tension. To assess the RhoA activity in the HGPS cell lines a FRET based activity sensor, called Raichu, was used (Yoshizaki et al., 2003). By measuring the FRET index of this sensor one can measure the activity of RhoA, with a greater FRET index relating to increased RhoA activation. Raichu-RhoA was transfected into primary cell lines and imaged using a spinning disk confocal microscope. Single plane images close to the cell bottom, incorporating the bulk of the cell body, were captured (Fig 5.1A). The background signal was subtracted, and the FRET index of each pixel calculated. The average FRET index for each cell was determined using a whole cell mask, using the direct acceptor excitation channel as the reference. This average FRET index per cell was then plotted (Fig 5.1B). This was conducted for one of the three pairs of cell lines (Pair 1: AG06917/GM00498), and within this pair the average FRET index was greater within the HGPS cell line than the healthy counterpart. This would suggest that RhoA activity is elevated within progerin-expressing cells, at least for this cell line.

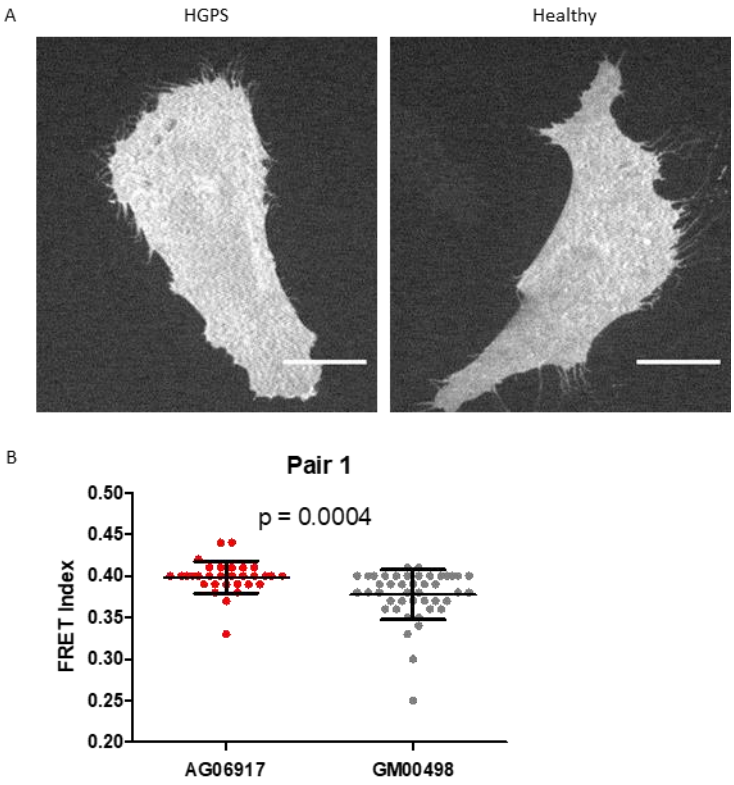

Figure 5.1: Measurement of RhoA activity via Raichu-FRET sensor. (A) FRET imaging of cell lines from pair 1 (AG06917/GM00498) was conducted, with the acceptor channel image shown. Scale bar = 20µm. (B) FRET index per pixel was calculated and averaged to yield the mean FRET index per cell. Mean ± SD plotted. Statistical significance tested using an unpaired t-test (Significance = $p < 0.05$). N = 3, $n \geq 31$.

5.3.2. RhoA Signalling as Driver of Adhesion Phenotype?

To investigate whether RhoA signalling plays a role in the increased adhesion area of the HGPS cell lines, the patient and healthy cell lines were treated with the ROCK inhibitor Y-27632 (Uehata *et al.*, 1997). This compound selectively inhibits both isoforms of ROCK, ROCK-I and ROCK-II, by competing with ATP for binding within the catalytic site (Ishizaki *et al.*, 2000). Cells were treated with 10µM Y-27632 for two days, grown on glass coverslips and then labelled with antibodies targeting paxillin and imaged using a confocal microscope (Fig 5.2A). Control cells were instead treated with an equivalent volume of DMSO to act as a vehicle control. The area of each of the focal adhesions was then analysed, as described previously (see section 3.3.3), and then the adhesions areas within each cell averaged to give an average adhesion area per cell (Fig 5.2B). For all three cell pairs a reduction in adhesion area was seen in the

HGPS cell lines upon Y-27632 treatment when compared to their respective vehicle control. This change was also seen in the healthy cell lines. The number of adhesions per cell was also counted and normalised to the cell area (Fig 5.2C). The adhesion number per μm^2 was significantly reduced in two of the three HGPS cell lines upon treatment (pair 1 and 3), which was again also seen in the healthy cell lines (Fig 5.2D).

5.3.3. Potential Alterations in Nuclear Import Mechanics?

The regulation of the nuclear import of transcription factors, such as YAP/TAZ, plays an important role in the cell's response to mechanical stresses. As such, a potential defect in nuclear import was explored by visualising the localisation of the Ran, the small GTPase critical to balancing the rates of import and export of actively transported cargo into and out of the nucleus. Cells were grown on glass coverslips coated with fibronectin and labelled with antibodies targeting Ran, which were then imaged via confocal microscopy (Fig 5.3A). Cells were also stained with Hoechst 33342 and phalloidin-alexafluor-670 to provide a nuclear and cellular marker respectively. The nucleus was then identified using an intensity threshold of the nuclear marker to generate a mask, and a nuclear ROI generated. The intensity of Ran labelling within this ROI was then measured (Fig 5.3B). A small but significant reduction in nuclear Ran levels was seen for two of the three cell pairs (pair 1 and 3) when compared to their healthy counterparts.

Mechanical stimuli can control the transport of the transcription factor YAP into the nucleus via direct action on the nucleus. This opening of the NPCs by force application may be facilitated by the interaction of Nup153, a nuclear basket constituent, and SUN1. The loss of this protein from the NPC could therefore indicate that there would be a loss of this mechanically linked nuclear import. To assess whether there was a loss of Nup153 within the HGPS cell lines in this study, cells were labelled for Nup153 and imaged via confocal microscopy (Fig 5.4A). With Hoechst as a nuclear marker, the intensity of the Nup153 labelling within the nucleus was analysed (Fig 5.4B). There was no significant change in Nup153 nuclear intensity within the individual HGPS cell lines, and in fact the nuclear levels of Nup153 were slightly increased in

two of the three cell lines. This shows that Nup153 was not lost from the nucleus in the HGPS cell lines analysed in this work.

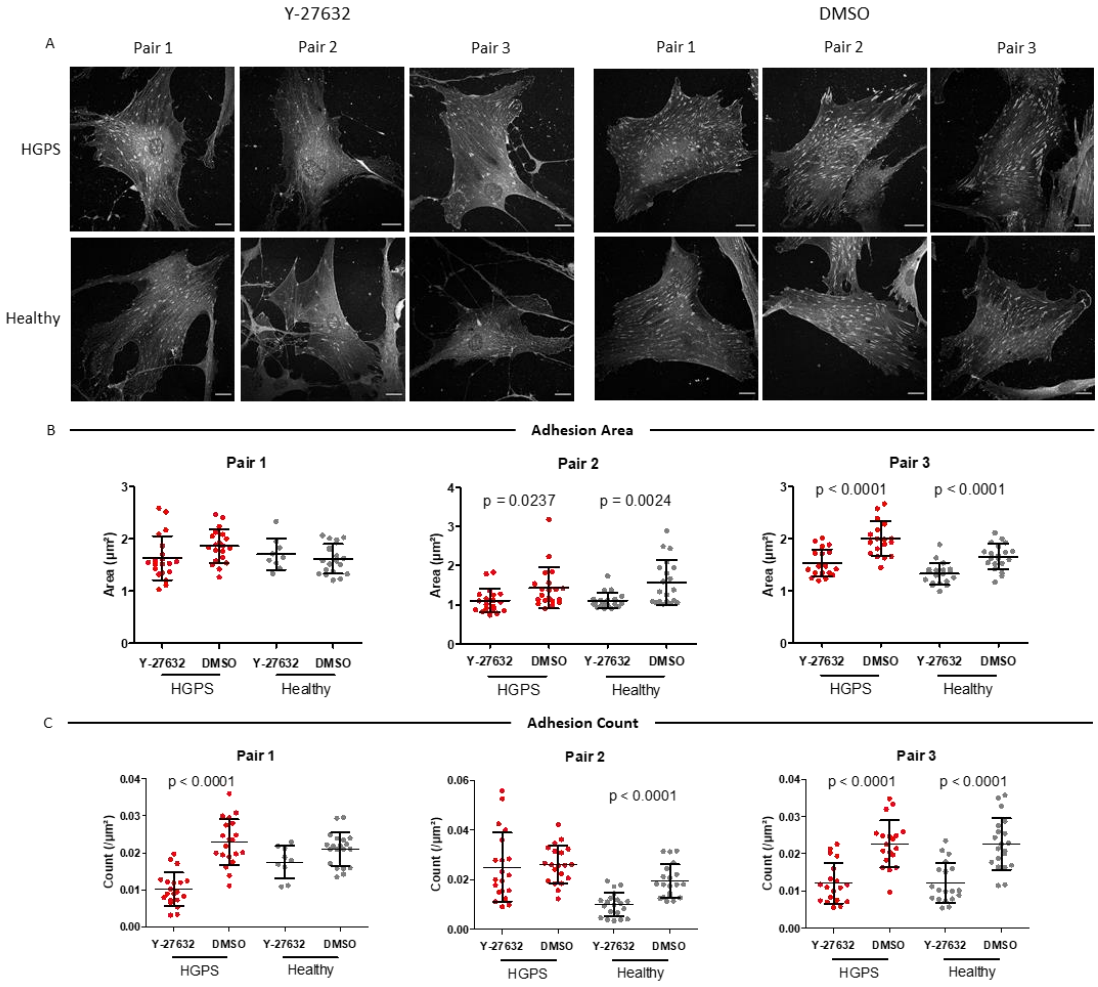

Figure 5.2: Assessment of focal adhesion phenotype upon ROCK inhibition. (A) Cell lines were either treated with 10µM Y-27632 or equivalent volume of vehicle control (DMSO), labelled for paxillin and imaged. Scale bar = 20µm (B) The average adhesion area for each cell was calculated. (C) The number of adhesions per cell was determined, normalised to the cell area. Mean ± SD plotted. Statistical significance tested using an unpaired t-test (Significance = $p < 0.05$). N = 2, $n \geq 20$.

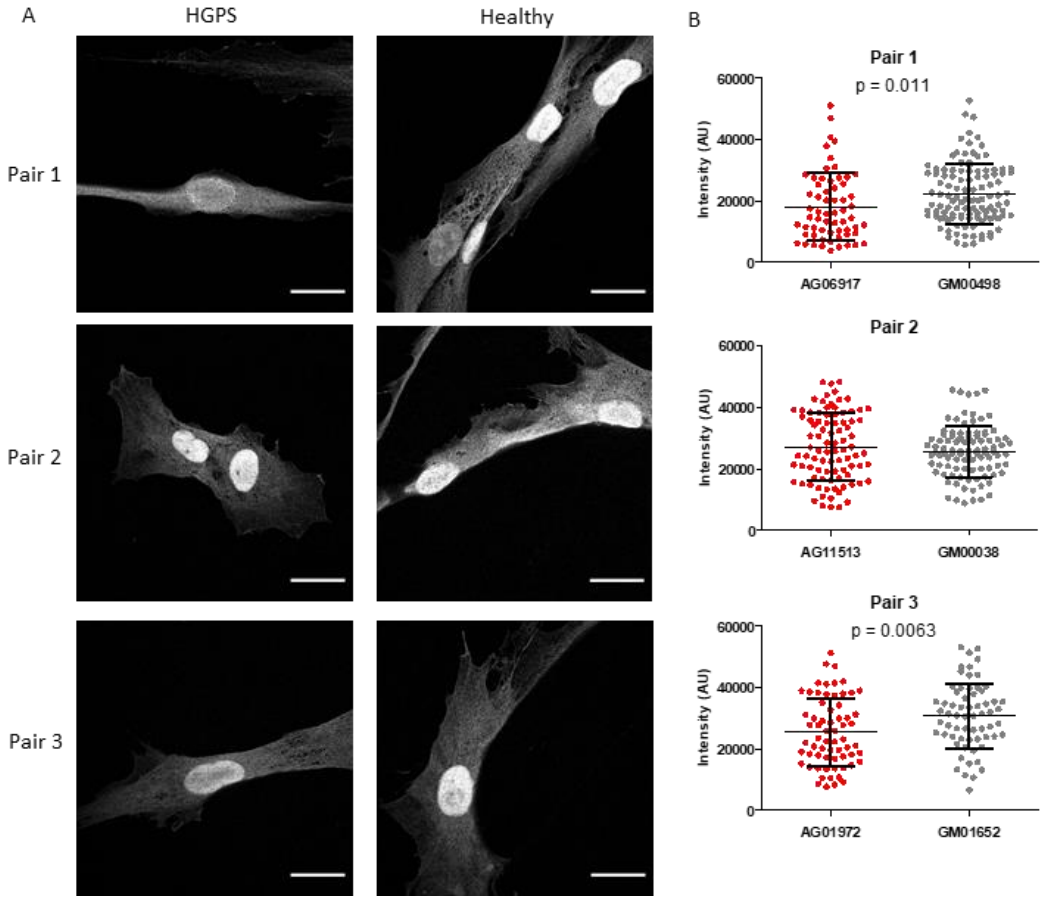

Figure 5.3: Nuclear localisation of Ran in HGPS cell lines. (A) Cells were labelled for Ran and imaged. Scale Bar = 20µm. (B) The intensity of Ran labelling within the nucleus was measured. Mean ± SD plotted. Statistical significance tested using an unpaired t-test (Significance = $p < 0.05$). N = 3, $n \geq 62$.

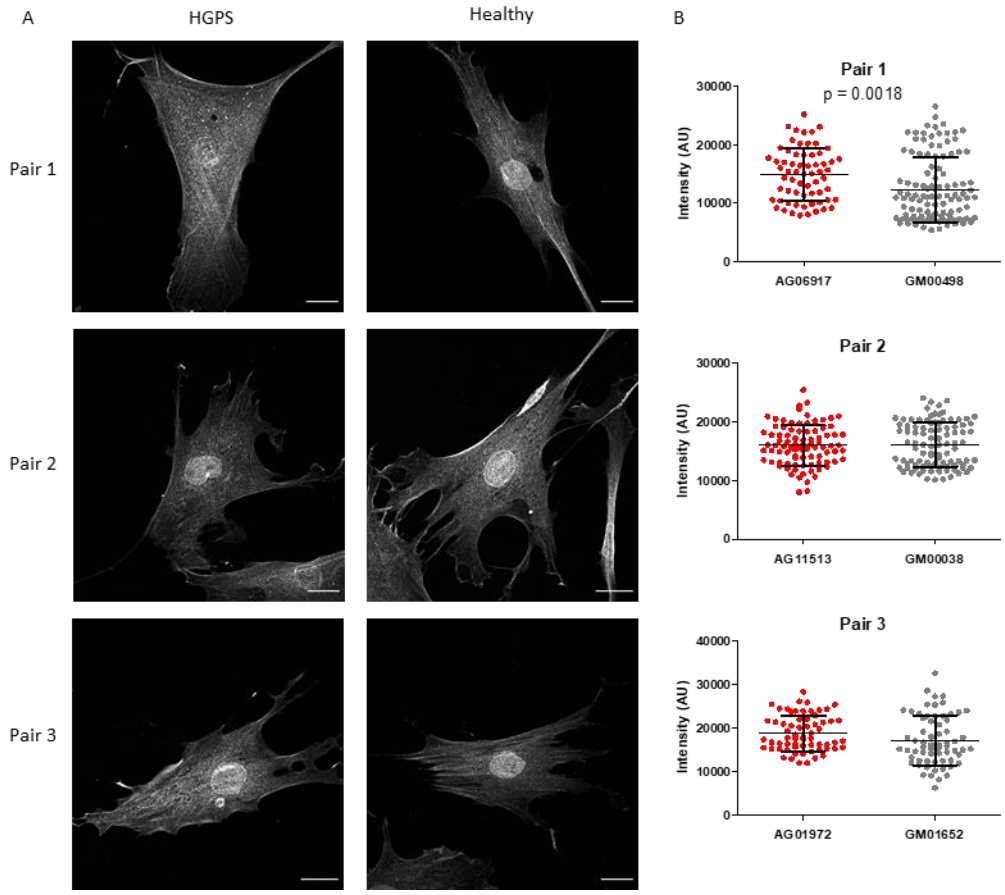

Figure 5.4: Nuclear localisation of Nup153 in HGPS cell lines. (A) Cells were labelled for Nup153 and imaged. Scale bar = 20µm. (B) The intensity of Nup153 labelling within the nucleus was measured. Mean ± SD plotted. Statistical significance tested using an unpaired t-test (Significance = $p < 0.05$). N = 3, $n \geq 62$.

5.3.4. Effect of HGPS Treatment on Focal Adhesion Phenotype

One of the prominent phenotypes that has been seen across all three of the HGPS cell lines used in this study has been an increase in the size of the focal adhesions. As inhibition of ROCK reduced the size and number of adhesions in these cells, it appears that RhoA/ROCK signalling plays a role in establishing this phenotype. However, this does not establish whether the changes in adhesion phenotype are directly related to the accumulation of progerin within the nuclei of these cells. HGPS cells can be treated with farnesyltransferase inhibitors to prevent the accumulation of progerin, and thus alleviate the HGPS pathology (Capell *et al.*, 2005; Glynn & Glover, 2005; Toth *et al.*, 2005). As such, treating cells with one such inhibitor, lonafarnib, was conducted. The cell lines from pair 1 (AG06917/GM00498) were treated with daily doses of the farnesyltransferase inhibitor lonafarnib (at 2µM) for three days, based upon the most

effective concentration used by Capell *et al.* (2005) in their assessment of lonafarnib treatment efficiency. To assess the effectiveness of the treatment, tile scan images of treated cells were captured and the number of nuclei displaying deformed appearance, namely invaginations of the NE and nuclear blebbing, were counted. The percentage of total nuclei that had a deformed appearance was then calculated for each cell line (Fig 5.5A). Hoechst 33342 staining or lamin A/C antibody labelling was used to mark the nuclei for this purpose (Fig 5.5B), and all images were blinded prior to manual categorisation of the nuclei. Treatment of HGPS with 2μM lonafarnib reduced the percentage of deformed nuclei from an average of 63.5% to 47.5%. This decrease is lower than would be expected for such a treatment regimen (Capell *et al.*, 2005), but does show that the treatment did reduce the proportion of cells displaying the characteristic nuclear phenotype of progerin accumulation. To test the dependence of the adhesion phenotype on progerin accumulation, AG06917 cells treated with lonafarnib were fixed and labelled for paxillin and imaged by confocal microscopy (Fig 5.6A). The focal adhesions were then identified as described previously and their area calculated; these were then averaged to give an average focal adhesion area per cell (Fig 5.6B). Lonafarnib treatment did not significantly alter the average focal adhesion area of the AG06917 HGPS cell line. The adhesion count was also determined for the treat cells (Fig 5.6C) and was found to be unchanged upon lonafarnib treatment.

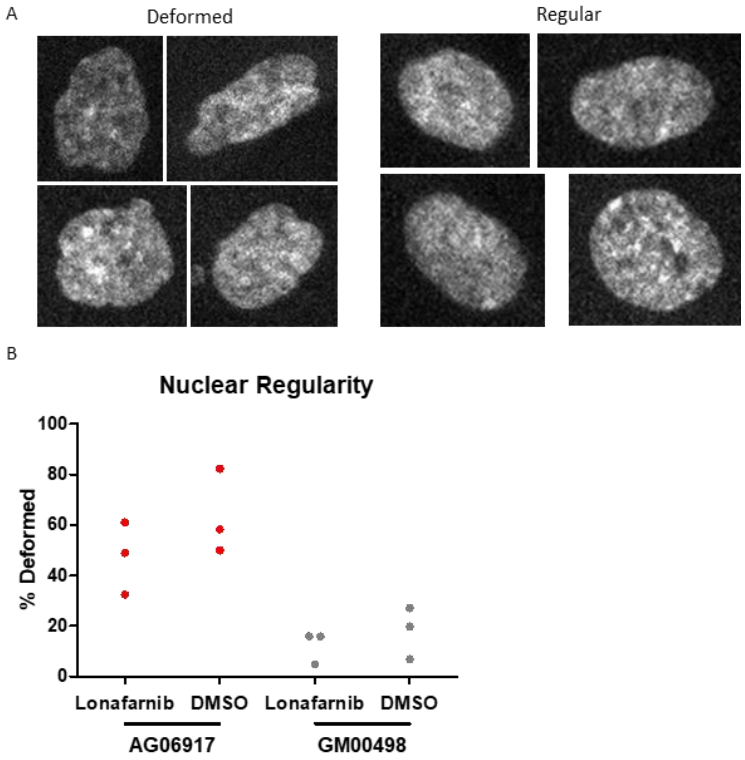

Figure 5.5: Characterisation of nuclear morphology upon lonafarnib treatment. (A) The nuclei of cells from pair 1 (AG06917/GM00498) were marked with either lamin A/C antibody labelling or Hoechst 33342 staining. Nuclei were then categorised as either "deformed" or "regular" based on visual assessment. (B) The percentage of deformed nuclei relative to the total nuclei count was calculated for cells treated with either 2µM lonafarnib or an equivalent volume of vehicle control (DMSO). Mean values plotted. Statistical significance tested using an unpaired t-test (Significance = $p < 0.05$). $N = 3$, $n \geq 441$.

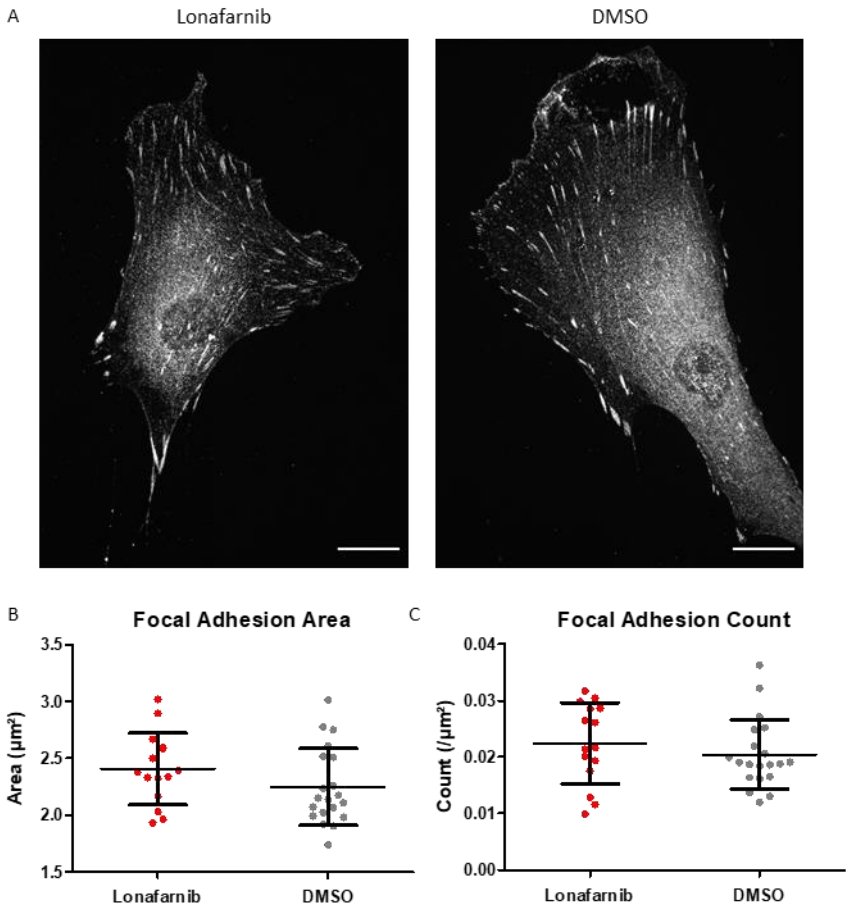

Figure 5.6: Assessment of effect of lonafarnib treatment on focal adhesion phenotype. (A) AG06917 cells were treated with either 2µM lonafarnib or an equivalent volume of vehicle control (DMSO) and labelled for paxillin. Scale bar = 20µm. (B) The average focal adhesion area for each cell was calculated. (C) The number of adhesions per cell was counted and normalised to the cell area. Mean ± SD plotted. Statistical significance tested using an unpaired t-test (Significance = $p < 0.05$). N = 3, $n \geq 15$.

5.4. Discussion

The aim of this chapter was to assess various mechanisms that could play a role in establishing the mechanical sensitivity of HGPS cells, as well as whether these factors had influence over the adhesion phenotype that was previously observed. Observation of RhoA activity in the AG06917 HGPS cell line showed an elevated level of RhoA activity relative to the healthy counterpart. Inhibition of ROCK, a downstream effector of RhoA, led to a reduction in both the area and number of focal adhesions within all the HGPS cell lines. While these observations do not establish RhoA signalling as the causative factor, it does demonstrate that the increased adhesion areas observed in the HGPS cell lines are influenced by RhoA activity, and that elevated RhoA activity presents a viable explanation for the phenotype seen in the HGPS cell lines. Given that increased RhoA/ROCK signalling has been reported to contribute to reduced mitochondrial function (Kang *et al.*, 2017) and cellular senescence (Mu *et al.*, 2020) in HGPS cells, this suggests that increased RhoA activity and signalling via ROCK may be highly influential in establishing the HGPS cellular phenotype.

Whilst elevated RhoA provides a potential explanation for the increased focal adhesion area and number in HGPS, it does not answer the question of whether the phenotype is the direct result of progerin accumulation within the nucleus. To try and address this question, the AG06917 cell line was treated with lonafarnib, a farnesyltransferase inhibitor that prevents the farnesylation of progerin and alleviates the HGPS nuclear phenotype (Capell *et al.*, 2005). This treatment did not have an influence on either the average focal adhesion area or the number of adhesions per cell in this cell line. This is surprising, as treatment with lonafarnib reversed the increased actin polymerisation phenotype observed by Mu *et al.* (2020), which was attributed to elevated RhoA activity. It is possible that the treatment within this experiment did not reduce progerin accumulation in a sufficient proportion of the cell population to have an observable effect upon the focal adhesions, and further work is needed to eliminate this possibility. However, based upon the data in this current work, it appears that reducing progerin accumulation within the nucleus alone is insufficient to trigger a reversal of the enlarged focal adhesions within the HGPS cells.

One potential mechanism by which HGPS cells may experience increased sensitivity to mechanical forces is through an inability to control the import of transcription factors in response to mechanical stimuli. This mechanism is suggested by the reduced nuclear YAP seen in the HGPS cell lines grown on 1.5kPa PDMS substrates (Fig 4.4B). Ran, whose concentration in the nucleus is important for regulating cargo import, has also been reported to be lost from the nucleus in HGPS cell lines (Kelly *et al.*, 2011; Larrieu *et al.*, 2018). The loss of nuclear YAP was also observed in this study, providing further evidence to the potential role of nuclear import in the HGPS phenotype. Nup153, a constituent of the nuclear basket which may facilitate force transmission to the NPC via SUN1 (Donnaloja *et al.*, 2019), could also play a role in the loss of mechanically controlled nuclear import in HGPS. It's loss from the nucleus has been shown in one HGPS cell line, AG11513 (Larrieu *et al.*, 2018), and this was demonstrated to play a role in maintaining the HGPS phenotype. However, assessment of the nuclear levels of Nup153 in this study did not find a loss of Nup153 from the nucleus when compared to their healthy counterparts, in agreement with the data from Snow *et al.* (2013). While this does not eliminate the possibility of reduced nuclear import in response to mechanical stimuli, it does eliminate the potential SUN1-Nup153 interaction as a causal factor.

6. Discussion

The ability of cells to sense and respond to the mechanical forces that surround them is vital to their development, function, and survival. The cell can respond to these forces thanks to a variety of mechanisms that are sensitive to the application of forces. One such mechanism is the ability to transmit forces directly from outside of the cell to the nucleus, where force stimuli can trigger both the import of transcription factors and alter the chromatin structure to control gene expression. These changes in gene expression then facilitate the cell's response to the force stimulus and promote the desired behaviour. An inability to respond appropriately to force stimuli will hamper a cell's function and may, if the force stresses are too great, result in the cell becoming damaged and ultimately die. This is especially important in tissues that experience greater force stresses than average, such as the muscle and vascular tissues. Patients afflicted with the premature ageing disease HGPS predominantly die due to cardiovascular disease (Gordon *et al.*, 2014), brought about by a breakdown of the arterial walls. This has led to the hypothesis that the expression and accumulation of the mutant form of lamin A, progerin, makes cells susceptible to damage due to mechanical stresses. However, the exact cause of this mechanical sensitivity has yet to be fully elucidated. The aim of this work was to explore the various components of the mechanotransduction pathway to ascertain whether there were any changes within these structures that might explain the force sensitivity within progerin-expressing cells.

Observation of the focal adhesions within HGPS cell lines demonstrated a consistent phenotype of enlarged focal adhesions for cells plated onto a fibronectin-coated substrate. The talin within these adhesions is under increased tension, demonstrating increased tensile forces at the adhesion. The enlarged adhesions were accompanied by increased actin fibre stiffness, suggesting elevated acto-myosin contractility. These increases would indicate an increased engagement of the cell to the extracellular environment, as well as increased force transmission across the adhesions and actin cytoskeleton. However, these increases were not accompanied by an increase in tension at the LINC complex, indicating that the increased force stimuli were not being transmitted across the NE. The fact that stable progerin expression within NIH-3T3 cells induced enlarged adhesions suggests that progerin expression alone is sufficient

to bring about this phenotype. Inhibition of RhoA signalling via ROCK influenced the adhesion phenotype, and RhoA activity was increased within the HGPS cell assessed. This suggests that RhoA signalling plays a role in facilitating the phenotype of the HGPS cells (Summarised by cell line in Table 6.1).

Table 6.1: Summary of experimental results by cell line. For each experiment conducted, the change in the average value of each HGPS cell line relative to its healthy control is noted. An upward green arrow indicates an increase, a grey dash indicates no change, and a downward red arrow indicates a decrease. Statistical significance was used as an indicator of increase/decrease; except for stress fibre tension, which was judged by observation of the image data as described previously.

Condition	Cell Line		
	AG06917 (Age 3)	AG11513 (Age 8)	AG01972 (Age 14)
Nuclear Tension	↓	–	–
Adhesion Tension	↑	↑	–
Adhesion Area	↑	↑	↑
Adhesion Count	–	↑	–
Adhesion Area (PDMS Substrates)	–	↑	↑
Stress Fibre Tension	↑	↑	↑
Cell Traction Force	–	–	↑
YAP Nuclear Localisation	↓	↑	–
YAP Nuclear Localisation (Stiff PDMS Substrate)	↓	↑	↓
YAP Nuclear Localisation (Soft PDMS Substrate)	↓	↑	↓
YAP Protein Level	–	↓	–
ROCK Inhibition – Adhesion Area Change	–	↓	↓
ROCK Inhibition – Adhesion Count Change	↓	–	↓

Based on these observations, this work presents a hypothesis that provides a potential model for progerin-based force sensitivity (Fig 6.1). Elevated RhoA activity and signalling via ROCK within HGPS cells stimulates acto-myosin contractility and promotes focal adhesion maturation. This results in increased tension across talin, as well as elevated force propagation within the cell. However, this force is not effectively transmitted to the NE via the LINC complex. This lack of force transmission prevents the dynamic regulation of RhoA in response to force stresses, and instead RhoA activity remains consistently high; promoted by the increased force transmission across the adhesions/stress fibres. This impairs the cell's ability to adequately respond to these stresses, leading the cell to become damaged and ultimately perish as a result, which on the larger scale leads to degradation in tissues subject to high force stresses. This tissue damage within the vasculature of HGPS patients results in atherosclerosis, cardiovascular disease and ultimately the death of the patient. This model would explain the increased cell death seen in the tissues subject to elevated force stresses (Booth *et al.*, 2015; Kim *et al.*, 2018; Verstraeten *et al.*, 2008) and fits alongside other observations made within the literature. Indeed, elevated RhoA activity has already been linked to the HGPS cellular phenotype (Kang *et al.*, 2017; Mu *et al.*, 2020), and a reduced response by the nucleus to force stresses has also been observed (Booth *et al.*, 2015). Dynamic regulation of RhoA activity is also vital for proper adaptation to shear stresses in endothelial cells (Tzima *et al.*, 2001). The activity of RhoA and RhoA signalling through ROCK is also known to play a role in the development of cardiovascular disease through a variety of different mechanisms that promote inflammation and result in tissue damage (Shimokawa *et al.*, 2016). The elevated RhoA activity resulting from a lack of mechanically induced response could therefore lead to atherosclerosis through these mechanisms.

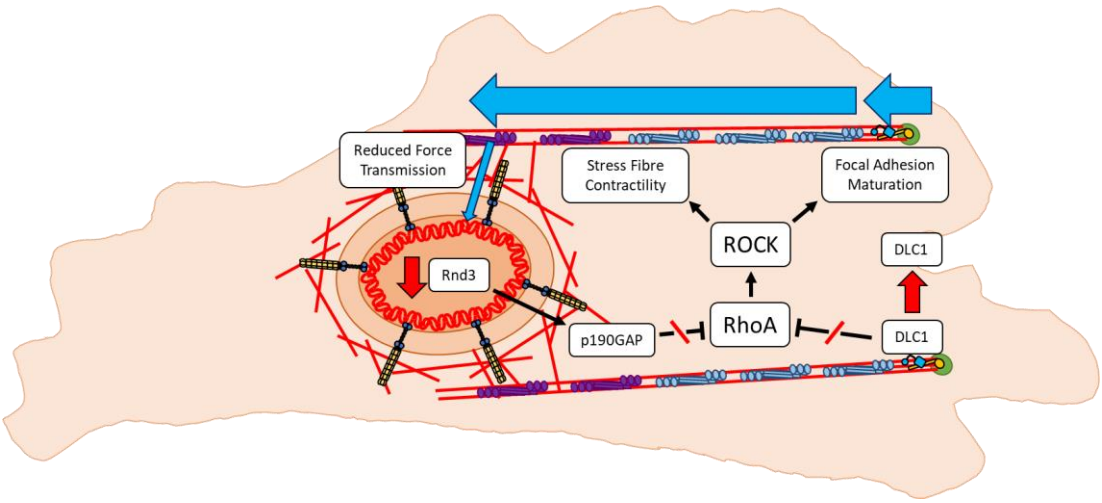

Figure 6.1. Proposed model for the causal factor of mechanical sensitivity in progerin-expressing cells. The accumulation of progerin within the nucleus creates a disconnect between the forces transferred across the actin cytoskeleton and the forces experienced by the NE, potentially as a result of changes in perinuclear actin structure. This disconnect prevents the dynamic regulation of RhoA activity in response to force stresses, and instead RhoA activity is consistently high. This promotes adhesion maturation and acto-myosin contractility, further reinforcing the phenotype of elevated RhoA activity. The cause of the increased RhoA activity may be due to either the loss of DLC1 from the adhesions or the downregulation of Rnd3, both of which act as antagonists of RhoA activity in response to mechanical forces.

However, there are two outstanding questions that remain to be answered before this model can provide a comprehensive explanation for the increased force sensitivity of HGPS cells. The first of those questions is what causes the disconnect between the forces transmitted across the acto-myosin cytoskeleton and those experienced at the NE. The disconnect is likely not a physical disconnect between the LINC complex and actin cytoskeleton, as disrupting this connection does not necessarily prevent mechanically regulated gene transcription (Lombardi *et al.*, 2011). Indeed, physically disconnecting the LINC complex from the actin cytoskeleton can in fact improve the survivability of HGPS cells subjected to mechanical stresses (Kim *et al.*, 2018). It has however been observed that the structure of the perinuclear actin cap, a cradle of actin filaments that is associated with and encompasses the ONM, is disrupted in HGPS cells (Khatau *et al.*, 2009). Transmembrane actin-associated nuclear (TAN) lines, concentrations of LINC complex proteins that bind to perinuclear actin cables (Luxton *et al.*, 2010), also have reduced engagement with perinuclear actin fibres in progerin-expressing NIH-3T3 cells (Chang *et al.*, 2019). This data would suggest that whilst the nucleus is still physically linked to the actin cytoskeleton, that connection is looser;

perhaps this loosening in actin engagement has a negative impact upon the ability to transmit forces from the wider actin cytoskeleton to the NE.

The second outstanding question for this model is what causes the increased RhoA activity within the HGPS cells. This increase in RhoA activity may be due to an inability to activate key RhoGAPs that are usually responsive to mechanical cues (Fig 6.1). Two key RhoGAPs that fulfil this function in healthy cells are p190GAP and Deleted in liver cancer 1 (DLC1). DLC1 is recruited to focal adhesions via it's binding to the R8 domain of talin (Haining *et al.*, 2018), where it is activated and inhibits RhoA activity (Li *et al.*, 2011). Unfolding of this domain by tensile forces prevents the binding of DLC1 and therefore inhibits its activity (Haining *et al.*, 2018). Usually, enlarged adhesions display reduced tension across individual talin molecules (Kumar *et al.*, 2016), however the enlarged adhesions of the HGPS cells demonstrated an increase in tension across talin. It is therefore possible that in a healthy context DLC1 is recruited to mature adhesions to inhibit RhoA activity and facilitate adhesion turnover (Burridge *et al.*, 2019), but in the context of HGPS this negative feedback does not occur due to elevated talin tension. p190GAP can also be activated in response to mechanical cues and has been shown to play an important role in regulating RhoA activity in response to elevated substrate stiffness (Monaghan-Benson *et al.*, 2018), as well as in regulating the response of endothelial cells to shear stress (Yang *et al.*, 2011). Rnd3, a member of the Rnd subfamily of small GTPases, has been shown to promote the activity of p190GAP and thus act as an antagonist for RhoA activity (Wennerberg *et al.*, 2003). The activity of Rnd3 in this capacity plays a role in regulating RhoA activity in response to substrate stiffness, and changes substrate stiffness are sufficient to alter the expression level of Rnd3 (Monaghan-Benson *et al.*, 2018). As such it is possible that Rnd3 expression, and thus control of RhoA activity, can be stimulated by mechanical stresses, and that the loss of Rnd3 expression due to a disconnect between nuclear and cytoskeletal forces is a driving factor behind the elevated RhoA activity in HGPS cells.

Whilst this work provides evidence toward this model, there are limitations to the approaches used that should be considered when interpreting the experimental results. The use of multiple age matched HGPS and healthy cell lines is designed to control both for the variability between genetically unique individuals and potential age-

related factors. However, the fact that the cells are taken from individuals of a certain age does not guarantee that the cells sampled will be in an equivalent point in the process of senescence. Since only a sample of the total population is taken during a skin biopsy, it is possible that the extracted cells are in a predominantly different senescent state to the total tissue population in that individual. Age matching therefore mitigates, but does not eliminate, the possibility that the cell line results are influenced by differences in senescent state.

The use of AFM as a means of measuring cell stiffness also has its limitations. The shape of the acquired force-distance curves, and the resulting young's modulus calculations, can be influenced by experimental factors other than the surface mechanics, including the shape of the indenter, the speed of approach and the force threshold used (Chiou *et al.*, 2013; Takechi-Haraya *et al.*, 2019). These factors were kept constant throughout the experiments in this study, allowing for relative comparison between samples. However, they need to be considered when assessing the measured values themselves, especially if comparing to values obtained in other studies.

The FRET biosensors also come with limitations. The process of FRET can occur between any two fluorophores with overlapping spectra so long as they are in proximity to one another. In the case of tension biosensors, it is the proximity/separation of the linked donor and acceptor fluorophores, and resulting intramolecular FRET changes, that is desired. However, if the sensor molecules are crowded together, then there is the possibility for FRET between adjacent donor/acceptor fluorophores, resulting in intermolecular FRET (Cost *et al.*, 2015); a FRET that is not directly related to applied forces. The level of intermolecular FRET can be measured using a pair of constructs, each containing one of the two fluorophores, which are then co-expressed in the same cell (Cost *et al.*, 2015). Such an evaluation has been conducted for the talin-TS used in this study (intermolecular FRET was found to be ~20% of intramolecular FRET) (Kumar *et al.*, 2015), however the nesprin-TS has not been evaluated in this fashion. Some proportion of the measured FRET index could therefore correspond to intermolecular FRET, which should be considered when evaluating the results within this study.

There is also a limitation to consider when interpreting the TFM data presented in this work, introduced by the method of average force calculation. The total force vector population for the entire field of view was used to calculate the averages, which would include measurements from areas of the gel where the cell of interest is not present. As such, the values shown in this study may be an underestimation of the cell traction forces and influenced by the cell area; both factors that should be considered when interpreting the data. The lonafarnib treatment data, namely the assessment of treatment effectiveness by nuclear morphology observation, is a subjective measurement based upon visual observation. Blinding the images prior to analysis can mitigate the subjective bias between conditions that this may introduce, however it does not eliminate subjective bias from the analysis. This bias will cause some variability in the results that must be considered when interpreting this data.

Answering the outstanding questions presented by this work will require additional experimentation, however it does provide a strong basis for a model that explains the mechanical sensitivity of cells due to progerin expression. A disconnect between the forces transmitted through the cytoskeleton and the NE prevents the mechanically regulated control of RhoA activity, which in turn prevents a dynamic response to force stresses. This loss of dynamic control leaves cells susceptible to mechanically induced damage in high force stress tissues, leading to degradation in these tissues. Inhibiting RhoA activity may therefore be a viable strategy for preventing the cardiovascular disease that acts as the predominant cause of death for HGPS patients, and thus extend the lifespan of these individuals. The parallels between HGPS and the natural ageing process also present the possibility that RhoA activity plays a role in age-related cardiovascular disease. Indeed, increased focal adhesion and stress fibre formation, as well as elevated FAK activity, have already been attributed to the senescent phenotype (Cho *et al.*, 2004).

Bibliography

Adelstein RS. ‘Regulation of contractile proteins by phosphorylation.’ *J Clin Invest*. 1983; 72(6):1863-6.

Aebi U, Cohn J, Buhle L, Gerace L. ‘The nuclear lamina is a meshwork of intermediate-type filaments.’ *Nature*. 1986 Oct 9-15; 323(6088): 560-4.

Akhremitchev BB, Walker GC. ‘Finite Sample Thickness Effects on Elasticity Determination Using Atomic Force Microscopy.’ *Langmuir*. 1999; 15(17): 5630–5634

Almendáriz-Palacios C, Gillespie ZE, Janzen M, Martinez V, Bridger JM, Harkness TAA, Mousseau DD, Eskiw CH. ‘The Nuclear Lamina: Protein Accumulation and Disease.’ Biomedicines. 2020 Jul 1; 8(7): 188.

Amano M, Ito M, Kimura K, Fukata Y, Chihara K, Nakano T, Matsuura Y, Kaibuchi K. ‘Phosphorylation and activation of myosin by Rho-associated kinase (Rho-kinase).’ *J Biol Chem*. 1996; 271(34): 20246-9.

Aragona M, Panciera T, Manfrin A, Giulitti S, Michielin F, Elvassore N, Dupont S, Piccolo S. ‘A mechanical checkpoint controls multicellular growth through YAP/TAZ regulation by actin-processing factors.’ *Cell*. 2013 Aug 29; 154(5): 1047-1059

Arribas SM, Hinek A, González MC. ‘Elastic fibres and vascular structure in hypertension.’ *Pharmacol Ther*. 2006 Sep; 111(3): 771-91.

Arsenovic PT, Ramachandran I, Bathula K, Zhu R, Narang JD, Noll NA, Lemmon CA, Gundersen GG, Conway DE. ‘Nesprin-2G, a Component of the Nuclear LINC Complex, Is Subject to Myosin-Dependent Tension.*’ Biophys J.* 2016; 110(1) :34-43.

Aumailley M, Bruckner-Tuderman L, Carter WG, Deutzmann R, Edgar D, Ekblom P, Engel J, Engvall E, Hohenester E, Jones JC, Kleinman HK, Marinkovich MP, Martin GR, Mayer U, Meneguzzi G, Miner JH, Miyazaki K, Patarroyo M, Paulsson M, Quaranta V, Sanes JR, Sasaki T, Sekiguchi K, Sorokin LM, Talts JF, Tryggvason K, Uitto J, Virtanen I, von der Mark K, Wewer UM, Yamada Y, Yurchenco PD. ‘A simplified laminin nomenclature.’ *Matrix Biol*. 2005 Aug; 24(5): 326-32.

Baarlink C, Wang H, Grosse R. ‘Nuclear actin network assembly by formins regulates the SRF coactivator MAL.’ *Science*. 2013 May 17; 340(6134): 864-7.

Balaban NQ, Schwarz US, Riveline D, Goichberg P, Tzur G, Sabanay I, Mahalu D, Safran S, Bershadsky A, Addadi L, Geiger B. ‘Force and focal adhesion assembly: a close relationship studied using elastic micropatterned substrates.’ *Nat Cell Biol*. 2001 May; 3(5): 466-72.

Barczyk M, Carracedo S, Gullberg D. ‘Integrins.’ *Cell Tissue Res*. 2010 Jan; 339(1): 269-80.

Belin BJ, Cimini BA, Blackburn EH, Mullins RD. 'Visualization of actin filaments and monomers in somatic cell nuclei.' *Mol Biol Cell*. 2013 Apr; 24(7): 982-94.

Bellis SL, Miller JT, Turner CE. 'Characterization of tyrosine phosphorylation of paxillin in vitro by focal adhesion kinase.' *J Biol Chem*. 1995; 270(29): 17437–17441.

Benham-Pyle BW, Pruitt BL, Nelson WJ. 'Mechanical strain induces E-cadherin-dependent Yap1 and β-catenin activation to drive cell cycle entry.' *Science*. 2015 May 29; 348(6238): 1024-7.

Bera M, Sengupta K. 'Nuclear filaments: role in chromosomal positioning and gene expression.' *Nucleus*. 2020 Dec; 11(1): 99-110.

Bergo MO, Gavino B, Ross J, Schmidt WK, Hong C, Kendall LV, Mohr A, Meta M, Genant H, Jiang Y, Wisner ER, Van Bruggen N, Carano RA, Michaelis S, Griffey SM, Young SG. 'Zmpste24 deficiency in mice causes spontaneous bone fractures, muscle weakness, and a prelamin A processing defect.' *Proc Natl Acad Sci USA*. 2002; 99(20): 13049-54.

Bershadsky AD, Ballestrem C, Carramusa L, Zilberman Y, Gilquin B, Khochbin S, Alexandrova AY, Verkhovsky AB, Shemesh T, Kozlov MM. 'Assembly and mechanosensory function of focal adhesions: experiments and models.' *Eur J Cell Biol*. 2006 Apr; 85(3-4): 165-73.

Birch HL. 'Extracellular Matrix and Ageing.' *Subcell Biochem*. 2018; 90: 169-190.

Booth-Gauthier EA, Alcoser TA, Yang G, Dahl KN. 'Force-Induced Changes in Subnuclear Movement and Rheology.' *Biophysical Journal*. 2012; 103(12): 2423-2431.

Booth EA, Spagnol ST, Alcoser TA, Dahl KN. 'Nuclear stiffening and chromatin softening with progerin expression leads to an attenuated nuclear response to force.' *Soft Matter*. 2015; 11(32): 6412-8.

Bos JL, Rehmann H, Wittinghofer A. 'GEFs and GAPs: critical elements in the control of small G proteins.' *Cell*. 2007; 129(5): 865-77.

Boutahar N, Guignandon A, Vico L, Lafage-Proust MH. 'Mechanical strain on osteoblasts activates autophosphorylation of focal adhesion kinase and proline-rich tyrosine kinase 2 tyrosine sites involved in ERK activation.' *J Biol Chem*. 2004; 279(29): 30588–30599.

Briand N, Collas P. 'Lamina-associated domains: peripheral matters and internal affairs.' *Genome Biol*. 2020 Apr 2; 21(1): 85.

Bridger JM, Foeger N, Kill IR, Herrmann H. 'The nuclear lamina. Both a structural framework and a platform for genome organization.' FEBS J. 2007 Mar; 274(6): 1354-61.

Bridger JM, Kill IR. ‘Aging of Hutchinson-Gilford progeria syndrome fibroblasts is characterised by hyperproliferation and increased apoptosis.’ *Exp Gerontol*. 2004 May; 39(5): 717-24.

Broers JL, Peeters EA, Kuijpers HJ, Endert J, Bouten CV, Oomens CW, Baaijens FP, Ramaekers FC. ‘Decreased mechanical stiffness in LMNA-/- cells is caused by defective nucleo-cytoskeletal integrity: implications for the development of laminopathies.’ *Hum Mol Genet*. 2004; 13(21): 2567-80.

Brown MC, Perrotta JA, Turner CE. ‘Identification of LIM3 as the principal determinant of paxillin focal adhesion localization and characterization of a novel motif on paxillin directing vinculin and focal adhesion kinase binding.’ *J Cell Biol*. 1996 Nov; 135(4): 1109-23.

Brown MC, Turner CE. ‘Paxillin: adapting to change.’ *Physiol Rev*. 2004; 84(4): 1315–1339.

Burridge K, Monaghan-Benson E, Graham DM. ‘Mechanotransduction: from the cell surface to the nucleus via RhoA.’ *Philos Trans R Soc Lond B Biol Sci*. 2019 Aug 19; 374(1779): 20180229.

Burridge K, Wittchen ES. ‘The tension mounts: stress fibers as force-generating mechanotransducers.’ *J Cell Biol*. 2013 Jan 7; 200(1): 9-19.

Cai S, Pestic-Dragovich L, O'Donnell ME, Wang N, Ingber D, Elson E, De Lanerolle P. ‘Regulation of cytoskeletal mechanics and cell growth by myosin light chain phosphorylation’. *Am J Physiol*. 1998; 275(5): C1349-56.

Cailleau R, Olivé M, Cruciger QV. ‘Long-term human breast carcinoma cell lines of metastatic origin: preliminary characterization.’ *In Vitro*. 1978; 14(11): 911-5

Calalb MB, Polte TR, Hanks SK. ‘Tyrosine phosphorylation of focal adhesion kinase at sites in the catalytic domain regulates kinase activity: a role for Src family kinases.’ *Mol Cell Biol.* 1995; 15(2): 954–963.

Calvo F, Ege N, Grande-Garcia A, Hooper S, Jenkins RP, Chaudhry SI, Harrington K, Williamson P, Moeendarbary E, Charras G, Sahai E. ‘Mechanotransduction and YAP-dependent matrix remodelling is required for the generation and maintenance of cancer-associated fibroblasts.’ *Nat Cell Biol*. 2013 Jun; 15(6): 637-46.

Campbell ID, Humphries MJ. ‘Integrin structure, activation, and interactions.’ *Cold Spring Harb Perspect Biol*. 2011 Mar 1; 3(3): a004994.

Candelario J, Sudhakar S, Navarro S, Reddy S, Comai L. ‘Perturbation of wild-type lamin A metabolism results in a progeroid phenotype.’ *Aging cell*. 2008; 7(3): 355-367.

Cao K, Capell BC, Erdos MR, Djabali K, Collins FS. ‘A lamin A protein isoform overexpressed in Hutchinson-Gilford progeria syndrome interferes with mitosis in progeria and normal cells.’ *Proc Natl Acad Sci USA*. 2007; 104(12): 4949-54.

Capell BC, Erdos MR, Madigan JP, Fiordalisi JJ, Varga R, Conneely KN, Gordon LB, Der CJ, Cox AD, Collins FS. 'Inhibiting farnesylation of progerin prevents the characteristic nuclear blebbing of Hutchinson-Gilford progeria syndrome.' Proc Natl Acad Sci U S A. 2005 Sep 6; 102(36): 12879-84.

Caridi CP, D'Agostino C, Ryu T, Zapotoczny G, Delabaere L, Li X, Khodaverdian VY, Amaral N, Lin E, Rau AR, Chiolo I. 'Nuclear F-actin and myosins drive relocalization of heterochromatic breaks.' *Nature*. 2018 Jul; 559(7712): 54-60.

Cartwright S, Karakesisoglou I. 'Nesprins in health and disease.' *Semin Cell Dev Biol*. 2014 May; 29: 169-79.

Chang W, Wang Y, Luxton GWG, Östlund C, Worman HJ, Gundersen GG. 'Imbalanced nucleocytoskeletal connections create common polarity defects in progeria and physiological aging.' *Proc Natl Acad Sci USA*. 2019 Feb 26; 116(9): 3578-3583.

Chen HC, Appeddu PA, Isoda H, Guan JL. 'Phosphorylation of tyrosine 397 in focal adhesion kinase is required for binding phosphatidylinositol 3-kinase.' *J Biol Chem*. 1996 Oct 18; 271(42): 26329-34.

Chen HC, Appeddu PA, Parsons JT, Hildebrand JD, Schaller MD, Guan JL. 'Interaction of focal adhesion kinase with cytoskeletal protein talin.' *J Biol Chem*. 1995; 270(28): 16995–16999.

Chhabra D, dos Remedios CG. 'Cofilin, actin and their complex observed in vivo using fluorescence resonance energy transfer.' *Biophys J*. 2005 Sep; 89(3): 1902-8.

Chiou YW, Lin HK, Tang MJ, Lin HH, Yeh ML. 'The influence of physical and physiological cues on atomic force microscopy-based cell stiffness assessment.' *PLoS One*. 2013 Oct 23; 8(10): e77384.

Cho KA, Ryu SJ, Oh YS, Park JH, Lee JW, Kim HP, Kim KT, Jang IS, Park SC. 'Morphological adjustment of senescent cells by modulating caveolin-1 status.' *J Biol Chem*. 2004 Oct 1; 279(40): 42270-8.

Chrzanowska-Wodnicka M, Burridge K. 'Rho-stimulated contractility drives the formation of stress fibers and focal adhesions.' *J Cell Biol*. 1996; 133(6): 1403–1415.

Chuang CH, Carpenter AE, Fuchsova B, Johnson T, de Lanerolle P, Belmont AS. 'Long-range directional movement of an interphase chromosome site.' *Curr Biol*. 2006 Apr 18; 16(8): 825-31.

Chuang HH, Wang PH, Niu SW, Zhen YY, Huang MS, Hsiao M, Yang CJ. 'Inhibition of FAK Signaling Elicits Lamin A/C-Associated Nuclear Deformity and Cellular Senescence.' *Front Oncol*. 2019 Jan 30; 9: 22.

Cooper LA, Shen TL, Guan JL. 'Regulation of focal adhesion kinase by its amino-terminal domain through an autoinhibitory interaction.' *Mol Cell Biol*. 2003 Nov; 23(22): 8030-41.

Corne TDJ, Sieprath T, Vandenbussche J, Mohammed D, Te Lindert M, Gevaert K, Gabriele S, Wolf K, De Vos WH. 'Deregulation of focal adhesion formation and cytoskeletal tension due to loss of A-type lamins.' *Cell Adh Migr*. 2017 Sep 3; 11(5-6): 447-463.

Cost AL, Ringer P, Chrostek-Grashoff A, Grashoff C. 'How to Measure Molecular Forces in Cells: A Guide to Evaluating Genetically-Encoded FRET-Based Tension Sensors.' *Cell Mol Bioeng*. 2015; 8(1): 96-105.

Courtemanche N, Pollard TD. 'Interaction of profilin with the barbed end of actin filaments.' *Biochemistry*. 2013 Sep 17; 52(37): 6456-66.

Crisp M, Liu Q, Roux K, Rattner JB, Shanahan C, Burke B, Stahl PD, Hodzic D. 'Coupling of the nucleus and cytoplasm: role of the LINC complex.' *J Cell Biol*. 2006 Jan 2; 172(1): 41-53.

Dahl KN, Kahn SM, Wilson KL, Discher DE. 'The nuclear envelope lamina network has elasticity and a compressibility limit suggestive of a molecular shock absorber.' *J Cell Sci*. 2004 Sep 15; 117(Pt 20): 4779-86.

Dahl KN, Scaffidi P, Islam MF, Yodh AG, Wilson KL, Misteli T. 'Distinct structural and mechanical properties of the nuclear lamina in Hutchinson-Gilford progeria syndrome.' *Proc Natl Acad Sci USA*. 2006; 103(27): 10271-6.

Davidson PM, Battistella A, Déjardin T, Betz T, Plastino J, Borghi N, Cadot B, Sykes C. 'Nesprin-2 accumulates at the front of the nucleus during confined cell migration.' *EMBO Rep*. 2020 Jul 3; 21(7): e49910.

Davidson PM, Lammerding J. 'Broken nuclei--lamins, nuclear mechanics, and disease.' *Trends Cell Biol*. 2014 Apr; 24(4): 247-56.

Deakin NO, Turner CE. 'Paxillin comes of age.' *J Cell Sci*. 2008 Aug 1;121(Pt 15): 2435-44.

Dechat T, Pfleghaar K, Sengupta K, Shimi T, Shumaker DK, Solimando L, Goldman RD. 'Nuclear lamins: major factors in the structural organization and function of the nucleus and chromatin.' *Genes Dev*. 2008 Apr 1; 22(7): 832-53.

Dekker J, Mirny L. 'The 3D Genome as Moderator of Chromosomal Communication.' *Cell*. 2016 Mar 10; 164(6): 1110-1121.

del Rio A, Perez-Jimenez R, Liu R, Roca-Cusachs P, Fernandez JM, Sheetz MP. 'Stretching single talin rod molecules activates vinculin binding.' *Science*. 2009 Jan 30; 323(5914): 638-41.

Deng L, Fairbank NJ, Fabry B, Smith PG, Maksym GN. 'Localized mechanical stress induces time-dependent actin cytoskeletal remodeling and stiffening in cultured airway smooth muscle cells.' *Am J Physiol Cell Physiol*. 2004; 287(2): C440-8.

Dominguez R. 'Actin filament nucleation and elongation factors--structure-function relationships.' *Crit Rev Biochem Mol Biol*. 2009 Nov-Dec; 44(6): 351-66.

Dominguez R, Holmes KC. 'Actin structure and function.' *Annu Rev Biophys*. 2011; 40: 169-86.

Domogatskaya A, Rodin S, Tryggvason K. 'Functional diversity of laminins.' *Annu Rev Cell Dev Biol*. 2012; 28: 523-53.

Donnaloja F, Jacchetti E, Soncini M, Raimondi MT. 'Mechanosensing at the Nuclear Envelope by Nuclear Pore Complex Stretch Activation and Its Effect in Physiology and Pathology.' *Front Physiol*. 2019 Jul 12; 10: 896.

Donnaloja F, Carnevali F, Jacchetti E, Raimondi MT. 'Lamin A/C Mechanotransduction in Laminopathies.' *Cells*. 2020 May 24; 9(5): 1306.
Doyle AD, Carvajal N, Jin A, Matsumoto K, Yamada KM. 'Local 3D matrix microenvironment regulates cell migration through spatiotemporal dynamics of contractility-dependent adhesions.' *Nat Commun*. 2015 Nov 9; 6: 8720.

Dorner D, Gotzmann J, Foisner R. 'Nucleoplasmic lamins and their interaction partners, LAP2alpha, Rb, and BAF, in transcriptional regulation.' *FEBS J*. 2007 Mar; 274(6): 1362-73.

Dundr M, Ospina JK, Sung MH, John S, Upender M, Ried T, Hager GL, Matera AG. 'Actin-dependent intranuclear repositioning of an active gene locus in vivo.' *J Cell Biol*. 2007 Dec 17; 179(6): 1095-103.

Dupont S. 'Role of YAP/TAZ in cell-matrix adhesion-mediated signalling and mechanotransduction.' *Exp Cell Res*. 2016 Apr 10; 343(1): 42-53.

Dupont S, Morsut L, Aragona M, Enzo E, Giulitti S, Cordenonsi M, Zanconato F, Le Digabel J, Forcato M, Bicciato S, Elvassore N, Piccolo S. 'Role of YAP/TAZ in mechanotransduction.' *Nature*. 2011 Jun 8; 474(7350): 179-83.

Eden S, Rohatgi R, Podtelejnikov AV, Mann M, Kirschner MW. 'Mechanism of regulation of WAVE1-induced actin nucleation by Rac1 and Nck.' *Nature*. 2002 Aug 15; 418(6899): 790-3.

Elosegui-Artola A, Andreu I, Beedle AEM, Lezamiz A, Uroz M, Kosmalska AJ, Oria R, Kechagia JZ, Rico-Lastres P, Le Roux AL, Shanahan CM, Trepat X, Navajas D, Garcia-Manyes S, Roca-Cusachs P. 'Force Triggers YAP Nuclear Entry by Regulating Transport across Nuclear Pores.' *Cell*. 2017 Nov 30; 171(6): 1397-1410.e14.

Elosegui-Artola A, Oria R, Chen Y, Kosmalska A, Pérez-González C, Castro N, Zhu C, Trepat X, Roca-Cusachs P. 'Mechanical regulation of a molecular clutch defines

force transmission and transduction in response to matrix rigidity.' *Nat Cell Biol*. 2016 May; 18(5): 540-8.

Engler AJ, Sen S, Sweeney HL, Discher DE. 'Matrix Elasticity Directs Stem Cell Lineage Specification.' *Cell*. 2006; 126(4): 677-89.

Eriksson M, Brown WT, Gordon LB, Glynn MW, Singer J, Scott L, Erdos MR, Robbins CM, Moses TY, Berglund P, Dutra A, Pak E, Durkin S, Csoka AB, Boehnke M, Glover TW, Collins FS. 'Recurrent de novo point mutations in lamin A cause Hutchinson-Gilford progeria syndrome.' *Nature*. 2003; 423(6937): 293-8.

Etienne-Manneville S, Hall A. 'Rho GTPases in cell biology.' *Nature*. 2002 Dec 12; 420(6916): 629-35.

Ferron F, Rebowski G, Lee SH, Dominguez R. 'Structural basis for the recruitment of profilin-actin complexes during filament elongation by Ena/VASP.' *EMBO J*. 2007 Oct 31; 26(21): 4597-606.

Fournier MF, Sauser R, Ambrosi D, Meister JJ, Verkhovsky AB. 'Force transmission in migrating cells.' *J Cell Biol*. 2010 Jan 25; 188(2): 287-97.

Frame MC, Patel H, Serrels B, Lietha D, Eck MJ. 'The FERM domain: organizing the structure and function of FAK.' *Nat Rev Mol Cell Biol*. 2010 Nov; 11(11): 802-14.

Galbraith CG, Skalak R, Chien S. 'Shear stress induces spatial reorganization of the endothelial cell cytoskeleton. Cell Motil Cytoskeleton.' 1998; 40(4): 317-30.

Gall JG. 'Cajal bodies: the first 100 years.' *Annu Rev Cell Dev Biol*. 2000; 16: 273-300.

Garcia-Mata R, Boulter E, Burridge K. 'The 'invisible hand': regulation of RHO GTPases by RHOGDIs.' *Nat Rev Mol Cell Biol*. 2011; 12(8): 493-504.

Ghassemi S, Meacci G, Liu S, Gondarenko AA, Mathur A, Roca-Cusachs P, Sheetz MP, Hone J. 'Cells test substrate rigidity by local contractions on submicrometer pillars.' *Proc Natl Acad Sci U S A*. 2012 Apr 3; 109(14): 5328-33.

Giannone G, Dubin-Thaler BJ, Döbereiner HG, Kieffer N, Bresnick AR, Sheetz MP. 'Periodic lamellipodial contractions correlate with rearward actin waves.' *Cell*. 2004 Feb 6; 116(3): 431-43.

Glynn MW, Glover TW. 'Incomplete processing of mutant lamin A in Hutchinson-Gilford progeria leads to nuclear abnormalities, which are reversed by farnesyltransferase inhibition.' *Hum Mol Genet*. 2005 Oct 15; 14(20): 2959-69.

Goksoy E, Ma YQ, Wang X, Kong X, Perera D, Plow EF, Qin J. 'Structural basis for the autoinhibition of talin in regulating integrin activation.' *Mol Cell*. 2008 Jul 11; 31(1): 124-33.

Goldberg MW, Allen TD. 'High resolution scanning electron microscopy of the nuclear envelope: demonstration of a new, regular, fibrous lattice attached to the baskets of the nucleoplasmic face of the nuclear pores.' *J Cell Biol*. 1992; 119(6): 1429-40.

Goldberg MW, Huttenlauch I, Hutchison CJ, Stick R. 'Filaments made from A- and B-type lamins differ in structure and organization.' *J Cell Sci*. 2008 Jan 15; 121(Pt 2): 215-25.

Goldman RD, Shumaker DK, Erdos MR, Eriksson M, Goldman AE, Gordon LB, Gruenbaum Y, Khuon S, Mendez M, Varga R, Collins FS. 'Accumulation of mutant lamin A causes progressive changes in nuclear architecture in Hutchinson-Gilford progeria syndrome.' *Proc Natl Acad Sci USA*. 2004; 101(24): 8963-8.

Goldstein IJ, Hollerman CE, Merrick JM. 'Protein-carbohydrate interaction. I. The interaction of polysaccharides with concanavalin A.' *Biochim Biophys Acta*. 1965 Jan 4; 97: 68-76.

Gonsior SM, Platz S, Buchmeier S, Scheer U, Jockusch BM, Hinssen H. 'Conformational difference between nuclear and cytoplasmic actin as detected by a monoclonal antibody.' *J Cell Sci*. 1999 Mar; 112 (Pt 6): 797-809.

Gonzalo S. 'DNA damage and lamins.' *Adv Exp Med Biol*. 2014; 773: 377-99.

Gonzalo S, Kreienkamp R. 'DNA repair defects and genome instability in Hutchinson-Gilford Progeria Syndrome.' *Curr Opin Cell Biol*. 2015; 34: 75-83.

Gordon LB, Massaro J, D'Agostino RB Sr, Campbell SE, Brazier J, Brown WT, Kleinman ME, Kieran MW. 'Progeria Clinical Trials Collaborative. Impact of farnesylation inhibitors on survival in Hutchinson-Gilford progeria syndrome.' *Circulation*. 2014 Jul 1; 130(1): 27-34.

Gordon LB, Shappell H, Massaro J, D'Agostino RB Sr, Brazier J, Campbell SE, Kleinman ME, Kieran MW. 'Association of Lonafarnib Treatment vs No Treatment With Mortality Rate in Patients With Hutchinson-Gilford Progeria Syndrome.' *JAMA*. 2018 Apr 24; 319(16): 1687-1695.

Goult BT, Yan J, Schwartz MA. 'Talin as a mechanosensitive signaling hub.*' J Cell Biol*. 2018 Nov 5; 217(11): 3776-3784.

Grashoff C, Hoffman BD, Brenner MD, Zhou R, Parsons M, Yang MT, McLean MA, Sligar SG, Chen CS, Ha T, Schwartz MA. 'Measuring mechanical tension across vinculin reveals regulation of focal adhesion dynamics.' *Nature*. 2010; 466(7303): 263-6.

Guilluy C, Swaminathan V, Garcia-Mata R, O'Brien ET, Superfine R, Burridge K. 'The Rho GEFs LARG and GEF-H1 regulate the mechanical response to force on integrins.' *Nat Cell Biol*. 2011 Jun; 13(6): 722-7.

Guimarães CF, Gasperini L, Marques AP, Reis RL. 'The stiffness of living tissues and its implications for tissue engineering.' *Nat Rev Mater* 2020 Feb; 5: 351–370.

Guolla L, Bertrand M, Haase K, Pelling AE. 'Force transduction and strain dynamics in actin stress fibres in response to nanonewton forces.' *J Cell Sci*. 2012 Feb 1; 125(Pt 3): 603-13.

Haining AWM, Rahikainen R, Cortes E, Lachowski D, Rice A, von Essen M, Hytönen VP, Del Río Hernández A. 'Mechanotransduction in talin through the interaction of the R8 domain with DLC1'. *PLoS Biol.* 2018 Jul 20; 16(7): e2005599.

Halder G, Dupont S, Piccolo S. 'Transduction of mechanical and cytoskeletal cues by YAP and TAZ.' *Nat Rev Mol Cell Biol*. 2012 Sep; 13(9): 591-600.

Hale CM, Shrestha AL, Khatau SB, Stewart-Hutchinson PJ, Hernandez L, Stewart CL, Hodzic D, Wirtz D. 'Dysfunctional connections between the nucleus and the actin and microtubule networks in laminopathic models.' *Biophys J*. 2008 Dec; 95(11): 5462-75.

Han DC, Guan JL. 'Association of focal adhesion kinase with Grb7 and its role in cell migration.' *J Biol Chem*. 1999 Aug 20; 274(34): 24425-30.

Haque F, Lloyd DJ, Smallwood DT, Dent CL, Shanahan CM, Fry AM, Trembath RC, Shackleton S. 'SUN1 interacts with nuclear lamin A and cytoplasmic nesprins to provide a physical connection between the nuclear lamina and the cytoskeleton.' *Mol Cell Biol*. 2006 May; 26(10): 3738-51.

Haque F, Mazzeo D, Patel JT, Smallwood DT, Ellis JA, Shanahan CM, Shackleton S. 'Mammalian SUN protein interaction networks at the inner nuclear membrane and their role in laminopathy disease processes.' *J Biol Chem.* 2010; 285(5): 3487-98.

Harada T, Swift J, Irianto J, Shin JW, Spinler KR, Athirasala A, Diegmiller R, Dingal PC, Ivanovska IL, Discher DE. 'Nuclear lamin stiffness is a barrier to 3D migration, but softness can limit survival.' *J Cell Biol*. 2014 Mar 3; 204(5): 669-82.

Heasman SJ, Ridley AJ. 'Mammalian Rho GTPases: new insights into their functions from in vivo studies.' *Nat Rev Mol Cell Biol*. 2008 Sep; 9(9): 690-701.

Heath JP. 'Behaviour and structure of the leading lamella in moving fibroblasts. I. Occurrence and centripetal movement of arc-shaped microfilament bundles beneath the dorsal cell surface.' *J Cell Sci*. 1983; 60: 331–354.

Helenius J, Heisenberg CP, Gaub HE, Muller DJ. 'Single-cell force spectroscopy.' *J Cell Sci*. 2008; 121(11): 1785-91.

Helfman DM, Levy ET, Berthier C, Shtutman M, Riveline D, Grosheva I, Lachish-Zalait A, Elbaum M, Bershadsky AD. 'Caldesmon inhibits nonmuscle cell contractility and interferes with the formation of focal adhesions.' *Mol Biol Cell*. 1999 Oct; 10(10): 3097-112.

Henderson NC, Rieder F, Wynn TA. 'Fibrosis: from mechanisms to medicines.' *Nature*. 2020 Nov; 587(7835): 555-566.

Heng YW, Koh CG. 'Actin cytoskeleton dynamics and the cell division cycle.' *Int J Biochem Cell Biol*. 2010 Oct; 42(10): 1622-33.

Heo SJ, Thorpe SD, Driscoll TP, Duncan RL, Lee DA, Mauck RL. 'Biophysical Regulation of Chromatin Architecture Instills a Mechanical Memory in Mesenchymal Stem Cells.' *Sci Rep*. 2015 Nov 23; 5: 16895.

Heo SJ, Han WM, Szczesny SE, Cosgrove BD, Elliott DM, Lee DA, Duncan RL, Mauck RL. 'Mechanically Induced Chromatin Condensation Requires Cellular Contractility in Mesenchymal Stem Cells.' *Biophys J.* 2016 Aug 23; 111(4): 864-874.

Hildebrand JD, Schaller MD, Parsons JT. 'Identification of sequences required for the efficient localization of the focal adhesion kinase, pp125FAK, to cellular focal adhesions.' *J Cell Biol*. 1993 Nov; 123(4): 993-1005.

Hildebrand JD, Schaller MD, and Parsons JT. 'Paxillin, a tyrosine phosphorylated focal adhesion-associated protein binds to the carboxyl terminal domain of focal adhesion kinase.' *Mol Biol Cell.* 1995; 6: 637–647.

Hofmann WA, Stojiljkovic L, Fuchsova B, Vargas GM, Mavrommatis E, Philimonenko V, Kysela K, Goodrich JA, Lessard JL, Hope TJ, Hozak P, de Lanerolle P. 'Actin is part of pre-initiation complexes and is necessary for transcription by RNA polymerase II.' *Nat Cell Biol*. 2004 Nov; 6(11): 1094-101.

Horton ER, Byron A, Askari JA, Ng DHJ, Millon-Frémillon A, Robertson J, Koper EJ, Paul NR, Warwood S, Knight D, Humphries JD, Humphries MJ. 'Definition of a consensus integrin adhesome and its dynamics during adhesion complex assembly and disassembly'. *Nat Cell Biol*. 2015 Dec; 17(12): 1577-1587.

Hu P, Wu S, Hernandez N. 'A role for beta-actin in RNA polymerase III transcription.' *Genes Dev*. 2004 Dec 15; 18(24): 3010-5.

Hu S, Chen J, Butler JP, Wang N. 'Prestress mediates force propagation into the nucleus.' *Biochem Biophys Res Commun*. 2005 Apr 8; 329(2): 423-8.

Hu S, Chen J, Fabry B, Numaguchi Y, Gouldstone A, Ingber DE, Fredberg JJ, Butler JP, Wang N. 'Intracellular stress tomography reveals stress focusing and structural anisotropy in cytoskeleton of living cells.' *Am J Physiol Cell Physiol*. 2003 Nov; 285(5): C1082-90.

Huang S, Ingber DE. 'The structural and mechanical complexity of cell-growth control.' *Nat Cell Biol*. 1999; 1(5): E131-8.

Humphries JD, Wang P, Streuli C, Geiger B, Humphries MJ, Ballestrem C. 'Vinculin controls focal adhesion formation by direct interactions with talin and actin.' *J Cell Biol*. 2007; 179(5): 1043–1057.

Humphrey JD, Dufresne ER, Schwartz MA. ‘Mechanotransduction and extracellular matrix homeostasis.’ *Nat Rev Mol Cell Biol*. 2014 Dec; 15(12): 802-12.

Hur SS, Jeong JH, Ban MJ, Park JH, Yoon JK, Hwang Y. ‘Traction force microscopy for understanding cellular mechanotransduction.’ *BMB Rep*. 2020 Feb; 53(2): 74-81.

Hynes RO. ‘Integrins: bidirectional, allosteric signaling machines.’ *Cell*. 2002 Sep 20; 110(6): 673-87.

Hynes RO, Naba A. ‘Overview of the matrisome--an inventory of extracellular matrix constituents and functions.’ *Cold Spring Harb Perspect Biol*. 2012 Jan 1; 4(1): a004903.

Ishizaki T, Uehata M, Tamechika I, Keel J, Nonomura K, Maekawa M, Narumiya S. ‘Pharmacological properties of Y-27632, a specific inhibitor of rho-associated kinases.’ *Mol Pharmacol*. 2000 May; 57(5): 976-83.

Iyer KV, Pulford S, Mogilner A, Shivashankar GV. ‘Mechanical activation of cells induces chromatin remodeling preceding MKL nuclear transport.’ *Biophys J*. 2012 Oct 3; 103(7): 1416-28.

Jaalouk DE, Lammerding J. ‘Mechanotransduction gone awry.’ *Nat Rev Mol Cell Biol*. 2009; 10(1): 63-73.

Jin P, Jan LY, Jan YN. ‘Mechanosensitive Ion Channels: Structural Features Relevant to Mechanotransduction Mechanisms.’ *Annu Rev Neurosci*. 2020 Jul 8; 43: 207-229.

Kabachinski G, Schwartz TU. ‘The nuclear pore complex--structure and function at a glance.’ *J Cell Sci*. 2015 Feb 1; 128(3): 423-9.

Kanchanawong P, Shtengel G, Pasapera AM, Ramko EB, Davidson MW, Hess HF, Waterman CM. ‘Nanoscale architecture of integrin-based cell adhesions.’ *Nature*. 2010 Nov 25; 468(7323): 580-4

Kandert S, Lüke Y, Kleinhenz T, Neumann S, Lu W, Jaeger VM, Munck M, Wehnert M, Müller CR, Zhou Z, Noegel AA, Dabauvalle MC, Karakesisoglou I. ‘Nesprin-2 giant safeguards nuclear envelope architecture in LMNA S143F progeria cells.’ *Hum Mol Genet.* 2007; 16(23): 2944-59.

Kang HT, Park JT, Choi K, Choi HJC, Jung CW, Kim GR, Lee YS, Park SC. ‘Chemical screening identifies ROCK as a target for recovering mitochondrial function in Hutchinson-Gilford progeria syndrome.’ *Aging Cell*. 2017 Jun; 16(3): 541-550.

Kang SM, Yoon MH, Park BJ. ‘Laminopathies; Mutations on single gene and various human genetic diseases.’ *BMB Rep*. 2018 Jul; 51(7): 327-337.

Kapoor P, Chen M, Winkler DD, Luger K, Shen X. ‘Evidence for monomeric actin function in INO80 chromatin remodeling.’ *Nat Struct Mol Biol*. 2013 Apr; 20(4): 426-32.

Kaunas R, Nguyen P, Usami S, Chien S. ‘Cooperative effects of Rho and mechanical stretch on stress fiber organization.’ *Proc Natl Acad Sci USA*. 2005 Nov 1; 102(44): 15895-900.

Keminer O, Peters R. ‘Permeability of single nuclear pores.’ *Biophys J*. 1999 Jul; 77(1): 217-28.

Ketema M, Kreft M, Secades P, Janssen H, Sonnenberg A. ‘Nesprin-3 connects plectin and vimentin to the nuclear envelope of Sertoli cells but is not required for Sertoli cell function in spermatogenesis.’ *Mol Biol Cell*. 2013 Aug; 24(15): 2454-66.

Khatau SB, Hale CM, Stewart-Hutchinson PJ, Patel MS, Stewart CL, Searson PC, Hodzic D, Wirtz D. ‘A perinuclear actin cap regulates nuclear shape.’ *Proc Natl Acad Sci U S A*. 2009 Nov 10; 106(45): 19017-22.

Kim DH, Khatau SB, Feng Y, Walcott S, Sun SX, Longmore GD, Wirtz D. ‘Actin cap associated focal adhesions and their distinct role in cellular mechanosensing.’ *Sci Rep*. 2012; 2: 555.

Kim DH, Wirtz D. ‘Cytoskeletal tension induces the polarized architecture of the nucleus.’ *Biomaterials*. 2015 Apr; 48: 161-72.

Kim AS, Kakalis LT, Abdul-Manan N, Liu GA, Rosen MK. ‘Autoinhibition and activation mechanisms of the Wiskott-Aldrich syndrome protein.’ *Nature*. 2000 Mar 9; 404(6774): 151-8.

Kim PH, Luu J, Heizer P, Tu Y, Weston TA, Chen N, Lim C, Li RL, Lin PY, Dunn JCY, Hodzic D, Young SG, Fong LG. ‘Disrupting the LINC complex in smooth muscle cells reduces aortic disease in a mouse model of Hutchinson-Gilford progeria syndrome.’ *Sci Transl Med*. 2018 Sep 26; 10(460): eaat7163.

Kimura K, Ito M, Amano M, Chihara K, Fukata Y, Nakafuku M, Yamamori B, Feng J, Nakano T, Okawa K, Iwamatsu A, Kaibuchi K. ‘Regulation of myosin phosphatase by Rho and Rho-associated kinase (Rho-kinase).’ *Science*. 1996; 273(5272): 245-8.

Kirschner J, Brune T, Wehnert M, Denecke J, Wasner C, Feuer A, Marquardt T, Ketelsen UP, Wieacker P, Bönnemann CG, Korinthenberg R. ‘p.S143F mutation in lamin A/C: a new phenotype combining myopathy and progeria.’ Ann Neurol. 2005; 57(1): 148-51.

Kovar DR, Harris ES, Mahaffy R, Higgs HN, Pollard TD. ‘Control of the assembly of ATP- and ADP-actin by formins and profilin.’ *Cell*. 2006 Jan 27; 124(2): 423-35.

Kumar A, Ouyang M, Van den Dries K, McGhee EJ, Tanaka K, Anderson MD, Groisman, A, Goult BT, Anderson KI, Schwartz MA. ‘Talin tension sensor reveals novel features of focal adhesion force transmission and mechanosensitivity.’ *The Journal of Cell Biology*. 2016; 213(3): 371-383.

Lam AJ, St-Pierre F, Gong Y, Marshall JD, Cranfill PJ, Baird MA, McKeown MR, Wiedenmann J, Davidson MW, Schnitzer MJ, Tsien RY, Lin MZ. 'Improving FRET dynamic range with bright green and red fluorescent proteins.' *Nat Methods*. 2012 Oct; 9(10): 1005-12.

Lambert MW. 'The functional importance of lamins, actin, myosin, spectrin and the LINC complex in DNA repair.' *Exp Biol Med (Maywood)*. 2019 Nov; 244(15): 1382-1406.

Lammerding J, Fong LG, Ji JY, Reue K, Stewart CL, Young SG, Lee RT. 'Lamins A and C but not lamin B1 regulate nuclear mechanics.' *J Biol Chem*. 2006 Sep 1; 281(35): 25768-80.

Lammerding J, Schulze PC, Takahashi T, Kozlov S, Sullivan T, Kamm RD, Stewart CL, Lee RT. 'Lamin A/C deficiency causes defective nuclear mechanics and mechanotransduction.' *J Clin Invest*. 2004; 113(3): 370-8.

Lanctôt C, Cheutin T, Cremer M, Cavalli G, Cremer T. 'Dynamic genome architecture in the nuclear space: regulation of gene expression in three dimensions.' Nat Rev Genet. 2007 Feb; 8(2): 104-15.

Langanger G, Moeremans M, Daneels G, Sobieszek A, De Brabander M, De Mey J. 'The molecular organization of myosin in stress fibers of cultured cells.' *J Cell Biol*. 1986; 102(1): 200–209.

Larrieu D, Viré E, Robson S, Breusegem SY, Kouzarides T, Jackson SP. 'Inhibition of the acetyltransferase NAT10 normalizes progeric and aging cells by rebalancing the Transportin-1 nuclear import pathway.' *Sci Signal*. 2018 Jul 3; 11(537): eaar5401.

Larson RS, Corbi AL, Berman L, Springer T. 'Primary structure of the leukocyte function-associated molecule-1 alpha subunit: an integrin with an embedded domain defining a protein superfamily.' *J Cell Biol.* 1989 Feb; 108(2): 703-12.

Le HQ, Ghatak S, Yeung CY, Tellkamp F, Günschmann C, Dieterich C, Yeroslaviz A, Habermann B, Pombo A, Niessen CM, Wickström SA. 'Mechanical regulation of transcription controls Polycomb- mediated gene silencing during lineage commitment'. *Nat Cell Biol*. 2016; 18(8): 864-75.

Lee HS, Lim CJ, Puzon-McLaughlin W, Shattil SJ, Ginsberg MH. 'RIAM activates integrins by linking talin to ras GTPase membrane-targeting sequences.' *J Biol Chem*. 2009 Feb 20; 284(8): 5119-27.

Lessey EC, Guilluy C, Burridge K. 'From mechanical force to RhoA activation.' *Biochemistry*. 2012; 51(38): 7420-32.

Leung T, Chen XQ, Manser E, Lim L. 'The p160 RhoA-binding kinase ROK alpha is a member of a kinase family and is involved in the reorganization of the cytoskeleton.' *Mol Cell Biol*. 1996 Oct; 16(10): 5313-27.

Li F, Higgs HN. 'Dissecting requirements for auto-inhibition of actin nucleation by the formin, mDia1.' *J Biol Chem*. 2005 Feb 25; 280(8): 6986-92.

Li G, Du X, Vass WC, Papageorge AG, Lowy DR, Qian X. 'Full activity of the deleted in liver cancer 1 (DLC1) tumor suppressor depends on an LD-like motif that binds talin and focal adhesion kinase (FAK)'. *Proc Natl Acad Sci U S A*. 2011 Oct 11; 108(41): 17129-34.

Li Q, Kumar A, Makhija E, Shivashankar GV. 'The regulation of dynamic mechanical coupling between actin cytoskeleton and nucleus by matrix geometry.' *Biomaterials*. 2014 Jan; 35(3): 961-9.

Li Q, Makhija E, Hameed FM, Shivashankar GV. 'Micropillar displacements by cell traction forces are mechanically correlated with nuclear dynamics.' *Biochem Biophys Res Commun*. 2015 May 29; 461(2): 372-7.

Lietha D, Cai X, Ceccarelli DF, Li Y, Schaller MD, Eck MJ. 'Structural basis for the autoinhibition of focal adhesion kinase.' *Cell*. 2007 Jun 15; 129(6): 1177-87.

Lim RY, Huang NP, Köser J, Deng J, Lau KH, Schwarz-Herion K, Fahrenkrog B, Aebi U. 'Flexible phenylalanine-glycine nucleoporins as entropic barriers to nucleocytoplasmic transport.' *Proc Natl Acad Sci USA*. 2006 Jun 20; 103(25): 9512-7.

Lin S, Gu L. 'Influence of Crosslink Density and Stiffness on Mechanical Properties of Type I Collagen Gel.' *Materials (Basel)*. 2015 Feb 6; 8(2): 551-560.

Liu B, Wang J, Chan KM, Tjia WM, Deng W, Guan X, Huang JD, Li KM, Chau PY, Chen DJ, Pei D, Pendas AM, Cadiñanos J, López-Otín C, Tse HF, Hutchison C, Chen J, Cao Y, Cheah KS, Tryggvason K, Zhou Z. 'Genomic instability in laminopathy-based premature aging.' *Nat Med*. 2005; 11(7): 780-5.

Liu J, Wang Y, Goh WI, Goh H, Baird MA, Ruehland S, Teo S, Bate N, Critchley DR, Davidson MW, Kanchanawong P. 'Talin determines the nanoscale architecture of focal adhesions.' *Proc Natl Acad Sci USA*. 2015 Sep 1; 112(35): E4864-73.

Lo CM, Wang HB, Dembo M, Wang YL. 'Cell movement is guided by the rigidity of the substrate.' *Biophysical Journal*. 2000; 79(1): 144-152.

Lombardi ML, Jaalouk DE, Shanahan CM, Burke B, Roux KJ, Lammerding J. 'The interaction between nesprins and sun proteins at the nuclear envelope is critical for force transmission between the nucleus and cytoskeleton.' *J Biol Chem*. 2011 Jul 29;286(30):26743-53.

López-Colomé AM, Lee-Rivera I, Benavides-Hidalgo R, López E. 'Paxillin: a crossroad in pathological cell migration.' *J Hematol Oncol*. 2017 Feb 18; 10(1): 50.

Lund EG, Duband-Goulet I, Oldenburg A, Buendia B, Collas P. 'Distinct features of lamin A-interacting chromatin domains mapped by ChIP-sequencing from sonicated or micrococcal nuclease-digested chromatin.' *Nucleus*. 2015; 6(1): 30-9.

Luo BH, Carman CV, Springer TA. ‘Structural basis of integrin regulation and signaling.’ *Annu Rev Immunol*. 2007; 25: 619-47.

Luxton GW, Gomes ER, Folker ES, Vintinner E, Gundersen GG. ‘Linear arrays of nuclear envelope proteins harness retrograde actin flow for nuclear movement.’ *Science*. 2010 Aug 20; 329(5994): 956-9.

Maekawa M, Ishizaki T, Boku S, Watanabe N, Fujita A, Iwamatsu A, Obinata T, Ohashi K, Mizuno K, Narumiya S. ‘Signaling from Rho to the actin cytoskeleton through protein kinases ROCK and LIM-kinase.’ *Science*. 1999 Aug 6;285(5429):895-8.

Maninova M, Caslavsky J, Vomastek T. ‘The assembly and function of perinuclear actin cap in migrating cells.’ *Protoplasma*. 2017 May; 254(3): 1207-1218.

Maninová M, Vomastek T. ‘Dorsal stress fibers, transverse actin arcs, and perinuclear actin fibers form an interconnected network that induces nuclear movement in polarizing fibroblasts.’ FEBS J. 2016 Oct; 283(20): 3676-3693.

Maniotis AJ, Chen CS, Ingber DE. ‘Demonstration of mechanical connections between integrins, cytoskeletal filaments, and nucleoplasm that stabilize nuclear structure.’ *Proc Natl Acad Sci USA.* 1997; 94(3): 849-854.

Martiel JL, Leal A, Kurzawa L, Balland M, Wang I, Vignaud T, Tseng Q, Théry M. ‘Measurement of cell traction forces with ImageJ.’ *Methods Cell Biol*. 2015; 125: 269-87.

Martinac B. ‘Mechanosensitive ion channels: molecules of mechanotransduction.’ *J Cell Sci*. 2004; 117(12): 2449-60.

Matsui H, Harada I, Sawada Y. ‘Src, p130Cas, and Mechanotransduction in Cancer Cells.’ *Genes Cancer*. 2012 May; 3(5-6): 394-401.

May CK, Carroll CW. ‘Differential incorporation of SUN-domain proteins into LINC complexes is coupled to gene expression.’ *PLoS One*. 2018 May 29; 13(5): e0197621.

McClintock D, Gordon LB, Djabali K. ‘Hutchinson-Gilford progeria mutant lamin A primarily targets human vascular cells as detected by an anti-Lamin A G608G antibody.’ *Proc Natl Acad Sci USA.* 2006; 103(7): 2154-9.

McClintock D, Ratner D, Lokuge M, Owens DM, Gordon LB, Collins FS, Djabali K. ‘The Mutant Form of Lamin A that Causes Hutchinson-Gilford Progeria Is a Biomarker of Cellular Aging in Human Skin.’ *PLoS ONE*. 2007; 2(12): e1269.

Melchior F, Paschal B, Evans J, Gerace L. ‘Inhibition of nuclear protein import by nonhydrolyzable analogues of GTP and identification of the small GTPase Ran/TC4 as an essential transport factor.’ *J Cell Biol*. 1993 Dec; 123(6 Pt 2): 1649-59.

Meng F, Sachs F. ‘Visualizing dynamic cytoplasmic forces with a compliance-matched FRET sensor.’ *J Cell Sci*. 2011; 124(Pt 2): 261-9.

Meng F, Suchyna TM, Sachs F. ‘A FRET based mechanical stress sensor for specific proteins in situ.’ *The FEBS journal*. 2008; 275(12): 3072-3087.

Mitra SK, Hanson DA, Schlaepfer DD. ‘Focal adhesion kinase: in command and control of cell motility.’ *Nat Rev Mol Cell Biol*. 2005; 6(1): 56-68.

Mockrin SC, Korn ED. ‘Acanthamoeba profilin interacts with G-actin to increase the rate of exchange of actin-bound adenosine 5'-triphosphate.’ *Biochemistry*. 1980 Nov 11; 19(23): 5359-62.

Moir RD, Yoon M, Khuon S, Goldman RD. ‘Nuclear lamins A and B1: different pathways of assembly during nuclear envelope formation in living cells.’ *J Cell Biol*. 2000 Dec 11; 151(6): 1155-68.

Monaghan-Benson E, Wittchen ES, Doerschuk CM, Burridge K. ‘A Rnd3/p190RhoGAP pathway regulates RhoA activity in idiopathic pulmonary fibrosis fibroblasts.’ *Mol Biol Cell.* 2018 Sep 1; 29(18): 2165-2175.

Morgan JT, Pfeiffer ER, Thirkill TL, Kumar P, Peng G, Fridolfsson HN, Douglas GC, Starr DA, Barakat AI. ‘Nesprin-3 regulates endothelial cell morphology, perinuclear cytoskeletal architecture, and flow-induced polarization.’ *Mol Biol Cell*. 2011 Nov; 22(22): 4324-34.

Morimoto A, Shibuya H, Zhu X, Kim J, Ishiguro K, Han M, Watanabe Y. ‘A conserved KASH domain protein associates with telomeres, SUN1, and dynactin during mammalian meiosis.’ *J Cell Biol*. 2012 Jul 23; 198(2): 165-72.

Moroianu J, Blobel G. ‘Protein export from the nucleus requires the GTPase Ran and GTP hydrolysis.’ *Proc Natl Acad Sci U S A*. 1995 May 9; 92(10): 4318-22.

Mounkes LC, Kozlov S, Hernandez L, Sullivan T, Stewart CL. ‘A progeroid syndrome in mice is caused by defects in A-type lamins.’ *Nature*. 2003 May 15; 423(6937): 298-301.

Mu X, Tseng C, Hambright WS, Matre P, Lin CY, Chanda P, Chen W, Gu J, Ravuri S, Cui Y, Zhong L, Cooke JP, Niedernhofer LJ, Robbins PD, Huard J. ‘Cytoskeleton stiffness regulates cellular senescence and innate immune response in Hutchinson-Gilford Progeria Syndrome.’ *Aging Cell* 2020; 19(8): e13152.

Nakajima H, Yamamoto K, Agarwala S, Terai K, Fukui H, Fukuhara S, Ando K, Miyazaki T, Yokota Y, Schmelzer E, Belting HG, Affolter M, Lecaudey V, Mochizuki N. ‘Flow-Dependent Endothelial YAP Regulation Contributes to Vessel Maintenance.’ *Dev Cell*. 2017 Mar 27; 40(6): 523-536.e6.

Nobes CD, Hall A. ‘Rho, rac, and cdc42 GTPases regulate the assembly of multimolecular focal complexes associated with actin stress fibers, lamellipodia, and filopodia.’ *Cell*. 1995 Apr 7; 81(1): 53-62.

O'Gorman S, Fox DT, Wahl GM. 'Recombinase-mediated gene activation and site-specific integration in mammalian cells.' *Science*. 1991 Mar 15; 251(4999): 1351-5.

Oda T, Iwasa M, Aihara T, Maéda Y, Narita A. 'The nature of the globular- to fibrous-actin transition.' *Nature*. 2009 Jan 22; 457(7228): 441-5. Erratum in: *Nature.* 2009 Sep 24; 461(7263): 550.

Ostlund C, Folker ES, Choi JC, Gomes ER, Gundersen GG, Worman HJ. 'Dynamics and molecular interactions of linker of nucleoskeleton and cytoskeleton (LINC) complex proteins.' *J Cell Sci*. 2009 Nov 15;122(Pt 22):4099-108.

Otomo T, Otomo C, Tomchick DR, Machius M, Rosen MK. 'Structural basis of Rho GTPase-mediated activation of the formin mDia1.' *Mol Cell*. 2005 Apr 29; 18(3): 273-81.

Overby DR, Matthews BD, Alsberg E, Ingber DE. 'Novel dynamic rheological behavior of individual focal adhesions measured within single cells using electromagnetic pulling cytometry.' *Acta Biomater*. 2005; 1(3):295-303.

Owen LM, Adhikari AS, Patel M, Grimmer P, Leijnse N, Kim MC, Notbohm J, Franck C, Dunn AR. 'A cytoskeletal clutch mediates cellular force transmission in a soft, three-dimensional extracellular matrix.' *Mol Biol Cell*. 2017 Jul 7; 28(14): 1959-1974.

Padmakumar VC, Libotte T, Lu W, Zaim H, Abraham S, Noegel AA, Gotzmann J, Foisner R, Karakesisoglou I. 'The inner nuclear membrane protein Sun1 mediates the anchorage of Nesprin-2 to the nuclear envelope.' *J Cell Sci*. 2005 Aug 1; 118(Pt 15): 3419-30.

Panciera T, Azzolin L, Cordenonsi M, Piccolo S. 'Mechanobiology of YAP and TAZ in physiology and disease.' *Nat Rev Mol Cell Biol*. 2017 Dec; 18(12): 758-770.

Pankov R, Yamada KM. 'Fibronectin at a glance.' *J Cell Sci*. 2002 Oct 15; 115(Pt 20): 3861-3.

Pasapera AM, Schneider IC, Rericha E, Schlaepfer DD, Waterman CM. 'Myosin II activity regulates vinculin recruitment to focal adhesions through FAK-mediated paxillin phosphorylation.' *J Cell Biol*. 2010 Mar 22; 188(6): 877-90.

Paterson HF, Self AJ, Garrett MD, Just I, Aktories K, Hall A. 'Microinjection of recombinant p21rho induces rapid changes in cell morphology.' J Cell Biol. 1990 Sep; 111(3): 1001-7.

Pathak A, Kumar S. 'Independent regulation of tumor cell migration by matrix stiffness and confinement.' *Proc Natl Acad Sci U S A*. 2012 Jun 26; 109(26): 10334-9.

Paul AS, Pollard TD. 'Review of the mechanism of processive actin filament elongation by formins.' *Cell Motil Cytoskeleton*. 2009 Aug; 66(8): 606-17.

Paulsson M. ‘Basement membrane proteins: structure, assembly, and cellular interactions.’ *Crit Rev Biochem Mol Biol*. 1992; 27(1-2): 93-127.

Pecci A, Ma X, Savoia A, Adelstein RS. ‘MYH9: Structure, functions and role of non-muscle myosin IIA in human disease.’ *Gene*. 2018 Jul 20; 664: 152-167.

Pellegrin S, Mellor H. ‘Actin stress fibres.’ *J Cell Sci*. 2007 Oct 15; 120(Pt 20): 3491-9.

Pendás AM, Zhou Z, Cadiñanos J, Freije JM, Wang J, Hultenby K, Astudillo A, Wernerson A, Rodríguez F, Tryggvason K, López-Otín C. ‘Defective prelamin A processing and muscular and adipocyte alterations in Zmpste24 metalloproteinase-deficient mice.’ *Nat Genet*. 2002; 31(1): 94-9.

Philimonenko VV, Zhao J, Iben S, Dingová H, Kyselá K, Kahle M, Zentgraf H, Hofmann WA, de Lanerolle P, Hozák P, Grummt I. ‘Nuclear actin and myosin I are required for RNA polymerase I transcription.’ *Nat Cell Biol*. 2004 Dec; 6(12): 1165-72.

Philip JT, Dahl KN. ‘Nuclear mechanotransduction: response of the lamina to extracellular stress with implications in aging.’ *J Biomech*. 2008; 41(15): 3164-70.

Poh YC, Shevtsov SP, Chowdhury F, Wu DC, Na S, Dundr M, Wang N. ‘Dynamic force-induced direct dissociation of protein complexes in a nuclear body in living cells.’ *Nat Commun*. 2012; 3: 866.

Polacheck WJ, Chen CS. ‘Measuring cell-generated forces: a guide to the available tools.’ *Nat Methods.* 2016; 13(5): 415-23.

Pollard TD. ‘Rate constants for the reactions of ATP- and ADP-actin with the ends of actin filaments.’ *J Cell Biol*. 1986 Dec; 103(6 Pt 2): 2747-54.

Pollard TD. ‘Actin and Actin-Binding Proteins.’ *Cold Spring Harb Perspect Biol*. 2016 Aug 1; 8(8): a018226.

Porter L, Minaisah RM, Ahmed S, Ali S, Norton R, Zhang Q, Ferraro E, Molenaar C, Holt M, Cox S, Fountain S, Shanahan C, Warren D. ‘SUN1/2 Are Essential for RhoA/ROCK-Regulated Actomyosin Activity in Isolated Vascular Smooth Muscle Cells.’ *Cells*. 2020 Jan 6; 9(1): 132

Postel R, Ketema M, Kuikman I, de Pereda JM, Sonnenberg A. ‘Nesprin-3 augments peripheral nuclear localization of intermediate filaments in zebrafish.’ *J Cell Sci*. 2011 Mar 1; 124(Pt 5): 755-64.

Prager-Khoutorsky M, Lichtenstein A, Krishnan R, Rajendran K, Mayo A, Kam Z, Geiger B, Bershadsky AD. ‘Fibroblast polarization is a matrix-rigidity-dependent process controlled by focal adhesion mechanosensing.’ *Nat Cell Biol*. 2011 Nov 13; 13(12): 1457-65.

Ragnauth CD, Warren DT, Liu Y, McNair R, Tajsic T, Figg N, Shroff R, Skepper J, Shanahan CM. 'Prelamin A acts to accelerate smooth muscle cell senescence and is a novel biomarker of human vascular aging.' *Circulation*. 2010; 121(20): 2200-10

Rahikainen R, Öhman T, Turkki P, Varjosalo M, Hytönen VP. 'Talin-mediated force transmission and talin rod domain unfolding independently regulate adhesion signaling.' *J Cell Sci*. 2019 Apr 3; 132(7): jcs226514.

Razafsky D, Wirtz D, Hodzic D. 'Nuclear envelope in nuclear positioning and cell migration.' *Adv Exp Med Biol*. 2014; 773: 471-90.

Reed CC, Iozzo RV. 'The role of decorin in collagen fibrillogenesis and skin homeostasis.' *Glycoconj J*. 2002 May-Jun; 19(4-5): 249-55.

Reichelt R, Holzenburg A, Buhle EL Jr, Jarnik M, Engel A, Aebi U. 'Correlation between structure and mass distribution of the nuclear pore complex and of distinct pore complex components.' *J Cell Biol*. 1990; 110(4): 883-94.

Reiner DJ, Lundquist EA. 'Small GTPases.' *WormBook*. 2018 Aug 16; 2018: 1-65.
Ren XD, Kiosses WB, Sieg DJ, Otey CA, Schlaepfer DD, Schwartz MA. 'Focal adhesion kinase suppresses Rho activity to promote focal adhesion turnover.' *J Cell Sci*. 2000 Oct; 113 (Pt 20): 3673-8.

Rexach M, Blobel G. 'Protein import into nuclei: association and dissociation reactions involving transport substrate, transport factors, and nucleoporins.' *Cell*. 1995 Dec 1; 83(5): 683-92.

Ribbeck K, Lipowsky G, Kent HM, Stewart M, Görlich D. 'NTF2 mediates nuclear import of Ran.' *EMBO J*. 1998; 17(22): 6587-98.

Ricard-Blum S. 'The collagen family.' *Cold Spring Harb Perspect Biol*. 2011 Jan 1; 3(1): a004978.

Ridley AJ, Hall A. 'The small GTP-binding protein rho regulates the assembly of focal adhesions and actin stress fibers in response to growth factors.' *Cell*. 1992 Aug 7; 70(3): 389-99.

Ris, H. 'Three-dimensional imaging of cell ultrastructure with high resolution low voltage SEM.*' Inst. Phys. Conf. Ser*. 1989; 98: 657-662.

Ris, H. 'The three dimensional structure of the nuclear pore complex as seen by high voltage electron microscopy and high resolution low voltage scanning electron microscopy.' *EMSA Bull.* 1991; 21, 54-56

Riveline D, Zamir E, Balaban NQ, Schwarz US, Ishizaki T, Narumiya S, Kam Z, Geiger B, Bershadsky AD. 'Focal contacts as mechanosensors: externally applied local mechanical force induces growth of focal contacts by an mDia1-dependent and ROCK-independent mechanism.' *J Cell Biol*. 2001 Jun 11; 153(6): 1175-86.

Roeder BA, Kokini K, Sturgis JE, Robinson JP, Voytik-Harbin SL. 'Tensile mechanical properties of three-dimensional type I collagen extracellular matrices with varied microstructure.' *J Biomech Eng*. 2002 Apr; 124(2): 214-22.

Rotty JD, Wu C, Bear JE. 'New insights into the regulation and cellular functions of the ARP2/3 complex.' *Nat Rev Mol Cell Biol*. 2013 Jan; 14(1): 7-12.

Rouiller I, Xu XP, Amann KJ, Egile C, Nickell S, Nicastro D, Li R, Pollard TD, Volkmann N, Hanein D. 'The structural basis of actin filament branching by the Arp2/3 complex.' *J Cell Biol.* 2008 Mar 10; 180(5): 887-95.

Rout MP, Aitchison JD, Suprapto A, Hjertaas K, Zhao Y, Chait BT. 'The yeast nuclear pore complex: composition, architecture, and transport mechanism.' *J Cell Biol*. 2000; 148(4): 635-51.

Roux KJ, Crisp ML, Liu Q, Kim D, Kozlov S, Stewart CL, Burke B. 'Nesprin 4 is an outer nuclear membrane protein that can induce kinesin-mediated cell polarization.' *Proc Natl Acad Sci USA*. 2009 Feb 17; 106(7): 2194-9.

Sagelius H, Rosengardten Y, Hanif M, Erdos MR, Rozell B, Collins FS, Eriksson M. 'Targeted transgenic expression of the mutation causing Hutchinson-Gilford progeria syndrome leads to proliferative and degenerative epidermal disease.' *J Cell Sci*. 2008 Apr 1; 121(Pt 7): 969-78.

Scaffidi P, Misteli T. 'Lamin A-Dependent Nuclear Defects in Human Aging.' *Science*. 2006; 312(5776): 1059-1063.

Schaller MD. 'Paxillin: a focal adhesion-associated adaptor protein.' *Oncogene*. 2001 Oct 1; 20(44): 6459-72.

Schaller MD, Hildebrand JD, Shannon JD, Fox JW, Vines RR, Parsons JT. 'Autophosphorylation of the focal adhesion kinase, pp125FAK, directs SH2-dependent binding of pp60src.' *Mol Cell Biol*. 1994 Mar; 14(3): 1680-8.

Schindelin J, Arganda-Carreras I, Frise E, Kaynig V, Longair M, Pietzsch T, Preibisch S, Rueden C, Saalfeld S, Schmid B, Tinevez JY, White DJ, Hartenstein V, Eliceiri K, Tomancak P, Cardona A. 'Fiji: an open-source platform for biological-image analysis.' *Nat Methods*. 2012 Jun 28; 9(7): 676-82.

Schneider M, Lu W, Neumann S, Brachner A, Gotzmann J, Noegel AA, Karakesisoglou I. 'Molecular mechanisms of centrosome and cytoskeleton anchorage at the nuclear envelope.' *Cell Mol Life Sci*. 2011 May; 68(9): 1593-610.

Schrank BR, Aparicio T, Li Y, Chang W, Chait BT, Gundersen GG, Gottesman ME, Gautier J. 'Nuclear ARP2/3 drives DNA break clustering for homology-directed repair.' *Nature*. 2018 Jul; 559(7712): 61-66.

Sellers JR. 'Myosins: a diverse superfamily.' *Biochim Biophys Acta*. 2000 Mar 17; 1496(1): 3-22.

Sept D, McCammon JA. ‘Thermodynamics and kinetics of actin filament nucleation.’ *Biophys J*. 2001 Aug; 81(2): 667-74.

Sharili AS, Kenny FN, Vartiainen MK, Connelly JT. ‘Nuclear actin modulates cell motility via transcriptional regulation of adhesive and cytoskeletal genes.’ *Sci Rep*. 2016 Sep 21; 6: 33893.

Shaw L, Sugden CJ, Hamill KJ. ‘Laminin Polymerization and Inherited Disease: Lessons From Genetics.’ *Front Genet*. 2021 Aug 12; 12: 707087.

Shevelyov YY, Ulianov SV. ‘The Nuclear Lamina as an Organizer of Chromosome Architecture.’ *Cells*. 2019 Feb 8; 8(2): 136.

Shimi T, Kittisopikul M, Tran J, Goldman AE, Adam SA, Zheng Y, Jaqaman K, Goldman RD. ‘Structural organization of nuclear lamins A, C, B1, and B2 revealed by superresolution microscopy.’ *Mol Biol Cell*. 2015 Nov 5; 26(22): 4075-86.

Shimi T, Pfleghaar K, Kojima S, Pack CG, Solovei I, Goldman AE, Adam SA, Shumaker DK, Kinjo M, Cremer T, Goldman RD. ‘The A- and B-type nuclear lamin networks: microdomains involved in chromatin organization and transcription.’ *Genes Dev*. 2008 Dec 15; 22(24): 3409-21.

Shimokawa H, Sunamura S, Satoh K. ‘RhoA/Rho-Kinase in the Cardiovascular System.’ *Circ Res.* 2016 Jan 22; 118(2): 352-66.

Shiu JY, Aires L, Lin Z, Vogel V. ‘Nanopillar force measurements reveal actin-cap-mediated YAP mechanotransduction.’ *Nat Cell Biol*. 2018 Mar; 20(3): 262-271.

Shumaker DK, Kuczmarski ER, Goldman RD. ‘The nucleoskeleton: lamins and actin are major players in essential nuclear functions.’ *Curr Opin Cell Biol*. 2003 Jun; 15(3): 358-66.

Sinensky M, Fantle K, Trujillo M, McLain T, Kupfer A, Dalton M. ‘The processing pathway of prelamin A.’ *J Cell Sci.* 1994; 107 (Pt 1): 61-7.

Singh P, Carraher C, Schwarzbauer JE. ‘Assembly of fibronectin extracellular matrix.’ *Annu Rev Cell Dev Biol*. 2010; 26: 397-419.

Singla S, Hu C, Mizeracki A, Mehta JL. ‘Decorin in atherosclerosis.’ *Ther Adv Cardiovasc Dis*. 2011 Dec; 5(6): 305-14.

Sit ST, Manser E. ‘Rho GTPases and their role in organizing the actin cytoskeleton.’ *J Cell Sci*. 2011 Mar 1; 124(Pt 5): 679-83.

Sjöblom B, Salmazo A, Djinović-Carugo K. ‘Alpha-actinin structure and regulation.’ *Cell Mol Life Sci*. 2008 Sep; 65(17): 2688-701.

Sosa BA, Rothballer A, Kutay U, Schwartz TU. ‘LINC complexes form by binding of three KASH peptides to domain interfaces of trimeric SUN proteins.’ *Cell*. 2012 May 25; 149(5): 1035-47.

Stehbens WE, Delahunt B, Shozawa T, Gilbert-Barness E. 'Smooth muscle cell depletion and collagen types in progeric arteries.' *Cardiovasc Pathol*. 2001 May-Jun; 10(3): 133-6.

Stewart-Hutchinson PJ, Hale CM, Wirtz D, Hodzic D. 'Structural requirements for the assembly of LINC complexes and their function in cellular mechanical stiffness.' *Exp Cell Res*. 2008 May 1; 314(8): 1892-905.

Stutchbury B, Atherton P, Tsang R, Wang DY, Ballestrem C. 'Distinct focal adhesion protein modules control different aspects of mechanotransduction.' *J Cell Sci*. 2017 May 1; 130(9): 1612-1624.

Stuurman N, Heins S, Aebi U. 'Nuclear lamins: their structure, assembly, and interactions.' *J Struct Biol*. 1998; 122(1-2): 42-66.
Sun Z, Costell M, Fässler R. 'Integrin activation by talin, kindlin and mechanical forces.' *Nat Cell Biol*. 2019 Jan; 21(1): 25-31.

Suo J, Ferrara DE, Sorescu D, Guldberg RE, Taylor WR, Giddens DP. 'Hemodynamic shear stresses in mouse aortas: implications for atherogenesis.' *Arterioscler Thromb Vasc Biol*. 2007 Feb; 27(2): 346-51.

Svitkina TM. 'Ultrastructure of the actin cytoskeleton.' *Curr Opin Cell Biol*. 2018 Oct; 54:1-8.

Swift J, Ivanovska IL, Buxboim A, Harada T, Dingal PC, Pinter J, Pajerowski JD, Spinler KR, Shin JW, Tewari M, Rehfeldt F, Speicher DW, Discher DE. 'Nuclear lamin-A scales with tissue stiffness and enhances matrix-directed differentiation.' *Science*. 2013 Aug 30; 341(6149): 1240104.

Tajik A, Zhang Y, Wei F, Sun J, Jia Q, Zhou W, Singh R, Khanna N, Belmont AS, Wang N. 'Transcription upregulation via force-induced direct stretching of chromatin.' *Nat Mater*. 2016 Dec; 15(12): 1287-1296.

Takechi-Haraya Y, Goda Y, Izutsu K, Sakai-Kato K. 'Improved Atomic Force Microscopy Stiffness Measurements of Nanoscale Liposomes by Cantilever Tip Shape Evaluation.' *Anal Chem*. 2019 Aug 20; 91(16): 10432-10440.

Tan JL, Tien J, Pirone DM, Gray DS, Bhadriraju K, Chen CS. 'Cells lying on a bed of microneedles: an approach to isolate mechanical force.' *Proc Natl Acad Sci U S A*. 2003 Feb 18; 100(4): 1484-9.

Thakar K, May CK, Rogers A, Carroll CW. 'Opposing roles for distinct LINC complexes in regulation of the small GTPase RhoA.' *Mol Biol Cell*. 2017 Jan 1; 28(1): 182-191.

Theocharis AD, Skandalis SS, Gialeli C, Karamanos NK. 'Extracellular matrix structure.' *Adv Drug Deliv Rev*. 2016 Feb 1; 97: 4-27.

Thomas DG, Yenepalli A, Denais CM, Rape A, Beach JR, Wang YL, Schiemann WP, Baskaran H, Lammerding J, Egelhoff TT. 'Non-muscle myosin IIB is critical for nuclear translocation during 3D invasion.' *J Cell Biol*. 2015 Aug 17; 210(4): 583-94

Tojkander S, Gateva G, Schevzov G, Hotulainen P, Naumanen P, Martin C, Gunning PW, Lappalainen P. 'A molecular pathway for myosin II recruitment to stress fibers.' *Curr Biol.* 2011 Apr 12; 21(7): 539-50.

Toth JI, Yang SH, Qiao X, Beigneux AP, Gelb MH, Moulson CL, Miner JH, Young SG, Fong LG. 'Blocking protein farnesyltransferase improves nuclear shape in fibroblasts from humans with progeroid syndromes.' *Proc Natl Acad Sci U S A*. 2005 Sep 6; 102(36): 12873-8.

Turgay Y, Eibauer M, Goldman AE, Shimi T, Khayat M, Ben-Harush K, Dubrovsky-Gaupp A, Sapra KT, Goldman RD, Medalia O. 'The molecular architecture of lamins in somatic cells.' *Nature*. 2017 Mar 9; 543(7644): 261-264.

Tzima E, del Pozo MA, Shattil SJ, Chien S, Schwartz MA. 'Activation of integrins in endothelial cells by fluid shear stress mediates Rho-dependent cytoskeletal alignment.' *EMBO J*. 2001 Sep 3; 20(17): 4639-47.

Uehata M, Ishizaki T, Satoh H, Ono T, Kawahara T, Morishita T, Tamakawa H, Yamagami K, Inui J, Maekawa M, Narumiya S. 'Calcium sensitization of smooth muscle mediated by a Rho-associated protein kinase in hypertension.' *Nature*. 1997 Oct 30; 389(6654): 990-4.

Vavylonis D, Kovar DR, O'Shaughnessy B, Pollard TD. 'Model of formin-associated actin filament elongation.' *Mol Cell*. 2006 Feb 17; 21(4): 455-66.

Verstraeten VL, Ji JY, Cummings KS, Lee RT, Lammerding J. 'Increased mechanosensitivity and nuclear stiffness in Hutchinson-Gilford progeria cells: effects of farnesyltransferase inhibitors.' *Aging Cell*. 2008; 7(3): 383-93.

Vicente-Manzanares M, Ma X, Adelstein RS, Horwitz AR. 'Non-muscle myosin II takes centre stage in cell adhesion and migration.' *Nat Rev Mol Cell Biol*. 2009 Nov; 10(11): 778-90.

Wang JH, Lin JS. 'Cell traction force and measurement methods.' *Biomech Model Mechanobiol*. 2007 Nov; 6(6): 361-71.

Wang N, Tolić-Nørrelykke IM, Chen J, Mijailovich SM, Butler JP, Fredberg JJ, Stamenović D. 'Cell prestress. I. Stiffness and prestress are closely associated in adherent contractile cells.' *Am J Physiol Cell Physiol*. 2002 Mar; 282(3): C606-16.

Wang N, Tytell JD, Ingber DE. 'Mechanotransduction at a distance: mechanically coupling the extracellular matrix with the nucleus.' *Nat Rev Mol Cell Biol*. 2009; 10(1): 75-82.

Wang W, Shi Z, Jiao S, Chen C, Wang H, Liu G, Wang Q, Zhao Y, Greene MI, Zhou Z. 'Structural insights into SUN-KASH complexes across the nuclear envelope.' *Cell Res*. 2012 Oct; 22(10): 1440-52.

Wang Y, Botvinick EL, Zhao Y, Berns MW, Usami S, Tsien RY, Chien S. 'Visualizing the mechanical activation of Src.' *Nature*. 2005 Apr 21; 434(7036): 1040-5.

Warren DT, Zhang Q, Weissberg PL, Shanahan CM. 'Nesprins: intracellular scaffolds that maintain cell architecture and coordinate cell function?' *Expert Rev Mol Med*. 2005 Jun 13; 7(11): 1-15.

Watanabe N, Kato T, Fujita A, Ishizaki T, Narumiya S. 'Cooperation between mDia1 and ROCK in Rho-induced actin reorganization.' *Nat Cell Biol*. 1999 Jul; 1(3): 136-43.

Webb DJ, Donais K, Whitmore LA, Thomas SM, Turner CE, Parsons JT, Horwitz AF. 'FAK-Src signalling through paxillin, ERK and MLCK regulates adhesion disassembly.' *Nat Cell Biol*. 2004 Feb; 6(2): 154-61.

Webb DJ, Schroeder MJ, Brame CJ, Whitmore L, Shabanowitz J, Hunt DF, Horwitz AR. 'Paxillin phosphorylation sites mapped by mass spectrometry.' *J Cell Sci*. 2005 Nov 1; 118(Pt 21): 4925-9.

Wegner A, Isenberg G. '12-fold difference between the critical monomer concentrations of the two ends of actin filaments in physiological salt conditions.' *Proc Natl Acad Sci U S A*. 1983 Aug; 80(16): 4922-5.

Wei F, Xu X, Zhang C, Liao Y, Ji B, Wang N. 'Stress fiber anisotropy contributes to force-mode dependent chromatin stretching and gene upregulation in living cells.' *Nat Commun*. 2020 Sep 29; 11(1): 4902.

Wennerberg K, Forget MA, Ellerbroek SM, Arthur WT, Burridge K, Settleman J, Der CJ, Hansen SH. 'Rnd proteins function as RhoA antagonists by activating p190 RhoGAP.' *Curr Biol*. 2003 Jul 1; 13(13): 1106-15.

Wente SR, Rout MP. 'The nuclear pore complex and nuclear transport.' *Cold Spring Harb Perspect Biol*. 2010 Oct; 2(10): a000562.

Weng Z, Taylor JA, Turner CE, Brugge JS, Seidel-Dugan C. 'Detection of Src homology 3-binding proteins, including paxillin, in normal and v-Src-transformed Balb/c 3T3 cells.' J *Biol Chem*. 1993 Jul 15; 268(20): 14956-63.

Wilhelmsen K, Litjens SH, Kuikman I, Tshimbalanga N, Janssen H, van den Bout I, Raymond K, Sonnenberg A. 'Nesprin-3, a novel outer nuclear membrane protein, associates with the cytoskeletal linker protein plectin.' *J Cell Biol*. 2005 Dec 5; 171(5): 799-810.

Wood CK, Turner CE, Jackson P, and Critchley DR. ‘Characterisation of the paxillin-binding site and the C-terminal focal adhesion targeting sequence in vinculin.’ *J Cell Sci* 1994; 107: 709–717.

Worman HJ, Bonne G. ‘"Laminopathies": a wide spectrum of human diseases.’ *Exp Cell Res*. 2007 Jun 10; 313(10): 2121-33.

Woroniuk A, Porter A, White G, Newman DT, Diamantopoulou Z, Waring T, Rooney C, Strathdee D, Marston DJ, Hahn KM, Sansom OJ, Zech T, Malliri A. ‘STEF/TIAM2-mediated Rac1 activity at the nuclear envelope regulates the perinuclear actin cap.’ *Nat Commun*. 2018 May 29; 9(1): 2124.

Wozniak MA, Chen CS. ‘Mechanotransduction in development: a growing role for contractility.’ *Nat Rev Mol Cell Biol*. 2009; 10(1): 34-43.

Xing Z, Chen HC, Nowlen JK, Taylor SJ, Shalloway D, Guan JL. ‘Direct interaction of v-Src with the focal adhesion kinase mediated by the Src SH2 domain.’ *Mol Biol Cell*. 1994 Apr; 5(4): 413-21.

Yang B, Radel C, Hughes D, Kelemen S, Rizzo V. ‘p190 RhoGTPase-activating protein links the β1 integrin/caveolin-1 mechanosignaling complex to RhoA and actin remodeling.’ *Arterioscler Thromb Vasc Biol*. 2011 Feb; 31(2): 376-83.

Yoshizaki H, Ohba Y, Kurokawa K, Itoh RE, Nakamura T, Mochizuki N, Nagashima K, Matsuda M. ‘Activity of Rho-family GTPases during cell division as visualized with FRET-based probes.’ *J Cell Biol.* 2003; 162(2): 223-32.

Zaidel-Bar R, Ballestrem C, Kam Z, Geiger B. ‘Early molecular events in the assembly of matrix adhesions at the leading edge of migrating cells.’ *J Cell Sci*. 2003; 116(Pt 22): 4605–4613.

Zanconato F, Forcato M, Battilana G, Azzolin L, Quaranta E, Bodega B, Rosato A, Bicciato S, Cordenonsi M, Piccolo S. ‘Genome-wide association between YAP/TAZ/TEAD and AP-1 at enhancers drives oncogenic growth.’ *Nat Cell Biol*. 2015; 17(9): 1218-27.

Zebda N, Dubrovskyi O, Birukov KG. ‘Focal adhesion kinase regulation of mechanotransduction and its impact on endothelial cell functions.’ *Microvasc Res*. 2012; 83(1): 71-81.

Zhang H, Liu KK. ‘Optical tweezers for single cells.’ *J R Soc Interface*. 2008; 5(24): 671-90.

Zhang Q, Skepper JN, Yang F, Davies JD, Hegyi L, Roberts RG, Weissberg PL, Ellis JA, Shanahan CM. ‘Nesprins: a novel family of spectrin-repeat-containing proteins that localize to the nuclear membrane in multiple tissues.’ *J Cell Sci*. 2001 Dec; 114(Pt 24): 4485-98.

Zhang X, Lei K, Yuan X, Wu X, Zhuang Y, Xu T, Xu R, Han M. 'SUN1/2 and Syne/Nesprin-1/2 complexes connect centrosome to the nucleus during neurogenesis and neuronal migration in mice.' Neuron. 2009; 64(2): 173-87.

Zhang XF, Schaefer AW, Burnette DT, Schoonderwoert VT, Forscher P. 'Rho-dependent contractile responses in the neuronal growth cone are independent of classical peripheral retrograde actin flow.' *Neuron*. 2003; 40(5): 931–944.

Zhao B, Ye X, Yu J, Li L, Li W, Li S, Yu J, Lin JD, Wang CY, Chinnaiyan AM, Lai ZC, Guan KL. 'TEAD mediates YAP-dependent gene induction and growth control.' *Genes Dev*. 2008; 22(14): 1962-71.

Zhao X, Guan JL. 'Focal adhesion kinase and its signaling pathways in cell migration and angiogenesis.' *Adv Drug Deliv Rev*. 2011; 63(8): 610-5.

Zhen YY, Libotte T, Munck M, Noegel AA, Korenbaum E. 'NUANCE, a giant protein connecting the nucleus and actin cytoskeleton.' *J Cell Sci*. 2002; 115(15): 3207-22.

Zhu R, Antoku S, Gundersen GG. 'Centrifugal Displacement of Nuclei Reveals Multiple LINC Complex Mechanisms for Homeostatic Nuclear Positioning.' *Curr Biol*. 2017; 27(20): 3097-3110.e5.